New devices for energy harvesting and storage: integrated third generation photovoltaic solar cells and electrochemical double layer capacitors

Doctoral Dissertation
Doctoral Program in Electrical, electronic and communications Engineering (31th Cycle)

New devices for energy harvesting and storage: integrated third generation photovoltaic solar cells and electrochemical double layer capacitors

Alberto Scalia
S224111
D39496

Supervisors:
Prof. Andrea Lamberti
Prof. Elena Tresso

PhD in electrical, electronics and communications engineering

Cycle XXXI

CONTENTS

1. INTRODUCTION

1.1 GLOBAL ENERGY DEMAND

The worldwide economy is facing a controversial and continuously mutable condition in which an enormous number of factors difficult to manage are playing a key role. In particular, the European continent has to deal with a series of geographical and political concerns that are undermining the stability of the union. In this complex scenario, for every country, energy procurement, conversion and storage in its different forms represents a main issue in order to have a stable and flourish future.

As declared by the International energy agency (IEA) the world total primary energy supply (TPES) is more than doubled by 1973 (6,101 Mtoe) to 2015 (13,647 Mtoe). This consumption is expected to still increase in the next future since the developing countries are increasing their own energetic expenditure in order to quickly get a development from the industrial viewpoint.

Regarding power generation (24,255 TWh per year), the most exploited energy source is coal (39.3 %), which is largely used in China. Even if natural gas has experienced a huge diffusion in the energy field, it accounts only for the 22.9% of the worldwide power production. Nevertheless, in the next future, it is expected a global increment in natural gas employment, due to its much less environmental impact with respect to the other fossil fuels. Hydro (16%) and Nuclear (10.6%) are also important components of the power generation puzzle. Instead, renewable and waste account only for the 7.1%. Even if grown with time, it is still a poor percentage if compared to the whole worldwide production.

In particular, photovoltaic power generation in 2015 has been 247 TWh, only 1% of the total.

Certainly, in order to attain a more diversified mix which would have positive implications from the economic and environmental viewpoint, PV massive diffusion is a primary step to be rapidly implemented.

1.2 PHOTOVOLTAIC TECHNOLOGIES

Photovoltaic (PV) cells core mechanism relates to a light absorbing material capable to generate electrons when absorbing photons. In fact, sunlight electromagnetic power radiation impinging onto a PV device imparts a certain amount of energy to electrons, which depends on the specific photon wavelength. If the photon energy is higher with respect to the energy gap of the semiconductor

material, an electron is promoted to the conduction band of the crystal and then passes from the "p" type towards the "n" type material. The p-n junction reacts in such a way to re-stabilize the initial condition and thus an internal polarization occurs (positive on the "n" type and negative on the "p" type). When the circuit is not externally closed, this polarization is the PV cell open circuit voltage.

$$V_{OC} = \frac{kT}{q} \ln\left(\frac{I_{ph}}{I_o}\right)$$

In the previous equation k is the Boltzmann constant, T is the temperature, q is the elementary charge (electron) I_{ph} is the current due to the photovoltaic effect and I_0 is the reverse saturation current. Inverters work to set the PV device voltage in order to maximize the product between current and voltage.[1], [2]

1.2.1 FIRST GENERATION

The first PV generation relates to crystalline silicon technology. From the beginning of the PV technology production, they have been continuously developed and nowadays represent the most widespread and robust PV technology in the market. In fact, despite of the initial short life which hindered its diffusion as an economically valuable technology, they have now attained a long life-time that makes them reliable and appealing for producing electrical energy also if compared to fossil fuels.

The most performing research solar cell of the first generation have attained an efficiency of 27.6% (NREL source).

Commercially available multi-crystalline modules possess an efficiency ranging from 14% to 19%.[2]

1.2.2 SECOND GENERATION

The second PV generation relates to the thin films technologies. In this generation are included: amorphous silicon (a-Si), cadmium telluride (CdTe), copper indium diselenide (CIS) and copper indium gallium diselenide (CIGS).

Amorphous silicon is probably the most popular thin-film PV technology. The best research cell has reached an efficiency of 14% (NREL source). In this technology, silicon atoms are randomly located. This randomness has implications on the electronic properties of the material. In fact, amorphous silicon has a higher band-gap (1.7 eV) with respect to crystalline silicon (1.1 eV). It implies a stronger absorption in the visible part of the electromagnetic spectrum than in the infrared region.[1]

Cadmium telluride (CdTe) has been reasonably recognized as the semiconductor material having the ideal bang-gap (1.45 eV).[1] In addition, it is easier to deposit and suitable for large scale production. Even if it has demonstrated good efficiency (22.1% NREL source), toxicity of cadmium and availability of Tellurium hindered its diffusion in the energy market.

Copper indium gallium diselenide (CIGS) is a PV technology constituted by multi-layered thin-film composites. CIGS technology has attained efficiencies above 20% for single cells (23.3% for research cell, NREL source), while for large area modules has attained 13%.[1] The most crucial challenge for CIGS modules fabrication has been the limited ability to scale up the process. Nevertheless, also cost has represented a limiting factor in commercializing this technology.

1.2.3 THIRD GENERATION

In the third generation are included: dye sensitized solar cells (DSSCs), organic solar cells, Perovskite solar cells, quantum dot solar cells and copper zinc tin sulphide (CZTS) solar cells. They represent the so-called "emerging PV technologies". Regarding DSSCs a deep discussion will be performed in chapter 2. Here, discussion is referred to the other PV technologies of the third generation.

Organic solar cells are fabricated as thin films of organic semiconductors: polymers or molecules. The typical thickness of the active material is nearly 100 nm since the average path of the electron-hole pair into the organic material is in the order of tens of nm. Electron-hole pair needs to reach the junction between a donor and an acceptor material in order to turn into free carriers. For this reason, a bulk hetero-junction is obtained throughout the whole active layer. Efficiencies of 12.6% have been attained to date (NREL source).

Perovskite solar cells have produced a huge interest in the scientific communities because of their fast increase in PV efficiency. To date, the best efficiency attained is 23.3% (NREL source). Perovskite absorber materials have the following chemical formula $CH_3NH_3PbX_3$, where X is a halogen atom: iodine, bromine, chlorine. [3]

Unfortunately, their limited stability over time hinders their employment in nowadays electrical energy production. To date, a perovskite PV module is not even present in the market. In addition, issues related to scalability processes and lead toxicity represent limiting factors in order to evaluate perovskite as a promising PV technology.

CTZS (quaternary semiconducting compound which lead to the fabrication of a thin film solar technology) solar cells and quantum dot solar cells (possessing

variable bandgaps by changing dots sizes) have demonstrated respectively 12.6% and 13.4% efficiencies (NREL source).

1.3 STANDARD TESTS CONDITIONS

Standard test conditions are the most commonly utilized conditions for testing PV solar cells or modules. They imply:

1) 100 mW cm^{-2} radiation intensity
2) 25 °C PV device temperature
3) Air mass 1.5 (AM1.5)

Air mass defines the direct optical path through the atmosphere that solar radiation has to pass through before reaching Earth's surface. It is expressed as the ratio between the actual path and the Zenith path length. In fact, when the sun is directly overhead the condition is of AM1.

AM1.5 implies a solar zenith angle of 48.2°.

These conditions were initially utilized for evaluating silicon PV technology performance and afterwards were adopted for assessing efficiency of all new technologies.

However, some technologies improve their efficiency by lowering the illumination conditions due to a different PV mechanism. In this perspective, evaluating PV performance in a wide range of radiation intensity, could be useful in order to have a clear idea of the electrical output a PV technology can produce.

1.4 CURRENT VOLTAGE MEASUREMENT

PV efficiency is expressed as the ratio between the electrical power output in the point where the product between current and voltage is maximum and the electromagnetic solar power impinging onto the PV device.

Indeed, efficiency can be easily calculated through the following equation:

$$\eta = \frac{I_{max}\, V_{max}}{G\, S} = \frac{I_{SC}\, V_{OC}\, FF}{G\, S}$$

Where I_{max} is the current in the maximum power point (A), V_{max} is the voltage in the maximum power point (V), I_{SC} is the short circuit current (A), V_{OC} is the open circuit voltage (V), FF is the fill factor, G is the electromagnetic power density expressed in mW cm^{-2} and S is the PV device surface (cm^{-2}, active or total).

The FF is defined as the ratio between the maximum produced power ($I_{max} \times V_{max}$) and the product between V_{OC} and I_{SC}.

Parameters of the previous equation are obtained through a potentiodynamic measurement (current-voltage (IV) measurement). A certain region is examined: from a slight negative voltage till a positive voltage, larger with respect to the open circuit condition.

The IV curve of a laboratory glass-based DSSC, obtained under STCs can be seen in Figure 1.

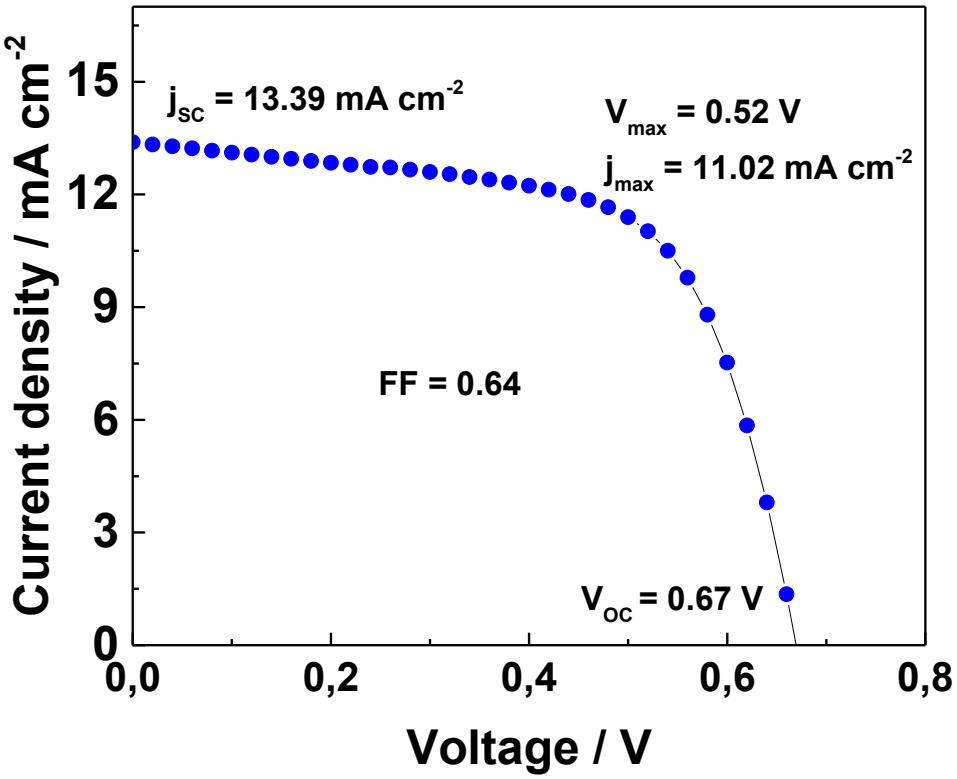

Figure 1: IV curve and peculiar PV parameter of a glass-based dye sensitized solar cell. j refers to the current density (current divided by the DSSC active surface).

1.5 AIM OF THE WORK

Renewable energy sources employment is a crucial point for lowering CO_2 emissions and decreasing global pollution. Their diffusion, especially PVs, could lead to energy self-sustainable buildings. Moreover, portable power packs able to

drive a certain application or re-charge electronic devices are nowadays obtaining more and more significance. What is usually missing in these power packs is an energy harvester, capable to disengage the energy device from the power grid, concerning subsequent uses. The PhD topic relates to the integration of dye sensitized solar cells (DSSCs) PV technology with electrochemical double layer capacitors (EDLCs) storage systems, in a single harvesting-storage device. Systems were characterized through photo-charges and subsequent discharges in dark conditions. Systematically, a different aspect was investigated: flexibility, high voltage, easiness of fabrication or simplification of the structure. Fabricated devices were systematically, critically analysed and compared with literature reports.

1.6 THESIS STRUCTURE

In this first chapter, the energy demand is critically discussed before presenting renewable energy sources and in particular PV technology. Topic and aim of this PhD are also proposed.

In chapter 2, DSSCs are presented, at first, regarding the typical glass-based configuration. Principal advantages are discussed as well as efficiency limits. Afterwards, flexible DSSCs configurations present in literature are reported, before focusing on the flexible configuration published as first work of this PhD.

In chapter 3, discussion about Electrochemical double layer capacitors (EDLCs) is proposed. In particular, principal testing modes and state-of-art materials (electrodes materials and electrolytes) are treated. At the end of this chapter, a physical and electrochemical study on an innovative co-solution of $Pyr_{14}TDI$ and Propylene carbonate is presented.

Chapter 4 is devoted to integrated PV-based harvesting-storage (HS) devices (PV-EDLC integration). The four configurations obtained in this PhD (DSSC-EDLC integration) are reported and deeply discussed also in comparison to literature reports.

Chapter 5 reports the conclusions and future prospects of HS devices.

2. DYE SENSITIZED SOLAR CELLS

Since 1991, when the first prototype was fabricated by O' Regan and Gratzel, Dye sensitized solar cells (DSSCs) have been considered as a promising route for the substitution of traditional silicon solar cells. In the past 20 years, this belief was strengthened, as they certainly possess peculiar features such as low-cost of the materials involved in the fabrication,[4], [5] easiness of production[5], [6] and improvement of the efficiency by lowering the intensity of the incoming radiation.[7] Moreover, they so far attracted considerable attention due to their unique characteristic of being able to be obtained in different colours and thus being employed in whimsical and creative buildings. In this perspective, DSSCs have been considered having a double purpose especially in new and smart edifices: power production and facades decoration.

Being DSSCs the photovoltaic (PV) technology with the lowest Payback time, they still remain one of the most studied solar cells category in spite of their limited efficiency (if compared to traditional silicon PV cells or even to emerging Perovskite solar cells).

In addition, even if not comparable to commercial PVs, their lifetime is undoubtedly higher than Perovskite solar cells.

For all of these reasons, from now on, DSSCs are commercially considered mainly for particular applications, and not for the employment in big PV power plant. Smart utilizations are related to windows facades, remote sensor networks, portable power-packs or power production in remote geographical regions.

The research group in Polito has many years of experience on this PV technology and was interested in the integration with an energy storage device. The electrochemical double layer capacitors have been chosen because the structure of the two energy systems is quite similar (two electrodes and an electrolyte in between).

In this perspective, when integrated to an energy storage device, DSSCs increase their significance as energy harvester and also their implications in nowadays life.

2.1 COMPONENTS OF THE CELL AND OPERATIONAL PRINCIPLE

DSSCs are PV devices which exploit the peculiar light absorption characteristic of some dyes in order to produce electrical power. The components of a traditional DSSC are:

1) A photo-anode consisting of a transparent conductive glass sheet (typically the conductive material onto the glass sheet is fluorine tin oxide (FTO) or Indium tin oxide (ITO)) onto which a micrometric layer of mesoporous semiconductor is deposited. Dye molecules are anchored onto the high surface area semiconductor in order to absorb electromagnetic radiation coming from the sun.
2) An electrolyte containing a redox couple having the aim to regenerate the dye.
3) A counter electrode obtained onto a glass conductive substrate onto which a nanometric Pt layer is deposited to act as catalyst of the reduction reaction in the electrolyte, closing the circuit.

When the cell is exposed to sunlight, the electromagnetic radiation passes through the photo-anode transparent glass and reaches the mesopourous semiconductor layer hosting the dye molecules. Here, dye absorbs the electromagnetic radiation in dependence of its absorption spectrum and turns into an excited state, promoting an electron from the highest occupied molecular orbital (HOMO) to the lowest unoccupied molecular orbital (LUMO). Since LUMO has a higher energy level with respect to the conduction band of the dye-hosting semiconductor, electrons are quickly transferred to the conduction band of the oxide semiconductor. Afterwards, electrons move into the mesoporous structure and reach the conductive glass. Once electrons pass through the external circuit, they reach the counter electrode where the reduction of tri-iodide to iodide occurs. Into the electrolyte ions diffuse and close the circuit.

The porosity and morphology of the semiconductor layer are dominant factors determining the amount of dye molecules adsorbed on its surface. The higher the surface area, the larger the reaction sites quantity for the monolayer dye molecules to harvest incident light.[8]

Regarding dye complexes employed in DSSC, a large variety of them was synthesized in the past. Peculiar features that perfect dye should have are: a) remarkable absorption in the visible range, b) stability in the excited state, c) suitable redox potential and d) remarkable electron injection in the semiconductor layer and easiness of being regenerated by electrolyte.[9]

The Dyes that have obtained the best efficiencies to date are Ruthenium-complexes. Some of them have already been successfully commercialized such as N3, N719 and Z907.[8]

To date, organic solvent-based electrolytes have been the most commonly used in literature. In particular, iodide/triiodide redox couple dissolved in organic matrices have found large use. Among the organic solvents, acetonitrile (ACN) have been the most employed in DSSCs, due to its lowest viscosity. Nevertheless, undesirable leakage and evaporation of organic liquid electrolytes, unavoidably affected DSSCs life and stability. In addition, their toxicity caused serious environmental issues. [8]

To overcome these shortcomings, research efforts have been focused for developing non-traditional electrolytes like room temperature ionic liquids or quasi-solid state and solid state electrolytes.

In addition, to solve environmental constraints water was considered as solvent for DSSCs. Unfortunately, its employment in the field remains quite incremental, leading to lower efficiencies with respect to organic counterparts.[10]

2.2 TESTING MODES

As for all the PV technologies, current-voltage measurement is the most utilized testing mode. It is used to evaluate solar cells/modules efficiency as the ratio between the maximum electrical power output and the electromagnetic power impinging onto the PV device area (active or total).

For a more explicative and analytical clarification of the efficiency equation and to deep realize which cells parameters are involved, refer to chapter 1.

2.2.1 ELECTROCHEMICAL IMPEDANCE SPECTROSCOPY

Electrochemical impedance spectroscopy (EIS) is based on the application of an alternating voltage to an electrochemical system (DSSC, EDLC, battery). A constant voltage is superimposed to an alternating signal, which has to be small enough in order to consider the system under study as pseudo-linear (small signal approximation).[11] Usually, 10 mV are employed as alternating sinusoidal signal

and voltages around the open circuit are investigated as constant superimposed value.

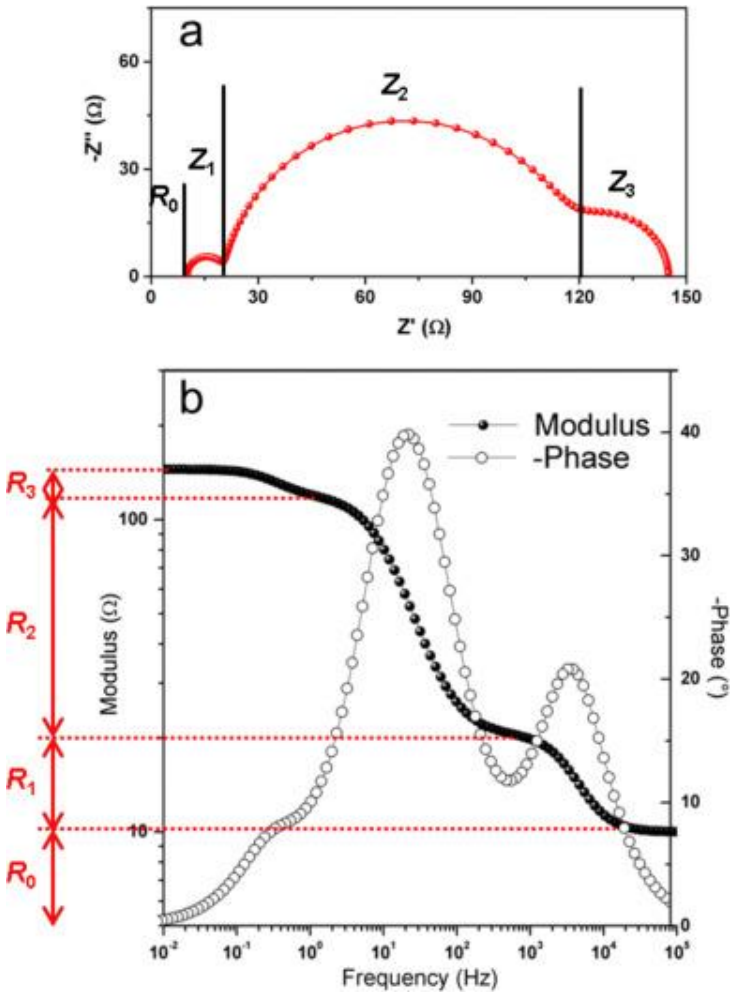

Figure 2: Impedance spectrum of a DSSC measured at open circuit voltage: (a) Nyquist and (b) Bode graphs. Reprinted with permission from reference*[11]*. Copyright 2017. Elsvevier.

The sinusoidal signal is applied in an appropriate range of frequencies (where it is possible to observe peculiar mechanisms) and the impedance is calculated by the Ohm's law.

In Figure 2A a typical Nyquist (- imaginary impedance vs real impedance) plot of a DSSC at an applied voltage around open circuit is proposed. Three semicircles representative of three different mechanisms occurring in the DSSC can be clearly recognized. For high frequencies above1 kHz, charge transfer process at counter

electrode (Z_1) is noticeable. It can be also identified in the Bode graph in Figure 2B, in which modulus (R_1) and phase of the impedance are plotted as a function of the frequency. The larger semicircle (Z_2) in the Nyquist plot, corresponding to the larger modulus variation in the Bode graph is representative of the electron transfer in the TiO_2 layer (electron-hole recombination, 1 Hz – 1 kHz). Last, Z_3 represents the diffusion into the electrolyte. This process occurs for very low frequencies, lower than 1 Hz.

2.3 WHAT ABOUT EFFICIENCY?

To date, the best efficiency reported in DSSCs literature is 14.3%. This remarkable efficiency (if compared to other third generation PV technologies) was achieved by Kakiage and co-workers in 2015 employing synergistic sensitization of silyl-anchor and carboxy-anchor dyes. [12] Overall, a quite slow constant increment in DSSC efficiency was experienced during years, thus testifying a persistent effort of the research community in pursuing performances capable to make DSSCs a worldwide utilized commercial technology.

Figure 3 shows the efficiency of the different PV technologies evaluated under standard test conditions (STC, see chapter 1) as a function of time (measurement year). Among the emerging PV technologies, DSSCs are certainly the oldest, but this longevity did not transmute into better performances, at least under 1 Sun illumination conditions. However, as they are still today under study,[7] their potentiality has to be researched in unconventional radiation settings, such as low illumination or indoor conditions.

In this perspective, Freitag and co-workers [7] attained this year an absolute outstanding efficiency record for DSSCs of 28.9%, employing an OsramWarmWhite 930 as light source (1000 lux). The incoming power density was measured to be 0.3066 mW cm-2, corresponding to 0.003% of the radiation intensity usually utilized in standard conditions to test PV cells. This extremely low power density is quite unusual in PV literature, but in that case DSSC power output of 88.5 μW cm-2 makes believe that indoor applications could be the smartest use and most feasible future employment regarding DSSCs. In that work, Freitag et al. used a copper redox mediator employing acetonitrile (ACN) as solvent and two complementary sensitizers.

Figure 4 shows the IV curves of the fabricated DSSCs (also another solvent was used as electrolyte: propionitrile) for illuminations of 200 lux (61.3 μW cm-2) and 1000 lux (306.6 μW cm-2).

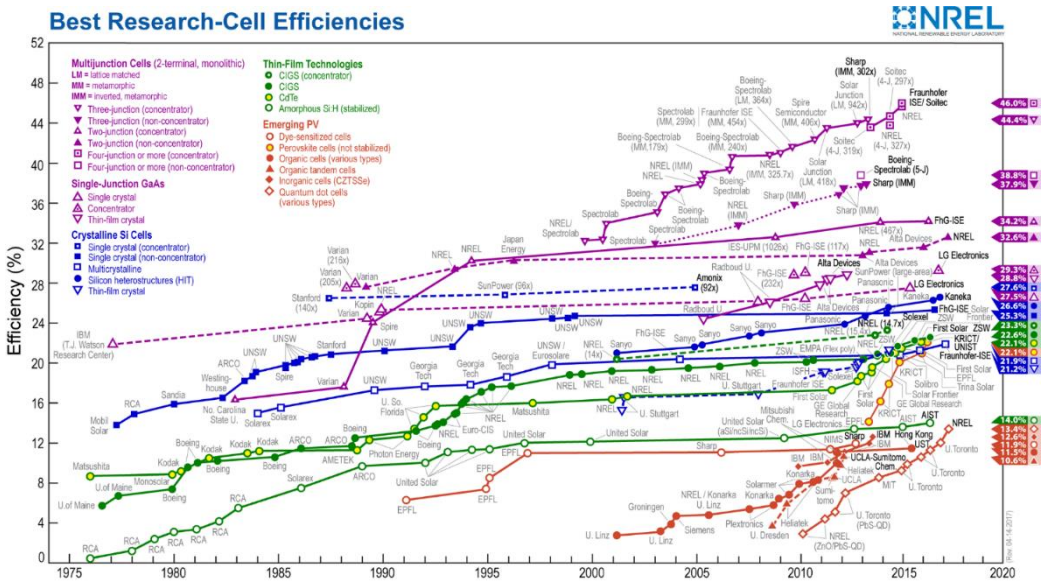

Figure 3: Best research-cell efficiencies graph. Efficiencies are reported as a function of the PV cell fabrication year.

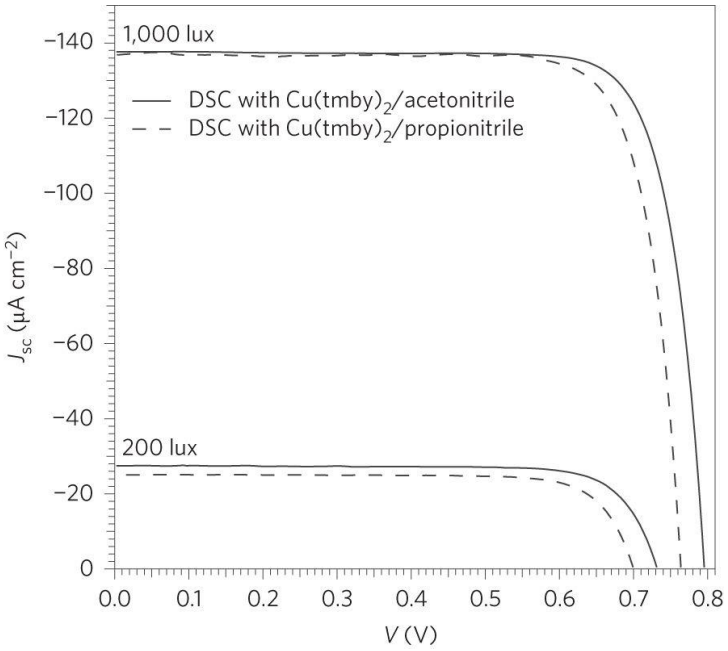

Figure 4: Current voltage characteristics of the co-sensitized DSSCs reported in Freitag et al.*[7]* under indoor-light conditions. Reprinted with permission from reference *[7]*. Copyright 2017 Nature publishing group.

2.4 PROGRESS IN FLEXIBLE DSSC

As already stated in this chapter, in their most efficient and widespread architecture DSSCs are fabricated onto planar conductive glass substrates. However, glass-based architecture possesses some critical constraints like rigidity, frangibility and weight. In addition, the largest part of the glass-based DSSC cost stands for the relatively expensive conductive glasses employed.

In order to extend the use of PVs to non-planar surfaces a series of flexible structures have been proposed in recent years.[13]

Since at least one of the two electrodes has to be fabricated onto a transparent substrate, the most commonly obtained architecture deals with devices fabricated onto plastic substrates: polyethylene terephthalate (PET) or polyethylene naphthalate (PEN). Nevertheless, cells containing a metal-substrate photo-anode and a plastic-substrate counter electrode have also been proposed in literature. In this case, DSSC has to be necessarily back-irradiated, since otherwise the electromagnetic power radiation could not reach the dye region, thus PV power generation would be eluded.

The main drawback of using a plastic photo-anode is related to low temperature (120 °C – 150 °C) TiO_2 semiconductor sintering, which usually requires temperatures in the range between 450 °C and 500 °C, since it guarantees an optimal bonding between nanoparticles and as a consequence a sufficiently long electron lifetime for effective charge collection. Inevitably, low temperature process leads to lower efficiencies. For this reason, alternative treatments were proposed in literature like ultra-violet (UV) assisted or compression methods.

Using a metallic substrate at the anode permits a high temperature sintering, but its opaqueness makes unavoidable a backward cell irradiation. In this way, light has to pass through the electrolyte layer which inevitably absorbs a fraction of the electromagnetic radiation, turning into a decrease of the PV efficiency. A solution to this problematic, could be obtaining a transparent electrolyte.[14] In this perspective, a 10% increase of the short circuit current density was experienced, with a deposition of submicron Sio_2 transparent beads onto the TiO_2 layer.[13]

In this way, transparent beads occupied a fraction of the opaque electrolyte and enhanced the number of photons which could reach the hosting dye mesoporous layer, improving the overall transmittance of the electrolyte chamber.

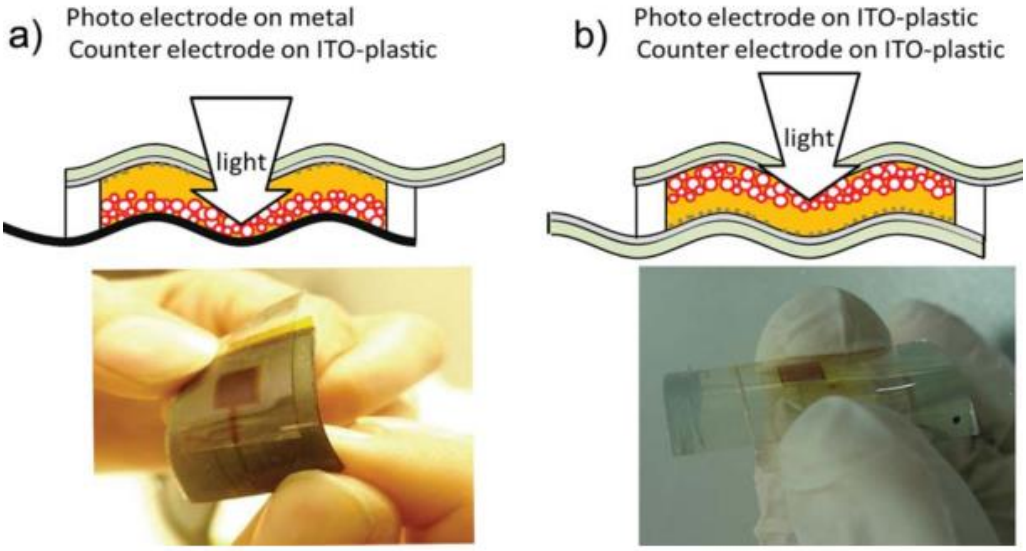

Figure 5: Literature widespread flexible DSSC architectures, presenting a backward illumination (metallic substrate at the photo-anode) a) or a forward illumination (plastic substrates both for the anode and cathode) b). Reprinted with permission from reference *[13]* Copyright 2014, Royal Society of Chemistry.

Figure 5 shows the two flexible DSSCs configurations before described. In particular, Figure 5A reports scheme and image of the metal-photo-anode architecture (backward irradiation) and Figure 5B shows the all plastic-substrate DSSC irradiated directly onto the anode side.

Differently, the approach followed in the projects related to this PhD was employing metallic grids as electrodes substrates, both for photo-anode or counter electrode fabrication. Metallic grids guaranteed good electrical conductivity and ease electrode processability, allowing to reach high temperature sintering. In addition, the device could be irradiated onto the photo-anode side, since semiconductor material completely covered the grid and light did not have to pass through a compact opaque metallic layer.

In a first project, the sealing of the flexible device was performed by means of a hot press employing plastic films, while in a second project in which a DSSC was coupled to a supercapacitor in a flexible configuration the integrated architecture was obtained employing PDMS slides by UV irradiating a liquid mixture of a radically cross-linkable silicone polyether acrylate and a photo-initiator.

2.5 NOVEL TOTALLY FLEXIBLE DYE-SENSITIZED SOLAR CELL EMPLOYING TITANIUM GRIDS AND POLYMERIC ELECTROLYTE

In this section, a quasi-solid and totally flexible Dye-Sensitized Solar Cell is presented. The designed structure was (at the time of publication) an absolute novelty in the DSSCs literature scenario. [15]

Peculiar employed materials were: metallic grids as electrodes substrates and a quasi-solid polymeric electrolyte.

Two rigid, planar structures were obtained before fabricating the flexible DSSC in order to previously examine the novel materials. The two planar configurations enabled to move from a rigid to a highly flexible device in a gradual way.

After fabrication, materials and devices were methodically characterized. Positively, performance of the flexible configuration was comparable to those provided by the rigid structures. A partial decrease in the PV efficiency (2.57% - 3.92%) was experienced due to a non-perfect electrode/electrolyte interface connection in terms of high resistance. Particularly, the counter electrode/ electrolyte connection resulted affected by the less effective use of two solid-state materials in contact with respect to the usage of a liquid electrolyte and also by the non-uniform platinum layer, which is traditionally adopted in glass-based DSSC.

2.5.1 EXPERIMENTAL SECTION

FLEXIBLE DSSC ELECTRODES FABRICATION

The flexible DSSC electrodes were fabricated onto Ti metallic grids. Regarding photoanode, commercial TiO_2 paste (18NR-AO) was diluted with isopropanol solvent in three different concentrations: 21.5%, 29% and 50% TiO2 paste by weight. The three solutions were stirred overnight before using.

Ti grids were cut into 1.4 cm side square shapes with a long tail working as electric contact. They were then cleaned in acetone and ethanol ultrasonic baths and left onto a hot plate to allow complete evaporation of solvents.

Subsequently, grids were dipped into TiO_2 solutions and left at room temperature in horizontal position till the TiO_2 layer appeared homogeneous and dry. Horizontal position was chosen in order to avoid agglomeration of the TiO_2 paste/isopropanol solution in the bottom part of the grid.

Grids were than annealed at a temperature of 525 °C for 30 min in order to obtain an anatase phase of the mesoporous structure. Photoanodes were incubated

for 12 h in a N719 0.3 mM solution employing ethanol as solvent. Unadsorbed dye was removed by rinsing grids with ethanol excess.

Counter electrode was fabricated onto the same Ti grid used for the photoanode by means of the sputtering technique. A nanometric layer of Pt was deposited in order to act as catalyst of the reduction reaction.

QUASI-SOLID ELECTROLYTE FABRICATION

Polymer electrolyte membrane (PEM) was prepared by means of a Ultra-violet light cured (UVLC) procedure, irradiating a blend composed by the two oligomers which are reported in Figure 6: Bisphenol A ethoxylate dimethacrylate (BEMA) and poly(ethylene glycol) methyl ether methacrylate (PEGMA).

The reaction was activated by a photosensitive molecule (Darocur 1173), which UV irradiated, could generate reactive radicals by a homolytic intramolecular scission. These radicals reacted with the two monomers in the blend. The first one (BEMA) contained two methacrylate groups; thus, its propagation reaction led to a 3-D crosslinked polymeric network. Conversely, PEGMA, contained a single functionality and could reduce the crosslinking density of the polymeric network making the membrane more flexible and once swelled in the iodine-based liquid electrolyte could increase the mobility of the iodide–triiodide redox couple in the polymer matrix. In this perspective, BEMA produced the self-standing and crosslinked skeleton of the polymeric membrane, while PEGMA ensured its flexibility, electrochemical, and functional properties.

A ratio of 35/65 between BEMA and PEGMA was chosen in order to obtain a satisfactory compromise regarding thermal stability, ionic conductivity, self-standing capability and above all flexibility.[16] The percentage of Darocur 1173 that was added as radical photoinitiator was 3 wt% (with respect to the BEMA/PEGMA blend) . The obtained mixture was sandwiched between two UV transparent lab glasses spaced by 100 μm thick tapes on the borders. Then, the blend was UV irradiated for 2.5 min employing a medium vapour pressure Hg lamp providing an irradiation intensity of 30 mW cm^{-2}. Crosslinked PEM was detached from the glass by means of a lab bistoury. Figure 6 also shows the PEM under extremely severe bending conditions.

Subsequently, PEM was soaked in an iodine-based liquid electrolyte: 0.45 M Sodium Iodide (NaI), 0.056 M Iodine (I_2), and 0.55M 4-tert-butylpyridine (TBP) dissolved in 3-methoxypropionitrile (MPN).

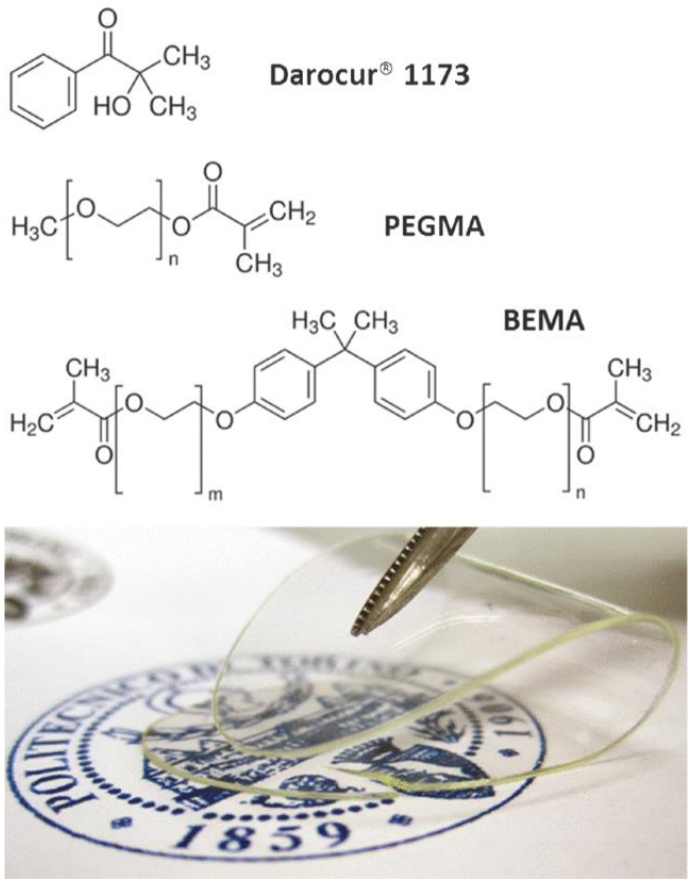

Figure 6: Structures of the reactive monomers and the photoinitiator used for the PEMs fabrication and a picture of a flexible UV-cured membrane. Reprinted with permission from reference *[15]*. Copyright 2016, IEEE.

PLASTIC ACTIVATION

DSSC sealing was performed employing 75 μm thick Polyethylene terephthalate (PET) films. In view of the sealing process, PET was previously chemically activated, under high vacuum conditions using a reactive atmosphere containing oxygen ions and radicals. In this way, a chemically active surface containing reactive groups (-OH, -COOH) was obtained.

To confirm the correct activation process, contact angle measurements were executed in order to check the hydrophobicity of the surface. This investigation enabled also to choose the best process parameters for the plasma treatment: 20 mtorr pressure, 30Wof RF power, an O2 flux of 20 sccm, and 1 min process time.

DEVICES ASSEMBLY

The three configurations obtained in this work are shown in Figure 7A. The first configuration was similar to a glass-based DSSC utilizing a quasi-solid electrolyte, except for the fact that the photoanode was fabricated onto a Ti metallic grid.

The glass at the photoanode was used just to keep fixed the cell structure, while in this configuration the counter electrode was still obtained sputtering a nanometric thick Pt layer directly onto the glass substrate.

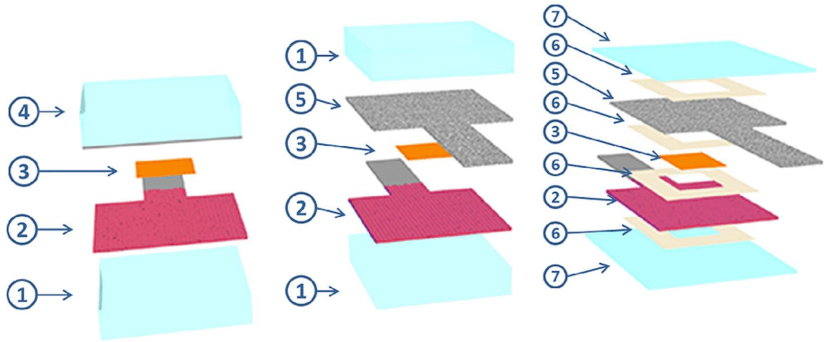

(a)

Cell #1 Cell #2 Cell #3

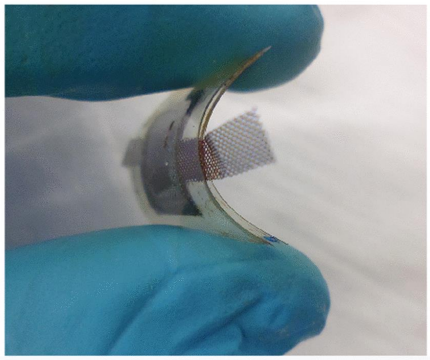

(b)

Figure 7: a) Schemes of the three cells configurations and b) picture of the flexible DSSC (final configuration). (1) Titanium grid with TiO2 and N719 (2), PEM (3), Pt-coated FTO/glass (4), Pt-coated Ti grid (5), Meltonix film (6), PET foil (7). Reprinted with permission from reference *[15]*. Copyright 2016, IEEE.

The second configuration differed from the previous only regarding the counter electrode that in this case was obtained onto the Ti grid, in view of the fabrication of the final flexible DSSC.

In this configuration both for the photoanode and the cathode sides the glasses were employed to keep fixed the structure and they did not provide any active purpose. In the first two configurations the DSSCs were kept fixed by using clips.

Final assembly was obtained employing 75 μm thick PET foils and Meltonix films. Each layer of the DSSC (PET, electrodes, electrolyte) was spaced by Meltonix films while two PET foils cut in a proper shape were used instead of glasses for the final sealing in order to obtain the flexible DSSC structure. While sealing, hot press was maintained at 85 °C. Picture of the flexible DSSC is shown in Figure 7B.

2.5.2 RESULTS AND DISCUSSION

FLEXIBLE PHOTOANODE

Commercial paste was diluted with isopropanol in order to obtain a less viscous material, easy to deposit. Thus, leading to a homogeneous semiconductor layer onto the metallic grid. Viscosity tests were performed on the commercial paste and on the diluted solutions by means of a Rheometer (MCR Rheometer series Anton Paar). The viscosity of each solution was calculated as the average of the values measured in a range of shear rate between 10^{-1} and 10^{3} s^{-1}. Results are reported in Table 1. As expected, increasing the solvent percentage, the viscosity of the entire solution decreased, allowing a more uniform dipping of the sample.

Different TiO_2 solutions were studied in viscosity, mainly to evaluate the correlation with the thickness of the mesoporous layer onto the Ti grid substrate. To estimate the thickness of TiO_2 present onto the Ti grid, optical microscopy and FESEM analysis were carried out.

As it is possible to notice in Figure 8A, the thickness of the bare grid was around 45 μm. When dipped into the 21.5% TiO2 solution, thickness increased to 60 μm, as testified by optical microscopy images (see Figure 8B).

This value was confirmed by FESEM cross-sectional images. In fact, a completely covered portion of the grid, presenting the same total thickness (grid and semiconductor layer) evaluated with optical microscope, is reported in Figure 8C.

FESEM analysis was performed also on the mesoporous semiconductor material. Figure 8D shows the TiO_2 semiconductor fine structure.

Table 1: TiO2 solutions viscosities and thicknesses of semiconductor layer onto the titanium grid for the different paste concentrations.

TiO2 weight percentage in solution with isopropanol [%]	Viscosity [Pa s]	TiO2 thickness for each side of the grid [µm]
21.5	0.03	8
29	0.05	12
50	0.48	42
100	78.5	80

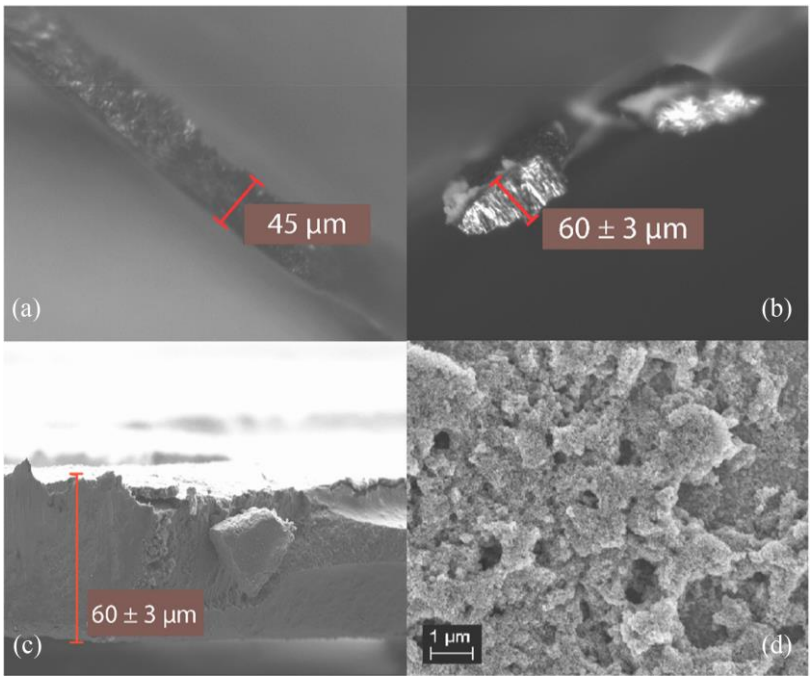

Figure 8: (a) Cross section of the bare Titanium grid, (optical microscopy image) . (b)Optical microscopy and (c) FESEM images of a portion of a metallic grid completely covered by TiO_2 (21.5%). (d) FESEM image of the fine structure of the semiconductor material. Reprinted with permission from reference *[15]*. Copyright 2016, IEEE.

Reducing isopropanol concentration, the thickness of the deposited TiO_2 layer increased till a value of 80 µm for no diluted paste.

Taking into account the uniformity of the obtained layer and the diffusion length of electrons in TiO_2 mesoporous structure, which is nearly 15 µm,[17] the solution which led to the most suitable semiconductor thickness was the 21.5%

semiconductor concentration, which led to a thickness of around 8 μm of Titanium dioxide for each side of the metal grid.

DSSC CHARACTERIZATION

PV response of the fabricated DSSCs was investigated through IV measurements. The recorded profiles are shown in Figure 9.

In order to better compare the performances of the three DSSCs, in Table 2 are summarized the peculiar PV parameters. Efficiencies were normalized to the effective photo-anode area.

The two rigid configurations (Cell 1 and Cell 2) present somewhat comparable PV parameters with respect to literature reports dealing with PEM as electrolyte.[18], [19] Changing the glass-based counter electrode (Cell 1) with the one obtained onto the metallic grid (Cell 2) did not dramatically affect the performances of the quasi-solid device. In fact, the PV efficiency slightly decreased from 4.45% (Cell 1) to 3.92% (Cell 2). This small reduction in the performance of the DSSC can be explained with the slower reduction kinetic of iodide to tri-iodide occurred at the cathode. This resulted in a decrease of the short circuit current density. The slowed reduction reaction in Cell 2 is ascribable to a lower surface percentage covered by Pt if compared to the uniform Pt layer sputtered onto the FTO glass of Cell 1. Remarkably, Cell 2 efficiency at time of publication was still higher if compared to the best result ever reported for a DSSC fabricated with a flexible anode and a rigid cathode. [17] In that case DSSC structure was quite similar to Cell 1, but with the difference of employing titania nanotubes instead of nanoparticles.

Even if, a quite interesting j_{sc} was found for Cell 3, the efficiency was limited with respect to the planar configurations. This was evidently due to the poor fill factor obtained for Cell 3. In fact, for the flexible configuration a quite high series resistance is observable from the IV slope near to the open circuit voltage.

Table 2: Peculiar PV parameters of the three DSSCs configurations

	FF	V_{OC} [V]	j_{SC} [mA cm^{-2}]	η_{corr} [%]
Cell 1	0.42	0.676	9.24	4.45
Cell 2	0.44	0.686	7.88	3.92
Cell 3	0.2	0.688	11.3	2.57

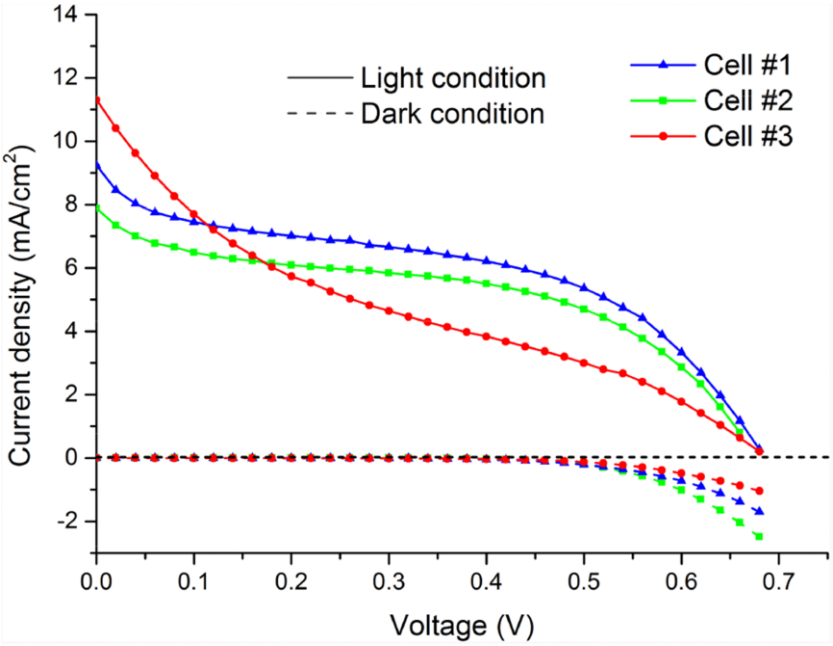

Figure 9: IV profiles of the three DSSCs configurations under 1 Sun irradiation and in dark conditions. Reprinted with permission from reference *[15]*. Copyright 2016, IEEE.

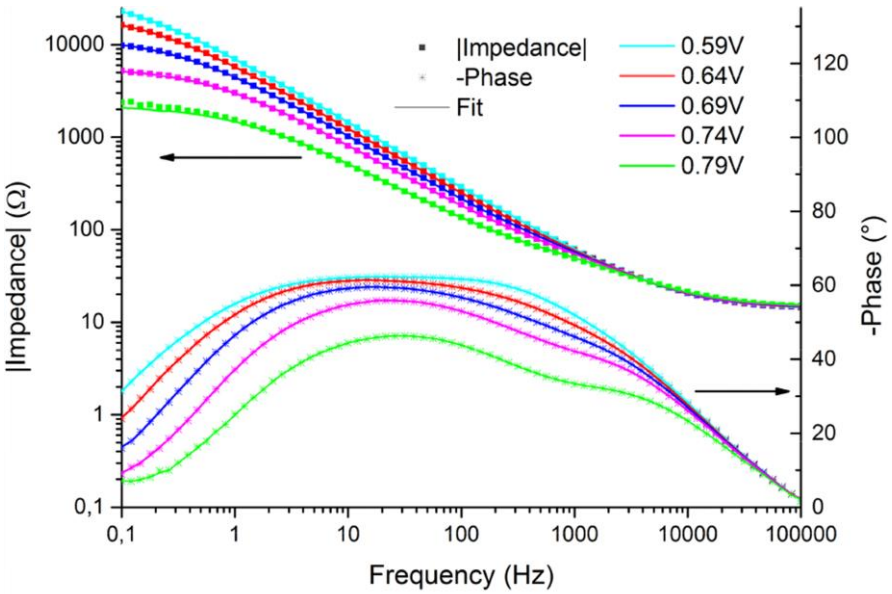

Figure 10: Bode graph of the flexible DSSC configuration: phase (right axis) and the modulus of the impedance (left axis). Impedance measuremnts were performed at values around the open circuit voltage. Reprinted with permission from reference *[15]*. Copyright 2016, IEEE.

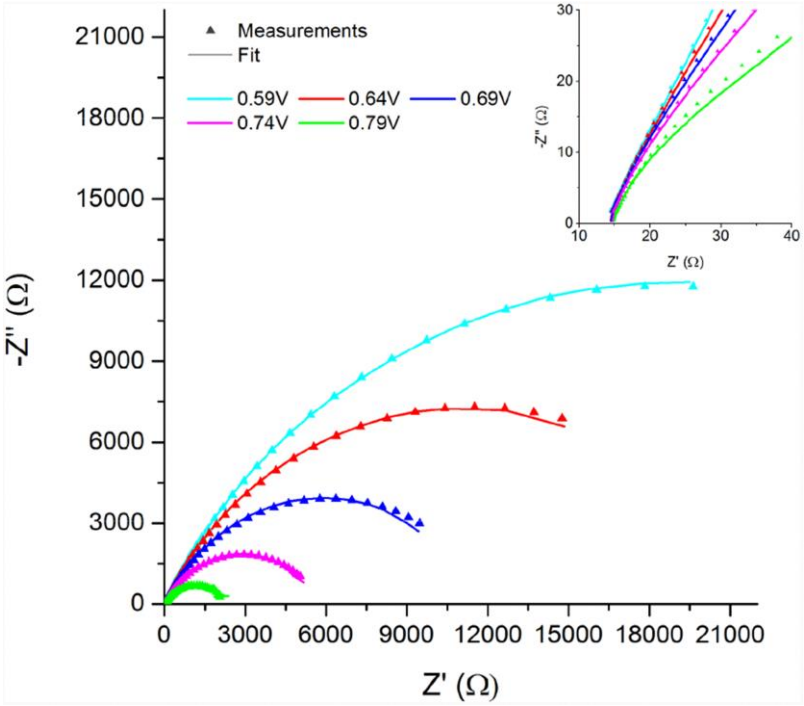

Figure 11: Nyquist plot of the flexible DSSC configuration. In the inset is shown the initial region in orderto appreciate the first semicircle. Points are measured values, while lines are the fitting curves. Reprinted with permission from reference *[15]*. Copyright 2016, IEEE.

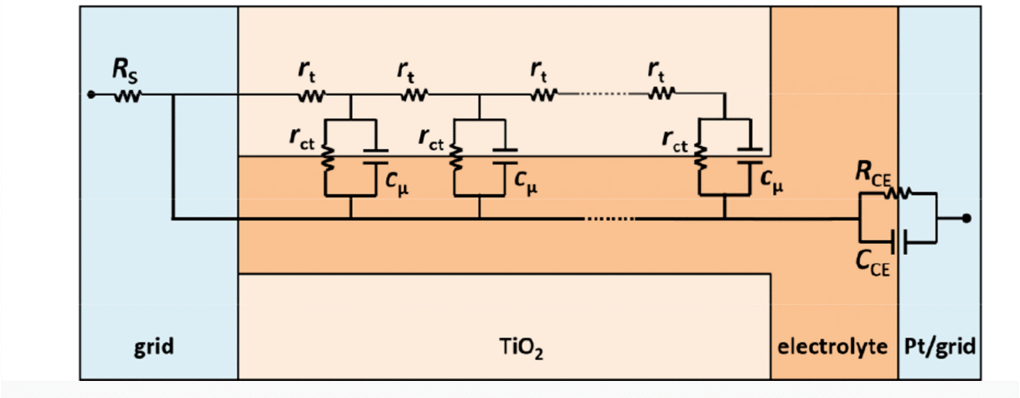

Figure 12: Equivalent circuit of the flexible DSSC configuration. Reprinted with permission from reference *[15]*. Copyright 2016, IEEE

Electrochemical Impedance spectroscopy (EIS) was performed in order to highlight and deeply understand the electrochemical mechanisms occurring in the flexible configuration. EIS was carried out for voltages close to the V_{OC}. Figure 10 shows Bode graph (impedance and phase) of the flexible DSSC. For higher applied voltages (0.79 and 0.74 V), two peaks are clearly recognizable. The peak at high frequency is related to the interface between cathode and electrolyte, while the peak at intermediate frequencies gives information on the electron recombination at the electrolyte/photo-anode interface.

The intermediate frequency peak shifts toward lower frequencies by lowering the applied voltage. It implies a larger lifetime for electrons. This phenomenon is related to the fact that less and less free electrons occupies the conduction band and thus recombination probability diminishes.

For high voltages the high frequency peak is discernible from the middle frequency peak. However, reducing the voltage a single peak is noticeable. This is related to the electronic transport into the titanium oxide layer. In fact, for lower voltages the transport resistance (in TiO_2) cannot be anymore neglected as it was for high voltages, when the TiO_2 could be considered sufficiently conductive.

Figure 11 shows the Nyquist plot. Here, the peaks of the Bode graph are visible as semicircles and the diameter of the semicircle is representative of the interface resistance.

The smaller semicircle (visible in the inset) represents the interface between cathode and electrolyte, while the bigger semicircle at intermediate frequencies represents the anode/electrolyte interface.

The plot was fitted according to the circuit in Figure 12, which models the flexible DSSC. Ohmic resistance (R_S in Figure 12), which is visible in the Nyquist plot as the distance of the first point obtained (for the highest frequency applied) from the origin. The calculated value (14.54 Ω cm^2) was found to be similar to values reported in literature. [17]

However, the cathode/electrolyte resistance (R_{CE}) was found to be excessively large (17.5 Ω cm^2). The low fill factor is certainly due to this anomalous value. In fact, for efficient DSSC, R_{CE} should be lower than 10 Ω cm^2.[20]

3. ELECTROCHEMICAL DOUBLE LAYER CAPACITORS

Electrochemical double layer capacitors (EDLCs) represent a mature energy storage technology, which can be complementary used with Lithium ion batteries (LIBs) in order to fulfill the complex scenario of nowadays electrical energy requirements. In fact, EDLCs and LIBs possess quite opposite features that could work balancing roles while driving the same application.

Differences between the two storage technologies rely in the dissimilar storage mechanism. In LIBs, energy is stored through redox reactions happening in the bulk of the cathode (reversible Li-insertion and de-insertion in the materials (anode and cathode) occurs), while EDLCs store electrical energy accumulating electrons at the surface of electrodes material, forming a double layer with ions present in the electrolyte which are electrostatically kept onto the porous electrode surface.

Reversible electrostatic storage mechanism occurring in EDLCs leads to impressive long-term cycling performance. In this perspective, they can tolerate 1,000,000 cycles before experiencing a significant capacitance decrease. [21] Conversely, LIBs can withstand 500-3000 cycles depending on the slowdown of the electrolyte decomposition or other materials (e.g. active material) degradation. Diminishing the surface directly exposed to the electrolyte by employing larger material particles or establishing a passivation solid electrolyte interphase may extend LIBs working lives, which however appear poor if compared to EDLCs.[22]

The other main difference arising from the dissimilar storage mechanism regards energy density and power density. In fact, redox reactions happening in LIBs permits to store a much higher energy per unit of volume compared to double layer electrostatic accumulation. On the other hand, batteries need more time to be charged and discharged involving relatively slow redox reactions. EDLCs instead, can exploit the accumulated charge in a short period if the application requires it, resulting in higher power densities.

Applications in which EDLCs have attracted more interest are automotive, transportation (electric or hybrid vehicles), current stabilizers and smart grids. They are all applications requiring fast response and less restrictive technical specifications than batteries.

3.1 RAGONE GRAPH

Figure 13 shows the Ragone plot, reporting specific power on the y-axis and specific energy on the x-axis. As observable from the graph, EDLCs are located between batteries and conventional capacitors regarding the energy density stored in the electrochemical device. In fact, EDLCs commonly have energy density lower than 10 Wh kg^{-1}. Challenges of future research are certainly represented by increasing their specific energy.

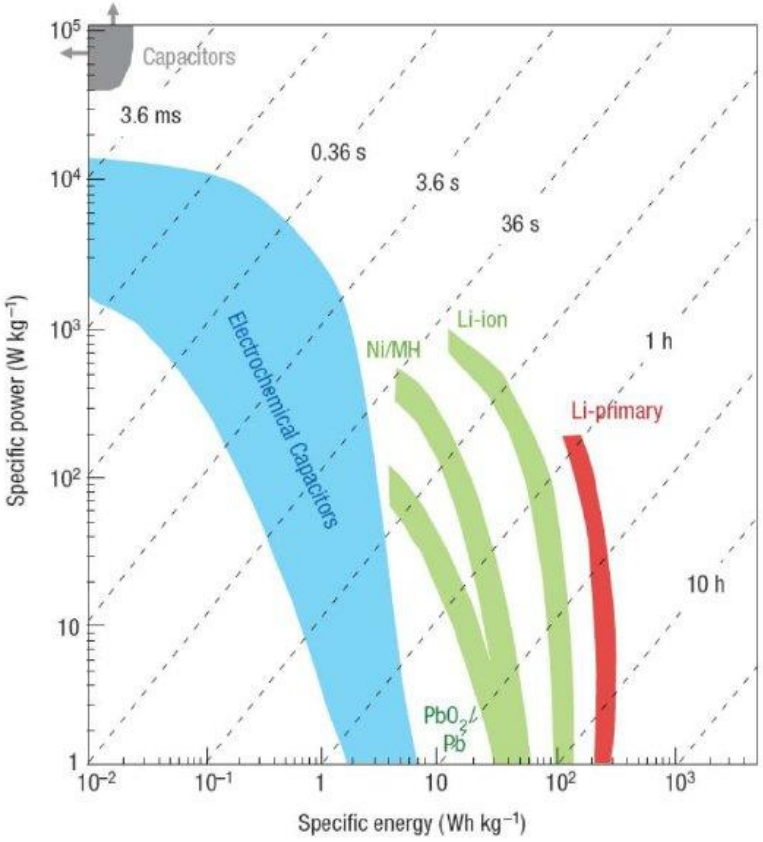

Figure 13: Ragone graph, reporting specific power on y-axis and specific energy on x-axis. Reprinted with permission from reference*[23]*. Copyright 2008, Nature publishing group.

Another important advantage (not stressed in the introductory part) EDLCs possess with respect to other technologies appear their outstanding versatility, since the area in the graph is clearly larger with respect to Li-ion, Li-primary, PbO_2 or capacitors.

3.2 TESTING MODES

Energy stored into an EDLC may be roughly estimated through the following equation:

$$E = \frac{1}{2} C V^2$$

Where C is the capacitance (F g^{-1}) and V is the voltage window reduced by the typical IR drop occurring when switching from charge to discharge in a galvanostatic measurement (refer to *Galvanostatic charge discharge* section of this paragraph).

Power density is instead evaluated as:

$$P = \frac{V^2}{4R}$$

in which R is the equivalent series resistance (EDLC resistance by treating the electrochemical energy storage as the series of a capacitor with a resistance).

The two previous equations can be used only for triangular galvanostatic profiles or for rectangular cyclic voltammetry curves (refer to the following sections of this paragraph). Generally, energy can be always evaluated through the discharge curve (whichever is the testing mode) integrating the product between voltage and current over time:

$$E = \int V(t) i(t) dt$$

3.2.1 CYCLIC VOLTAMMETRY

Cyclic voltammetry (CV) is a potentiodynamic measurements which applies a linear potential sweep between positive and negative electrodes in a 2-electrodes cell configuration and between working and reference electrodes in a 3-electrodes cell configuration. Voltage or potential change (scan rate) is expressed in mV s^{-1}. Potential is varied in a certain voltage window. When testing new materials or electrolytes, voltage window can be progressively enlarged (anodic and cathodic sweeps) in order to test efficiency and determine the maximum operating voltage. From a 3-electrodes CV measurement it is possible to adjust electrodes mass for the final device configuration (refer to the last paragraph of this chapter, where an electrochemical study of a novel electrolyte is proposed).

Carbon-based EDLCs CVs present a quite rectangular shape, mainly depending on the resistance of the EDLC under study. In the following chapter dedicated to integrated devices a quite distorted CV can be observed for an EDLC obtained onto

conductive glass substrates, having larger resistivity if compared to usual current collectors employed in EDLCs fabrication.

Conversely the CVs showed in this chapter (co-solutions of ILs and PC) are rectangular and present resistance values comparable to literature.

Capacitance can be evaluated through the following equation as reported by Zhang et al.:[21]

$$C = \frac{\int_0^{V/\nu} |i|\, dt}{V\, m}$$

where V is the potential attained during scanning, ν is the imposed scan rate, i is the recorded current and m is the electrodes active material weight.

3.2.2 GALVANOSTATIC CHARGE DISCHARGE

Galvanostatic charge discharge (GCD) is the most used measurement for characterizing EDLCs. A constant current is applied to the EDLCs while charging and the same current value is applied in the opposite verse while discharging. GCD presents a triangular profile for carbon-based EDLCs which do not envisage faradaic reactions. Equivalent series resistance can be evaluated by the voltage IR drop occurring when switching from charging to discharging phase, by simply applying Ohm's law.[24]

$$R_{ES} = \frac{\Delta V}{\Delta I}$$

Where ΔI is the total change in current ($I_2 - I_1 = 2I$) and ΔV the measured voltage drop.

Capacitance can instead be evaluated by the linear slope of the discharge curve as reported in the following equation:[25]

$$C\ [F\ g^{-1}] = \frac{i\ [A]}{s\ [V\ s^{-1}]\ m\ [g^{-1}]}$$

where s is the slope of the linear discharge profile, m is the electrodes mass and i is the applied current.

This technique is also largely used for testing the long-term performances of an EDLC. In this chapter, a commonly employed approach to evaluate EDLCs cycling stability is applied to an IL-PC co-solution. 5 steps of 1 000 consecutive GCD cycles were performed at 1, 2, 5, 10 and again 1 A g^{-1}. After this initial protocol, 50 000 cycles were performed at 2 A g^{-1}.

When the discharge profile of a GCD measurement is not perfectly linear, capacitance should be calculated taking into account the energy effectively provided by the EDLC while discharging, in order to avoid overestimation.

Energy and power can also be evaluated from GCD as follows:

$$E_{average}\ (Wh\ kg^{-1}) = i \int \frac{U}{m_{am}\ 3.6}\ dt_d$$

$$P\ (W\ kg^{-1}) = \frac{E_{average}\ 3600}{t_d}$$

in which, t_d is the discharge time expressed in seconds, i is the current expressed in Ampere, U is the voltage expressed in Volt, m is the mass of the active material expressed in gram.

3.2.3 FLOATING TESTS

An alternative technique that can be used to evaluate cycling stability is the float test. This method, which has been recently proposed, refers to holding the device at the maximum voltage allowed by the electrochemical stability window for at least 50–100 hours while periodically sampling capacitance through GCD, CV or EIS.

3.2.4 ELECTROCHEMICAL IMPEDANCE SPECTROSCOPY

Electrochemical impedance spectroscopy (EIS) measures the impedance of the EDLC in a wide frequency range, by applying a low-amplitude alternative voltage superimposed on a steady state potential.[21] Being the equivalent circuit of an EDLC the series of a capacitor and a resistance the Nyquist plot of an EDLC should ideally be a parallel line to the y-axis. Instead, a real EDLC shows in the high frequency region a semicircle profile, typical of the circuital model of a capacitor in parallel to a resistance. The semicircle profile is related to contact problems among the particles or to contact problems with the current collector. In the intermediate frequency region, a linear profile with a slope of approximately 45°is recognizable and is associated to the limited ion diffusion in the pores of the electrodes. In addition, for very low frequencies the spectrum is not completely vertical (90°) meaning that the behaviour differs from that of an ideal capacitor.

Typical parameters that can be obtained from an EIS regards the equivalent series resistance and the capacitance. However, EIS is mainly performed when charge transfer (e.g. pseudo-capacitive materials), mass transport and charge storage mechanism need to be clarified (especially for new EDLCs components).

In Figure 14 is reported the EIS of an organic solvent-based EDLC. Test was performed in an EL cell with carbon-based EDLC electrodes having an 18 mm diameter circular shape. In the inset is clearly noticeable the high frequency semicircle discussed above.

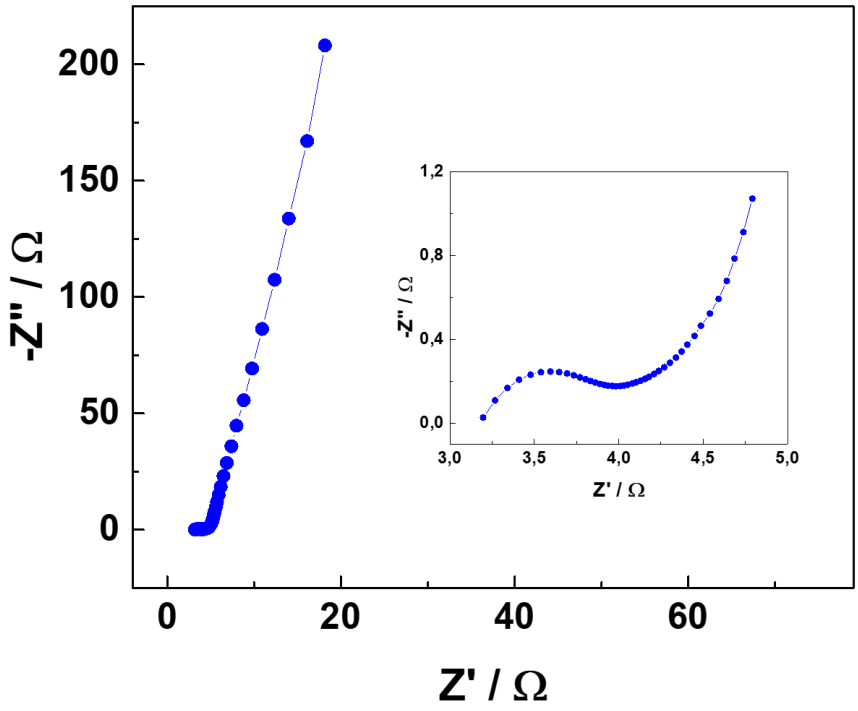

Figure 14: Electrochemical Impedance Spectroscopy of a Propylene Carbonate-TEABF$_4$ EDLC. Measurement was carried out in a EL cell with circular electrodes having 18 mm diameter.

3.3 CARBON MATERIALS

Commercially available EDLCs make use of porous carbon materials for electrodes. Usually, capacitance values grow increasing the specific surface area (SSA). However, it must be stated that this assumption cannot be always considered, as demonstrated by Chmiola and co-workers.[26]

Overall, important roles are played by carbon structure, pore shapes, surface functional groups and electrical conductivity. Porous activation by employing CO_2 or KOH treatments was considered in literature in order to exploit the obstructed or clogged pores. [27]

When designing a proper EDLC, average pore size of the active material and ions sizes of the salts present in the electrolyte need to be considered in order to avoid problematics related to ion sieving or pore saturation.[27]–[30]

Overall, carbon materials play a dominant role in increasing EDLCs capacitance values, thus turning also into a large variation of power density.

A large variety of carbon materials were studied in the recent past (graphene, carbon nanotubes, carbon nanofibers, microporous carbons, metal enriched carbons), testifying willingness of the research community in obtaining highly performing carbon-based EDLCs.[27], [28]

3.4 EDLCs ELECTROLYTES

Since energy stored into an EDLC is proportional to the square of the voltage window, a crucial point to enlarge EDLCs utilization is undoubtedly researching electrolyte capable to withstand higher voltages with respect to the conventional and industrially employed organic electrolytes.

Commercial EDLCs use acetonitrile (ACN) or propylene carbonate (PC). These solvents, employing tetraethylammonium tetrafluoroborate ($TEABF_4$) as salt, work with a voltage window of 2.7 V, which is much higher with respect to the 1.23 V water splitting limit of aqueous electrolyte. [22], [27], [31]

Their ionic conductivity, when employed in solutions with commonly used organic salts, is lower with respect to aqueous electrolyte. For example, a 1 M H_2SO_4 aqueous solution at 25 °C possesses an ionic conductivity of nearly 0.8 S cm^{-1}. This value is at least one order of magnitude higher if compared to organic electrolytes. In fact, a 0.65 M (1 M) $TEABF_4$ in ACN electrolyte has an ionic conductivity of 49.6 mS cm-1 (0.06 S cm-1), and ACN is the solvent with the lowest viscosity among the organic solvents employed in EDLCs. An electrolyte employing PC with the same salt ($TEABF_4$) and concentration (0.65 M) provides only 10.6 mS cm^{-1}. [31] However, ACN has more environmentally issues if compared to PC. This is the reason why PC in spite of the lower ionic conductivity is also widely used for industrial EDLCs, especially in developed countries where safety and environmental policies are significant constraints. Furthermore, organic electrolytes require complicated purification and assembling has to be done in a strictly-controlled environment in order to remove any residual impurities (especially water) that can lead to large performance degradation and serious self-discharge issues. This is one of the reason which renders EDLCs highly expensive also compared to batteries if normalized to the energy stored or even to the device weight.

Even if the voltage window of aqueous electrolyte is narrow in comparison to organic electrolytes they were recently profusely studied due to the fact that they are inexpensive and do not require a controlled environment to be fabricated. In literature, the employment of aqueous electrolytes has led to impressive device

capacitance values (300 F g^{-1}) [31] even in EDLCs employing no pseudo-capacitive active material (mainly carbon-based materials). An epochal turning point was represented by Fic et al. [32] attempt, when they proved that no capacitance fade was experienced in an aqueous EDLC employing 1M Li_2SO_4 salts working at 2.2 V, giving significance to neutral medium electrolyte. However, as they stated in their paper, their laboratory Swagelok cell was far from a commercial EDLC system.

As I started my research activity with DSSCs (and in that field water electrolytes remain quite a dream) I find that water-based EDLCs demonstrating by far the best literature capacitances and power densities values deserve to be deeply studied in order to try to make this technology commercially available.

On the other hand, research community has recently valued the possibility to use ionic liquids (ILs) in EDLCs since they can effectively and substantially increase the voltage cell up to 3.5 V, or even higher voltages. They are salts (exclusively ions) with melting points below 100 °C.

Usually, ILs possess several advantages including high thermal, chemical and electrochemical stability, negligible volatility, and non-flammability. [31]

Additionally, ILs can be tuned in order to get desired physical and chemical properties. This feature is given by the large variety of cations and anions (virtually unlimited), that can be combined. Regarding cations, imidazolium-based ILs have the highest conductivities, while pyrrolidinium-based ILs possess the largest operating voltage windows. Typical ILs anions employed in EDLCs are: tetrafluoroborate ($BF4^-$), hexafluoro-phosphate ($PF6^-$) and bis(trifluoromethanesulfonyl)imide ($TFSI^-$).

ILs have lower ionic conductivities with respect to aqueous or organic electrolytes. This is certainly related to their higher viscosity. In order to increase capacitance values provided by ILs EDLCs they have recently been investigated in co-solutions with organic solvents, [22], [27], [31]still providing a large voltage window.[33]–[37]

Nowadays, since portable or wearable electronics demand is continuously growing, as well as the need to have in the market performing flexible devices, solid-state electrolytes have been thoroughly investigated for EDLCs. [38]–[40] To date, the majority of the solid-state electrolytes developed for EDLCs were polymer-based electrolytes.

Regarding ELDCs electrolytes, the projects related to my research were focused on ILs and PC co-solutions (part of this chapter), quasi-solid electrolytes (polymer matrix soaked into aqueous electrolyte) and solid electrolytes (PEO-

Pyr_{14}TFSI). In particular, the last two types were employed in integrated PV-EDLC devices (refer to chapter 4, *Integrated harvesting-storage devices*).

3.5 NOVEL ELECTROLYTES BASED ON PYR_{14}TDI-PC CO-SOLUTIONS

In this paragraph are shown and discussed the first results ever obtained regarding the use of N-butyl- N-methyl-pyrrolidinium 4,5-dicyano-2-(trifluoromethyl) imidazole (Pyr14TDI) as electrolyte component for EDLC applications. In particular, different co-solutions were obtained with propylene carbonate (PC) and investigated in terms of physical and electrochemical properties. A wide concentration range was studied, from diluted (25% Pyr_{14}TDI by weight) to extremely concentrated solutions (75% Pyr_{14}TDI by weight). Figure 15 reports the electrolyte components schemes.

At first, physical properties of the electrolytes were evaluated: viscosity, ionic conductivity, density and flash point. Then, an electrochemical study was performed in order to evaluate the overall voltage stability windows of the electrolytes. Even if the highest voltage window was obtained for the extremely concentrated co-solution, this did not turn into the highest energy density among the different concentrated electrolytes, since capacitance value was definitely lower if compared to the 25 wt% or 50 wt% IL.

3.5.1 EXPERIMENTAL SECTION

PREPARATION OF THE ELECTROLYTES AND CHARACTERIZATION

Three concentrations of Propylene carbonate (PC) and N-butyl-N-methyl-pyrrolidinium 4,5-dicyano-2-(trifluoromethyl) imidazole (Pyr_{14}TDI) were studied, namely 25% (IL-25), 50% (IL-50) and 75% (IL-75) IL by weight. Co-solutions were prepared in a Ar-filled glovebox having oxygen and water content lower than 0.1 ppm. The viscosities of the electrolytes were determined by means of an Anton-Paar Physica MCR301 rheometer using the cone-plate geometry, while the densities were estimated with an Anton-Paar density meter (DMA 4100M) using the ASTM D6450 standard. Viscosities and densities were investigated in the range between 20 °C and 60 °C. these measurements were conducted inside a dry-room with dew point lower than -70 °C.

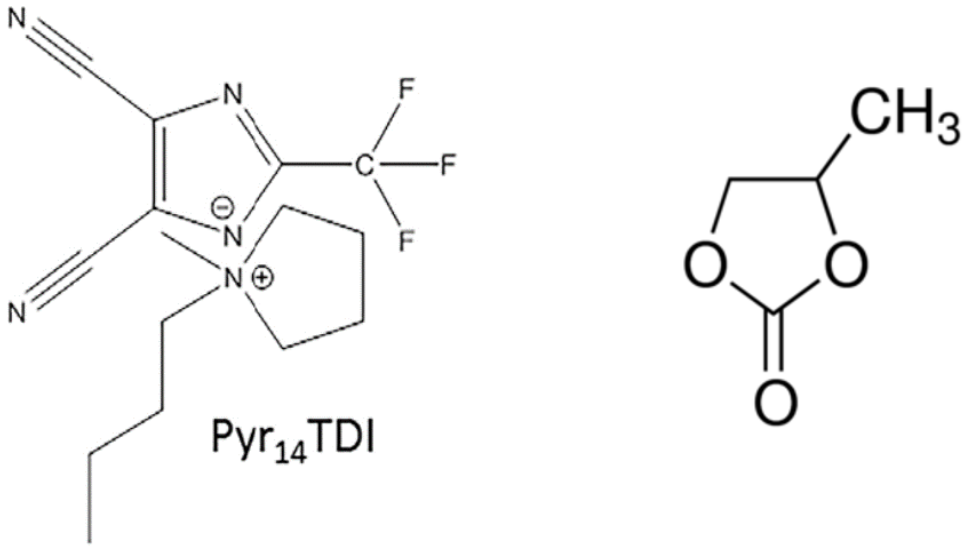

Figure 15: Schemes of the $Pyr_{14}TDI$ and Propylene carbonate.

Ionic conductivities were measured using an automated conductimeter equipped with the frequency analyzer and thermostatic chamber (Biologic). Before conductivity measurements were performed, the cell constants were determined using the 0.01M KCl standard solution. The measurements were conducted in the temperature range from -30°C to 60°C with a step of 2°C and an equilibration time at each temperature of 1 h.

ELECTROCHEMICAL TESTS

Electrodes composition was the following: 85 wt% activated carbon (DLC Super30, Norit), 10 wt% conductive additive (Super C45, Imerys Graphite and Carbon, Switzerland) and 5 wt% binder (Sodium carboxymethyl cellulose (CMC), Walocell CRT GA07, Dow Wolff Chemicals).

The use of CMC as binder permitted to work with an aqueous slurry which was coated onto an aluminium current collector. Once cut in 1.13 cm^2 discs, electrodes were dried for 12 h under the following conditions: 10^{-3} mbar, 180 °C. For the electrochemical characterization Swagelok type cells were employed, at first in 3-electrodes configuration to evaluate anodic and cathodic limits and subsequently after balancing the electrodes weights in 2-electrodes configuration.

In the 3-electrodes configuration the counter electrode was obtained with the following composition: 80 wt% activated carbon, 10 wt% conductive carbon and

10 wt% PTFE as binder. It was fabricated having a much larger mass with respect to the working electrode. As reference electrode was used an Ag wire.

In both 2- and 3-electrodes configurations a Whatman GF/ D (diameter: 12 mm, thickness: 675 mm) was employed as separator. 120 µL electrolyte solution was used for each cell.

Electrochemical measurements were performed with a VMP multichannel potentiostatic- galvanostatic system (Biologic Science instruments) at a temperature of 20 °C.

Constant current measurements were conducted in a current density range between 1 A g^{-1} and 10 A g^{-1}. Capacitance was evaluated through the discharge curve as reported in the paragraph *Galvanostatic charge discharge* of this chapter.

Energy and power densities were evaluated from discharge curves as reported in *Galvanostatic charge discharge* paragraph.

Floating measurements were carried out holding the EDLCs fabricated with IL-25 and IL-50 to 3 V and the EDLC employing IL-75 to 3.3 V. Every 20 h capacitance was measured by GCD discharge profile (1 A g^{-1}).

3.5.2 RESULTS AND DISCUSSION

Electrolytes properties are summarized in table 3. It was decided to use these three compositions in order to evaluate a wide concentration range, being IL-25 a very diluted solution and IL-75 an almost solvent-in-salt electrolyte.

Table 3: Composition and properties of the investigated electrolyte solutions (20 °C). Adapted with permission. Copyright 2018, Wiley.

Co-solution	IL/ PC w/w	Density (g cm^{-3})	Viscosity (mPa s)	Conductivity (mS cm^{-1})	Flash point (°C)
IL-25	1:3	1.195	3.4	8.7	127
IL-50	1:1	1.184	9.2	9.8	135
IL-75	3:1	1.175	32.1	6.0	153

Figure 16A shows ionic conductivity measurements in a temperature range between -30 °C and 60 °C for the three different electrolyte concentrations.

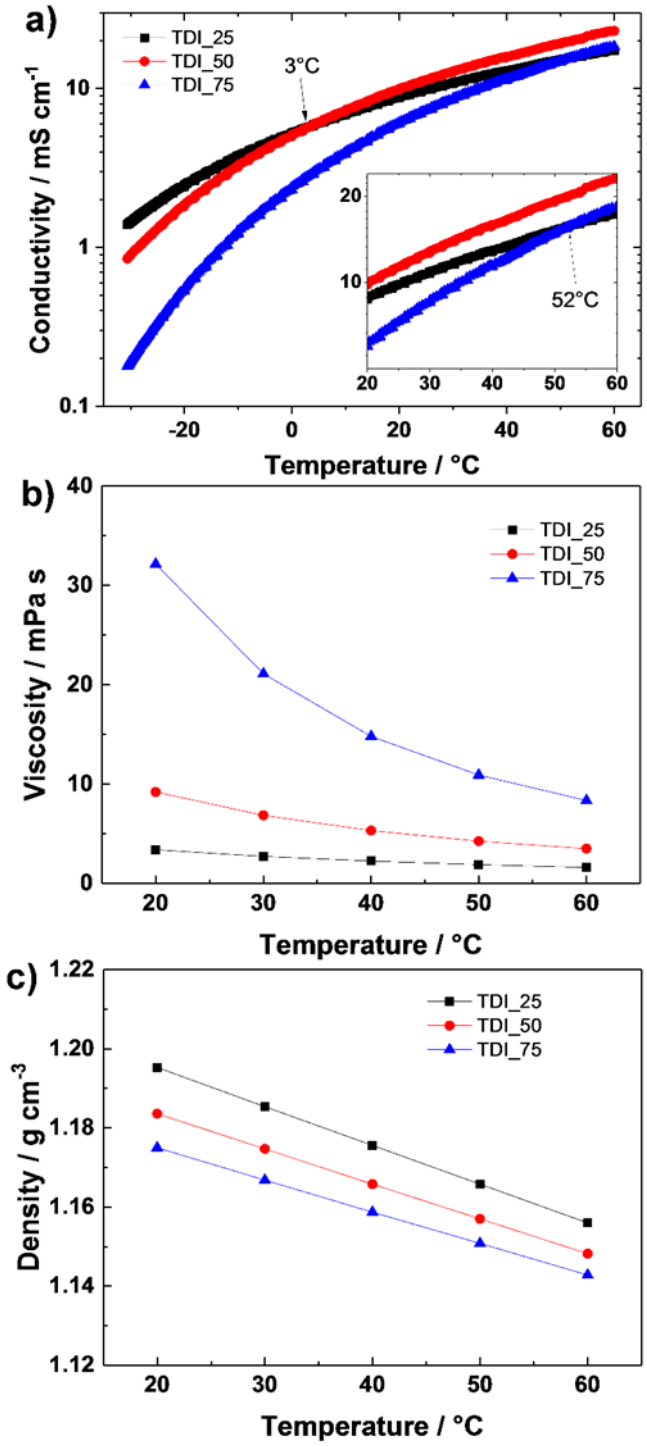

Figure 16: (a) Ionic conductivity, (b) viscosity and (c) density of the Pyr_{14}TDI-PC co-solutions. Reprinted with permission. Copyright 2018, Wiley.

For low temperatures, the highest ionic conductivity was found for the most diluted concentration (IL-25). It was due to the lower viscosity (3.4 mPa s) with respect to IL-50 (9.2 mPa s) and IL-75 (32.1 mPa s). At 3 °C IL-50 conductivity exceeded that of IL-25 due to the higher number of carriers present in the solution. In fact, at ambient temperature the highest ionic conductivity was possessed by IL-50 (9.8 mS cm^{-1}). It appears a good value also in comparison to PC-based conventional electrolytes.

Above ambient temperature IL-50 conductivity increased due to diminished viscosity and enhanced carrier mobility, as can clearly observed in Figure 16B. Another crossing point was found at 52°C (inset in Figure 16B), when IL-75 conductivity exceeded IL-25 conductivity.

In Figure 16C are reported densities of the investigated solutions as a function of the temperature. The range in between 20 °C and 60 °C was investigated. Results showed an unconventional behaviour. In fact, despite the expected decrement while increasing the temperature, density diminished for higher solute concentrations. This behaviour suggests repulsive interactions between the electrolyte components. Flash point measurements were conducted in order to evaluate safety features of such electrolytes. The highest flash point was found for the most concentrated co-solution (153 °C) according to Kühnel et al.[41]

Electrochemical measurements were first conducted in 3-electrodes setups, in order to define the maximum operative voltage EDLCs employing Pyr_{14}TDI-PC co-solutions could withstand. Anodic and cathodic CVs are shown in Figure 17. They were performed in order to determine positive and negative potential limits. In fact, for every increment of the voltage window, coulombic efficiency was evaluated. Results are reported in Figure 18A (threshold was set to 99%). As expected, the most concentrated solution (IL-75) was the one which could tolerate the larger voltage window (3.3V). As average, specific capacitance was almost 100 F g^{-1} (Figure 18B). These results are fully in agreement with previously reported EDLCs works employing the same activated carbon and PC-Il co-solutions as electrolytes.[33]–[35], [42]

In the negative domain the profiles of the CVs are not entirely box-shaped. This behaviour has been also observed in literature for ionic liquids presenting the same cation (Pyr_{14}^{+})[34] or Azp_{14}^{+}[37], [43] even if it was less evident. The extremely slow scan rate (if compared to similar works) emphasized a broad peak at -0.7 V vs Ag, probably due to organic groups (quinones), present on the active material surface, which give faradic reactions.[44]

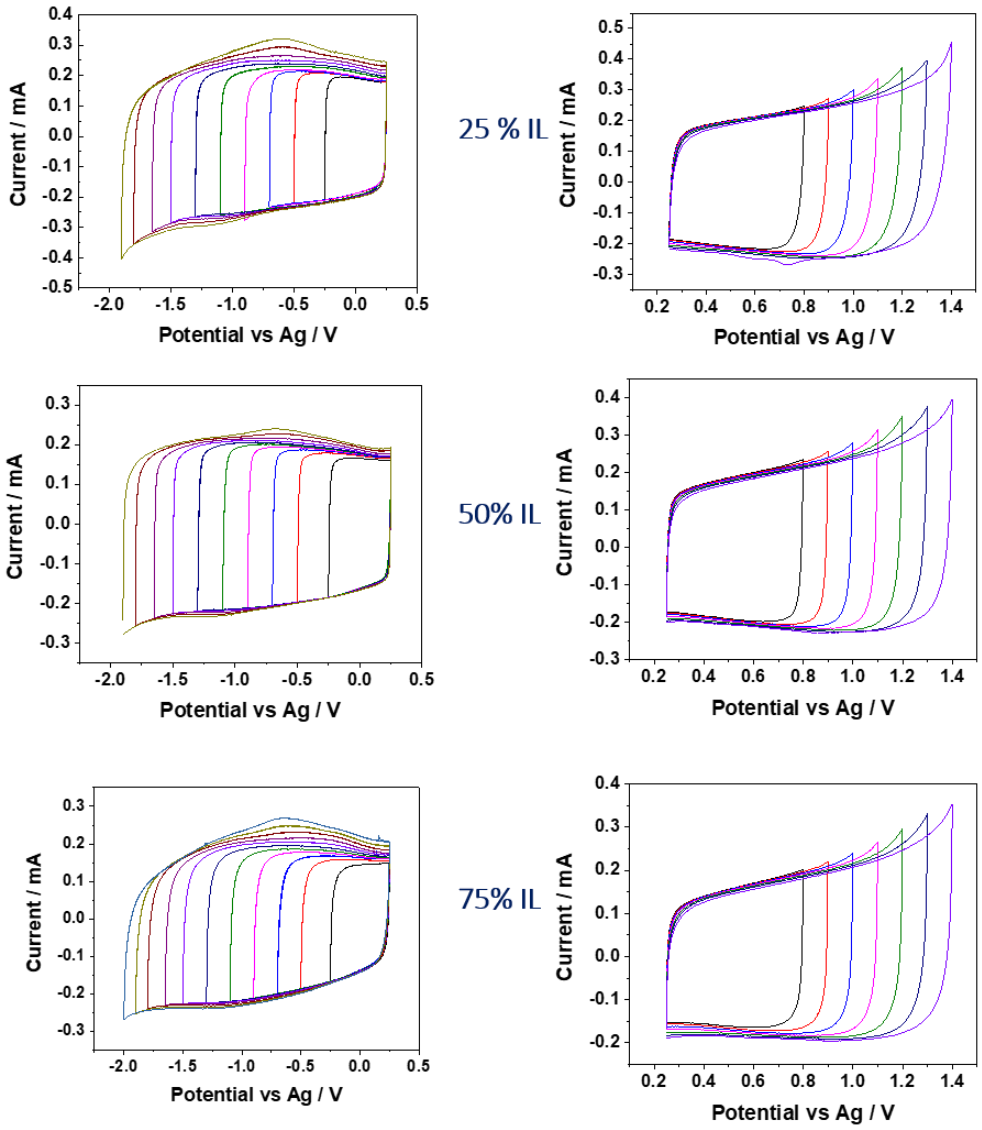

Figure 17: Anodic and cathodic CV measurements for the Pyr_{14}TDI-PC co-solutions performed in a 3-electrodes setup. Reprinted with permission. Copyright 2018, Wiley.

Electrodes masses were adjusted according to the following equation:

$$m_+C_+V_+ = m_-C_-V_-$$

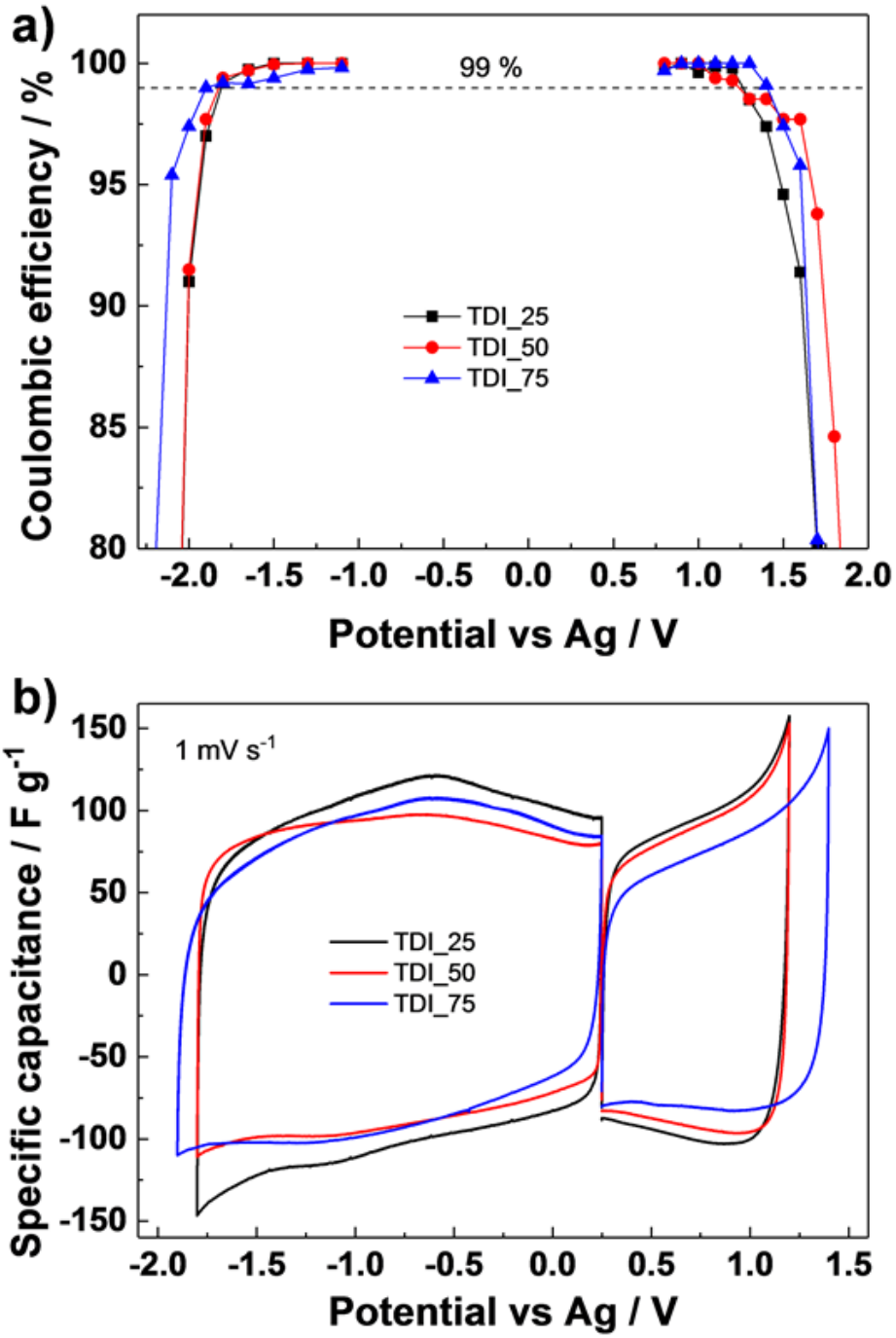

Figure 18: Stability window of the various $Pyr_{14}TDI$-PC mixtures determined by CV in 3-electrode setups. (a) Coulombic efficiency as function of the anodic and cathodic cut-off potentials (b) CV profiles obtained at 1 mV s^{-1} using the maximum voltage (ensuring efficiencies higher than 99%). Reprinted with permission. Copyright 2018, Wiley.

In which *m* is the electrode mass, *C* is the capacitance evaluated through cyclic voltammetry and *V* is the maximum anodic or cathodic voltage with respect to the open circuit voltage. + and – stand for anode and cathode. The same ratios were found between positive and negative electrodes masses for IL-25 and IL-50 (2), while a slightly higher value was found for IL-75.

Figure 19A shows the CVs carried out at 10 mV s^{-1} for the balanced EDLCs. Potentiodymanic measurement led to the typical rectangular shape demonstrating appreciable double layer features. Even for voltages close to the stability limit, evident current increment was not experienced, thus proving that EDLCs cycled in the proper voltage windows. A progressive capacitance decrease was found increasing the IL content. In particular, even if IL-75 voltage window was higher with respect to the other two tested concentrations its capacitance was evidently lower than IL-25 and IL-50 capacitances.

IL-25 had the highest capacitance among the investigated co-solutions. Even slight higher than IL-50, which conversely possessed the highest ionic conductivity. This result demonstrates that factors other than conductivity have an important role in EDLCs capacitance, as electrodes wettability and pores accessibility.

Figure 19B reports EDLCs specific capacitances evaluated through CVs in the range 10 mV s^{-1} - 200 mV s^{-1}.

Afterwards, EDLCs were subjected to a protocol composed of 5 GCD steps with currents ranging from 1 A g^{-1} to 10 A g^{-1}, each one comprising 1,000 GCD cycles. In the last step current was set again to 1 A g^{-1} in order to check if capacitance recovery was successfully experienced. Results are shown in Figure 20A. The figure provides also coulombic efficiencies of the GCD cycles. As for CV measurements, IL-25 demonstrated the best performance.

Specific capacitances are in agreement with published works employing the same activated carbon material.[34], [42] In particular, IL-25 results are comparable with PC-based IL co-solutions employing $Pyr_{14}BF_4$ and $Pyr_{14}TFSI$.

After this initial protocol, EDLCs were subjected to long-term cycling measurements at an imposed constant current of 2 A g^{-1}. Figure 20B shows the capacitance retention for 50 000 cycles. IL-25 demonstrated the best capacitance retention and is consistent with other IL published works.[34] In Figure 20C EDLCs specific energy and power are reported in the Ragone plot. Although, IL-75 possessed the highest voltage window, this did not turn into the highest energy density due to the much lower capacitance value. Instead IL-25 showed the best performance for all the currents applied.

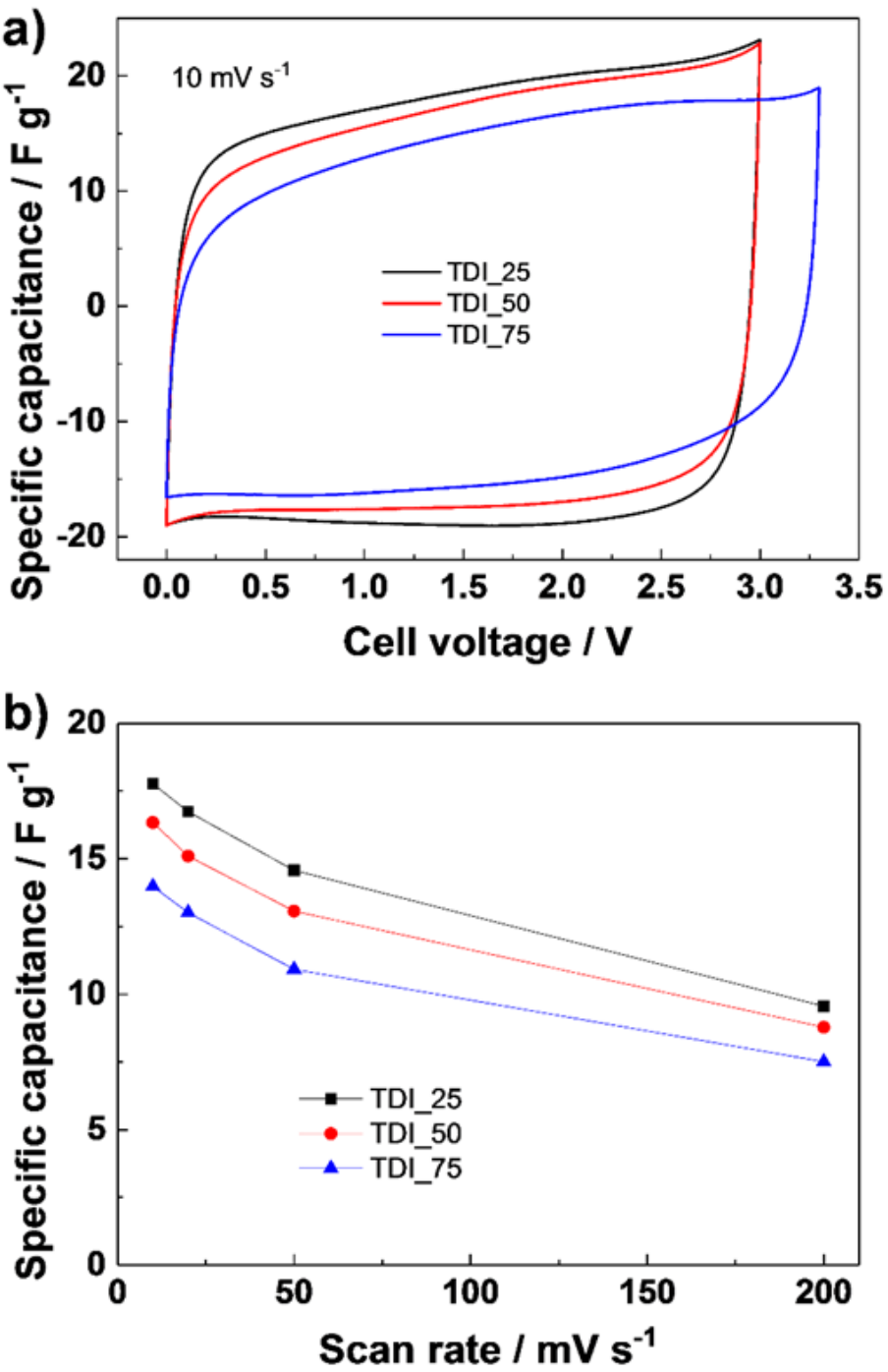

Figure 19 : (a) CV measurements for the three IL-PC co-solutions in a 2-electrodes configuration (b) specific capacitance reported as a function of the scan rate. Reprinted with permission. Copyright 2018, Wiley.

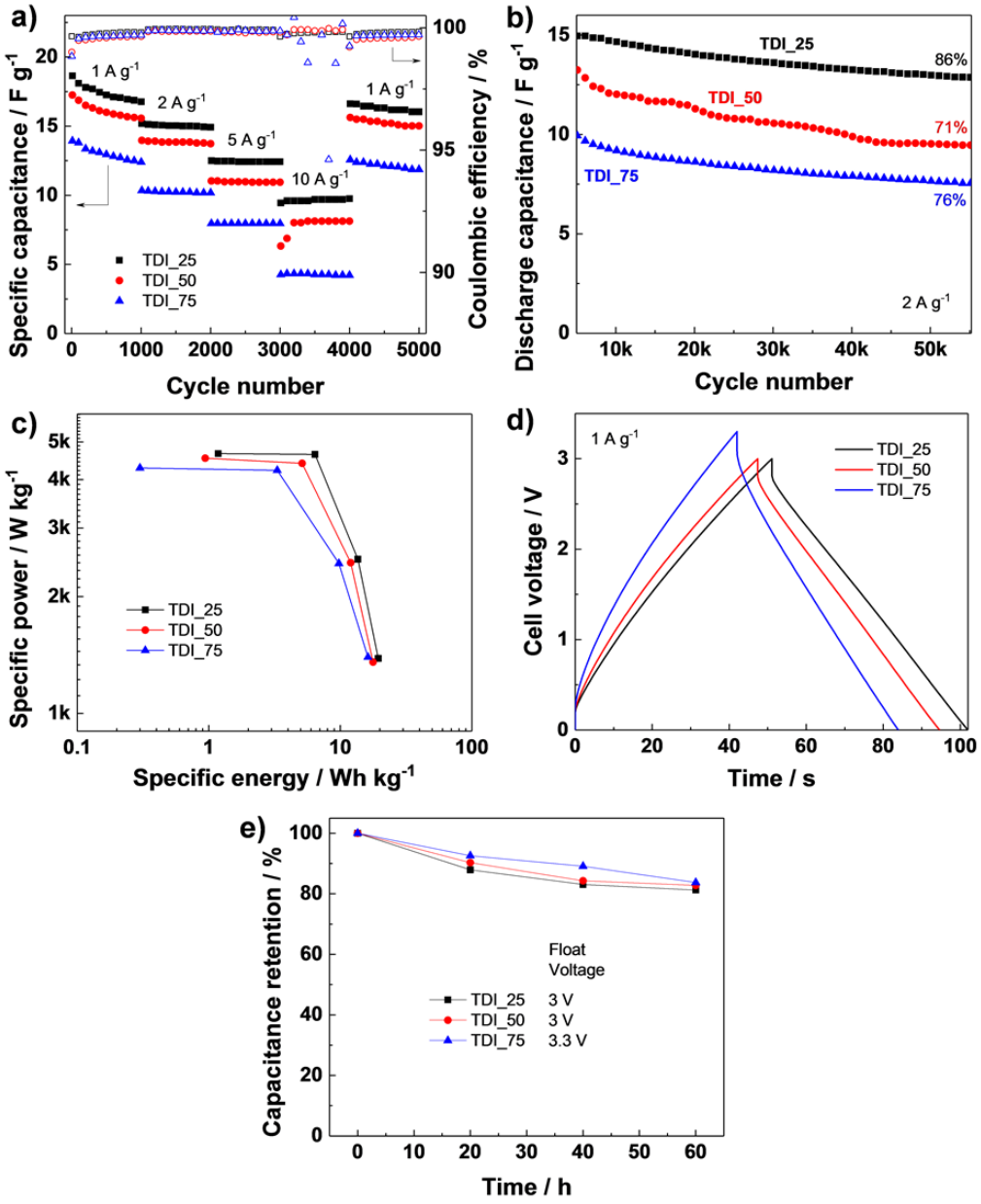

Figure 20: Electrochemical performance of balanced EDLCs employing the various $Pyr_{14}TDI$- PC co-solutions. (a) Specific capacitance and coulombic efficiency upon GCD cycling performed with an increasing imposed current (1, 2, 5, 10 and 1 A g^{-1}). (b) Cycling stability over 50,000 cycles performed at 2 A g^{-1}. (c) Ragone plot for the three tested co-solutions. (d) GCD curves recorded at 1 A g^{-1} (e) Float tests. Reprinted with permission. Copyright 2018, Wiley.

Overall, IL-75 reduced performance has to be examined considering the large internal resistance of the cell, which is a consequence of the high viscosity. This is evident from the higher voltage drop of IL-75 1 A g^{-1} GCD measurement proposed in Figure 20D and also from the less defined triangular shape if compared to IL-25 and IL-50.

Figure 20E shows float voltage tests outcomes. IL-75 co-solution demonstrated the best retention performance. In this perspective, this particular co-solution appears promising for high temperature applications, as testified by ionic conductivity measurements in the range between -30 and 60 ° However, positively, at the end of the floating test the capacitance retention of all the tested co-solutions resulted capped to almost 85% of the initial values.

4. INTEGRATED ENERGY HARVESTING-STORAGE DEVICES

4.1 THE SIGNIFICANCE OF INTEGRATED ENERGY HARVESTING-STORAGE TECHNOLOGY

The most critical issue regarding renewable power generation is related to the uncertainty of the renewable source availability. The likely lack of perfect synchronism between electrical energy production and power utilization could render renewable energy plants less appealing with respect to thermoelectric power plants. In addition, power plants which work continuously and give a fixed output are easy to implement in a power grid. Conversely, the implementation of a big photovoltaic or wind power plant can cause severe fluctuation in the electrical energy that the power grid has to manage. In order, to exploit the enormous potentiality of the solar radiation and use the photo-generated power even when the electromagnetic radiation is unavailable an energy storage system is required. In this perspective, in a future in which hopefully fossil fuels will be less and less employed, self-sustainable housing or buildings will have to dedicate a certain volume to an energy storage section. In this way, even during the night time or during a cloudy day all the utilities could be powered if the storage system was properly designed.

For the off-grid conditions the energy industry has produced a series of portable rechargeable batteries capable to easily recharge common electronic devices. However, the charge that can be stored in these items is limited and they are not usually provided of an energy harvester yet. For this reason, intense research activity and manufacturing tests of new integrated systems appear to be the possible prelude of new industrial products spread in the market.

During the last years the number of scientific publications dedicated to combined energy harvesting and storage devices/installations radically increased. This growth testifies a mutual behaviour implemented by the research community in order to actively promote this fascinating energy sector. In particular, the increment in the publications dedicated to photovoltaic (PV) harvester-based self-sustainable systems testifies how PV technology can be easily implemented with a storage section. Figure 21 was obtained typing the words “photovoltaic” and “capacitor” in the Scopus scientific database. The word “capacitor” was chosen in

order to highlight the works strictly related to the topic of this PhD thesis and avoid to extend the research to different type of energy storage. The research was performed with the guidelines to search the combination of these words in the title, abstract or in the keywords. In less than ten years the number of publications per year with these characteristics has gone from few tens to over three hundred. Thus, once more testifying an increasing interest in this type of self-sustainable energy harvesting and storage (HS) systems.

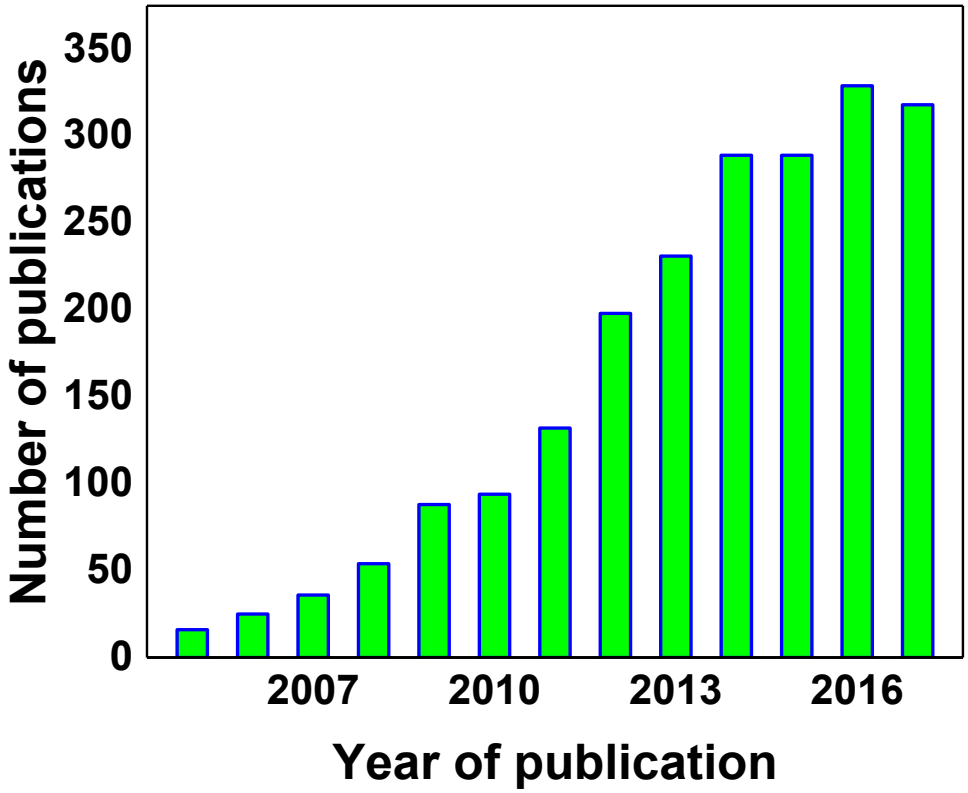

Figure 21: Number of scientific publications per year in the field of PV-based integrated energy conversion and storage systems. The research was conducted (25/7/2018) typing the words photovoltaic and capacitor in the Scopus scientific database.

4.2 WHY DYE SENSITIZED SOLAR CELL AND ELECTRICAL DOUBLE LAYER CAPACITOR FOR INTEGRATED DEVICES?

As previously discussed in chapter 2, among the different photovoltaic technologies, Dye sensitized solar cells (DSSCs) appear a highly appreciable compromise regarding cost, production easiness, efficiency and improved performance under real environment conditions or cloudy circumstances. These qualities render DSSCs one of the most interesting solution for implementation in HS integrated devices.

Certainly, a potential industrial scale-up of HS devices needs an as much as possible decrement in production cost, since it would lead to a more accessible cost of sale for customers. HS devices in fact could have a huge impact on the energy market, since nowadays it seems surely a useful item in order to recharge portable electronic devices or smartphones. In this perspective, an accessible price could represent an appealing incentive for a fast dissemination in the technological energy scenery.

Since a HS device is composed of two sections, it is intrinsically more difficult fabricating it with respect to a single component device. Thus, lowering as much as possible the difficulty of fabricating the two parts, results of preeminent importance. From this point of view, DSSCs represent one of the easiest technology to be manufactured in the panorama of PV cells. In addition, the DSSC structure is similar to the structure of an energy storage electrochemical cell (two electrodes and an electrolyte). For this reason, integration between harvester and storage cells can be performed in different configurations. In particular, in literature two, three or four electrodes HS devices arrangements were proposed. This is due to the possibility to share a common electrode or even physically separate the two sections and obtain a "two electrodes" HS device. This last structure is not effectively recognizable as a two-electrodes layout but more like a differentiated-electrolyte sandwiched between two layers where the electrodes are located. The four-electrodes configuration is the simplest to be implemented but it needs electrical connections between the electrodes of the solar cell and the electrodes of the storage device. In this case the integration is physically obtained and the fabrication of the two devices is easier to perform, since it occurs separately. However, a proper integration has to be carefully thought in order to have a compact device to be easily and smartly used in everyday life.

For DSSCs, efficiency has always been considered a drawback from the scientific community. In comparison to crystalline silicon solar cells technology,

the electrical output per unit of surface area is effectively lower. In the last years also Perovskite solar cells produced diffuse consideration in the PV research field due to an outstanding and fast growth of their electrical output efficiency. Recently, they were considered for integrated HS devices, leading to an overall photon to electrical conversion and storage efficiency (OPECSE, relate to chapter 4) which is much higher compared to DSSCs-based HS devices present in literature. However, it must be stated, that an increase over time was experienced in the DSSCs efficiency and that being the theoretical efficiency not reached yet, research can further improve DSSCs record efficiency.

An even more important appealing feature is given by the increment in DSSCs performances lowering the incoming electromagnetic radiation intensity: characteristic profusely testified by literature reports. This is mainly due to a lower recombination process occurring (in percentage) when the conduction band of titanium oxide semiconductor is less populated of electrons.

Regarding the energy storage section of HS devices, the two categories that have gathered more interest are obviously represented by batteries and Supercapacitors (SCs).

Even if batteries represent a more mature, widely utilized technology and possess a much higher energy density with respect to SCs, the majority of scientific integration reports deals with SCs and in particular with Electrical double layer capacitors (EDLCs). This is due to a series of reasons which make particularly appealing and extremely reliable using EDLCs in an integrated self-sustainable powerpack.

SCs generally, but more specifically EDLCs withstand an extraordinary long cycle life of approximately 1 000 000 cycles.[22], [24] Evidences of this outstanding reliability over cycling are testified by literature but also by commercial devices. From this point of view, batteries evidently suffer performance degradation due to electrodes/electrolyte interfaces instability, chemical degradation or structural changes of the electrode and parasitic decomposition processes of the electrolyte which reduces the number of operational cycles before obtaining a substantial decrease in capacity.

This feature assumes a predominant significance, since the number of expected HS charge-discharge cycles could be of several tens or even hundreds in a single day. Assuming this intense activity, a HS device storage section like a battery would lead to only one month of uninterrupted operation or less. With the same daily number of cycles an HS device with an EDLC as energy storage section would last 27 years. In this case, before the EDLC undergoes performance degradation the

DSSC section would stop its harvester function and presumably even a Silicon-based PV harvester section would go out of operation.

The second reason which yields EDLCs being suited for integration with a PV harvester is given by the much higher power density they can sustain with respect to usual batteries. Since a PV cell or module produces a variable current output depending on the radiation intensity, the incoming power into the storage section is not fixed and is a function of environmental conditions and consequently of time. Because of this reason, EDLCs are certainly more appropriate for working under these circumstances. They possess in fact a versatility that let them accept power under different rate conditions with a marginal difference in the energy stored. The absence of redox reactions and the relatively fast storage mechanism through ions adsorption in the electrodes pores plays a key role in this aspect.

Another important feature which renders EDLCs employable in integration with a PV harvester is given by the less technical specifications required with respect to batteries in terms of voltage. In fact, batteries require to be charged to a specific voltage in order to let the electrochemical reactions occur. On the other hand, EDLCs do not need a specific voltage to store energy since the adsorption and desorption of cations and anions at the electrodes surfaces do not require a specific voltage value to occur. The typical EDLC Galvanostatic charge discharge (GCD) triangular shape testifies that for a fixed current the charging behaviour is unvarying.

The last advantage in using EDLCs instead of batteries in HS integrated devices is given by the fact that they are intrinsically safer. As aforementioned, no redox reactions involving the formation of dangerous compounds take place in EDLCs. For example, the growth of Li metal dendrites or O_2 evolution might occur while over-charging a lithium ion battery.[45]

Care must be taken when designing a HS PV-based device, since the uninterrupted exposure of the solar section to the sunlight increases irremediably its temperature and the proximity to the storage media might trigger hazardous side-reactions.

4.3 HS DEVICES SIGNIFICANT PARAMETERS

Since HS devices are obtained by combining two different energy units, both sections need to be optimized in order to get the best overall performance. In this paragraph, the most important PV-based HS devices parameters will be presented and discussed.

4.3.1 OVERALL PHOTON-TO-ELECTRON CONVERSION AND STORAGE EFFICIENCY (OPECSE)

The most critical and problematic to evaluate parameter, regarding HS devices, is certainly the efficiency. For PV cells and EDLCs, evaluating the efficiency is quite immediate since in literature a common behaviour was established by research community. In addition, for both the energy items involved, as for all the devices which transform an energy vector into another one appear easy to define an efficiency. For a PV cell it is represented by the ratio between the electrical power produced (voltage and current product) and the electromagnetic power incoming onto the solar cell. Regarding EDLCs, coulombic efficiency, defined as the ratio between discharging and charging capacity or energy efficiency, similarly defined as the ratio between discharging and charging energy, are quite immediate concepts.

Accordingly, the efficiency of a PV-based integrated device should be calculated as the ratio between the energy re-obtained during EDLC discharge phase (or stored into the EDLC) and the electromagnetic energy which impinged onto the solar cell while exposed to the solar radiation. However, discharge capacity and energy are functions of the applied current. Thus, a first random variable arises, which makes difficult a comparison between two devices discharged with a different galvanostatic current.

A second random variable is referred to the photo-charging time. In fact, the incoming energy vector is directly proportional to radiation power density, PV active surface and time. However, conversely, the output gain is hindered by the voltage window of the EDLC or to the open circuit voltage of the solar cell, since the energy stored in the EDLC is proportional to the square of the voltage. In fact, in first approximation, as reported in the previous chapter the following formula can be used for EDLCs showing a fairly linear discharge:

$$E = \frac{1}{2} C V^2$$

When connecting a PV harvester under illumination and an EDLC, in the first part of the photo-charge the voltage of the EDLC rapidly increases. Then the voltage increases more slowly till a voltage plateau is attained. This plateau is related to the PV Voc (maximum voltage achievable during photo-charge). For better understanding this mechanism relates to the following paragraphs.

Even if a voltage plateau within the EDLC voltage window limits could be useful in order to allow ions to arrange themselves into the porous structure, during this plateau the incoming electromagnetic energy coming from the sun is wasted since it does not lead to an EDLC voltage increase.

To date, in literature reports, the most widespread method to calculate the overall HS efficiency was through the following equation:

$$OPECSE = \frac{\frac{1}{2} C V^2}{G t S}$$

Where *OPECSE* stands for overall photon-to-electron conversion and storage efficiency, *C* is the capacitance of the EDLC section, *V* is the maximum voltage achieved during photo-charge, *G* is the electromagnetic power density impinging onto the PV solar cell or module, *t* is the photo-charging time and *S* is the PV harvester surface.

As previously reported, HS devices who do not show linear discharge could not use this formula. However, since this equation caught on in literature, all new works are somewhat addicted to it. Nevertheless, standardising capacitance evaluation would be a first step in order to get consistency among literature HS devices (using a fixed current density while discharging the EDLC). In the majority of the works dealing with photo-capacitors, capacitance is evaluated through GCD or CV.

By the way, as clearly exposed in Xu et al.,[46] photo-charge is a *dynamic process* because the *charging current of the capacitor is not constant*. During this dynamic process, if a series of OPECSE values are calculated at short constant time intervals and then are reported in a graph as a function of time, the values form a profile that reaches its maximum in a relatively short time period and then decreases exponentially when a voltage plateau is attained (see figures 40A, 49A, 55A). In this perspective, from an energy saving point of view, charge should be stopped when EDLC approaches the voltage plateau (close to the open circuit voltage of the PV harvester). However, in this case the discharge capacity and capacitance decrease with respect to a PV-EDLC system that is kept under continuous solar radiation for a somewhat long period.

A common belief is that for a fixed discharge current density, the capacitance calculated from discharge subsequent to photo-charge is lower with respect to capacitance evaluated through GCD cycles. However, this is not always true.

To this purpose, here follows a case in which the exact opposite happened: Skunik-Nuckowska and co-workers, using the same discharge current (0.1 A g^{-1}), found a higher capacitance after photo-charge (407 F g^{-1}) with respect to GCD measurements (370 F g^{-1}).[47] This, once more confirms that the charging history is crucial in defining discharge properties and as a consequence OPCSE parameter. Hence, when comparing OPECSE of two HS devices, charging profiles and discharge currents have to be nearly the same, otherwise misleading considerations could be done.

My approach in evaluating OPECSE (capacitance) followed literature reports published before 2017, in order to make possible a comparison with previous related works. Thus, capacitance was mainly calculated from GCD or CV measurements. However, in most of the cases discharge capacitance subsequent to photo-charge was linear and capacitance calculated from the slope of the discharge subsequent to photo-charge was nearly the same of the capacitance evaluated referring only to the EDLC (GCD or CV).

4.3.2 STORAGE EFFICIENCY

Overall efficiency (OPECSE) as so far reported in literature can be expressed as follows:

$$OPECSE = \eta_{PV}\,\eta_{STORAGE}$$

Where PV efficiency is the maximum photovoltaic efficiency calculated through the IV curve of the harvester section (product between current and voltage in the maximum power point). PV efficiency here assumes the highest value OPECSE ideally can reach and storage efficiency represents how close the HS device is from the ideal case in which all the produced power is stored in the EDLC without losses. As an average among all the HS devices literature reports which claim a storage efficiency value, this parameter is close to 70%. The highest the value, the best the integration between harvester and storage units.

4.3.3 DISCHARGE CAPACITY DENSITY

Another important parameter which is usually not considered when comparing two or more HS devices is the discharge capacity density the EDLC or pseudo-capacitor can deliver while discharging. Many works claiming for outstanding OPECSE showed really poor discharge capacity density. These HS devices are certainly appealing from an energetic point of view, but represent no technological advancement for HS devices practical use in nowadays life.

At the end of the following paragraph, which deals with PV-based HS devices state of the art, table 4 which compares photo-capacitors produced to date, is provided. In table 4, photo-capacitors peculiar parameters (if stated in the manuscript) are reported.

4.4 INTEGRATED HARVESTING-STORAGE DEVICES STATE OF THE ART

The first report regarding photo-rechargeable capacitor (photo-capacitor) was proposed by Miyasaka et al.[48] In this work, a 2 electrodes device was obtained. The characteristic photo-anode of a DSSC was directly in contact with an activated carbon (AC) EDLC electrode and a separator filled with an electrolyte solution containing 15% $(CH_3CH_2)_4NBF_4$ in propylene carbonate separated the two AC electrodes. This configuration led to a maximum photo-voltage of almost 0.45V.

Considering the low voltage output, a considerably high discharge capacity of 75 mC cm^{-2} after photo-charge was obtained.

An advancement of this layout was obtained by Murakami et al.,[49] that in the usual 3-electrodes photo-capacitors configuration with two different electrolytes for the harvesting and storage sections, reached a voltage during photo-charge of 0.82 V. The EDLC electrodes and electrolyte were fabricated with the same materials as in the previous 2-electrodes system, but in this case an outstanding discharge capacity of 470 mC cm^{-2} and a discharge capacitance of 0.65 F cm^{-2} were measured, testifying that this 3-electrodes configuration is intrinsically more stable than the one previously proposed. This discharge capacity value remains to date, to the best of my knowledge a record regarding DSSC-EDLC HS devices.

The first example, to the best of my knowledge, in which pseudo-capacitive materials were employed in the fabrication of the storage SC section, was proposed by Hsu and co-workers.[50] The harvester section was as usual for the first fabricated HS devices prototypes a DSSC, while the SC section was realized with PProDOT-Et_2 electrodes. The maximum voltage during photo-charge was 0.75 V and the discharge capacity was measured to be 260 mC cm^{-2}. This was the first report in which calculation regarding overall efficiency of the integrated device was implemented in the manuscript discussion. This first pseudo-capacitor-based integrated device reported an OPECSE of 0.6 %.

Skunik-Nuckowska et al.,[47] obtained a solid-state photo-capacitor, which is to date the only example present in literature regarding the integration of a dye-sensitized solar cell and a ruthenium oxide based electrochemical capacitor (in Figure 22A is reported the photo-capacitor scheme). The supercapacitor electrodes were separated by Nafion membrane which served as proton-conductive solid electrolyte. The DSSC electrolyte employed was instead a hole-conducting polymer, namely poly-(3-hexylthiophene-2,5-diyl) (P3HT). The system was also tested under different illumination conditions. In Figure 22B are reported photo-charge curves for 1, 0.5 and 0.1 Sun illumination conditions. It was the first time

that this analysis was carried out for a photo-capacitor. However, differently from DSSC typical behaviour, the OPECSE decreased lowering sunlight radiation. The discharge capacity in this case was 1440 mC cm^{-2}. This value was three times higher the discharge capacity obtained by Murakami and co-workers.[49] However, this was largely expected, because of the much higher capacity provided by Ruthenium oxide electrodes with respect to AC. The OPECSE value was calculated to be 0.8%.

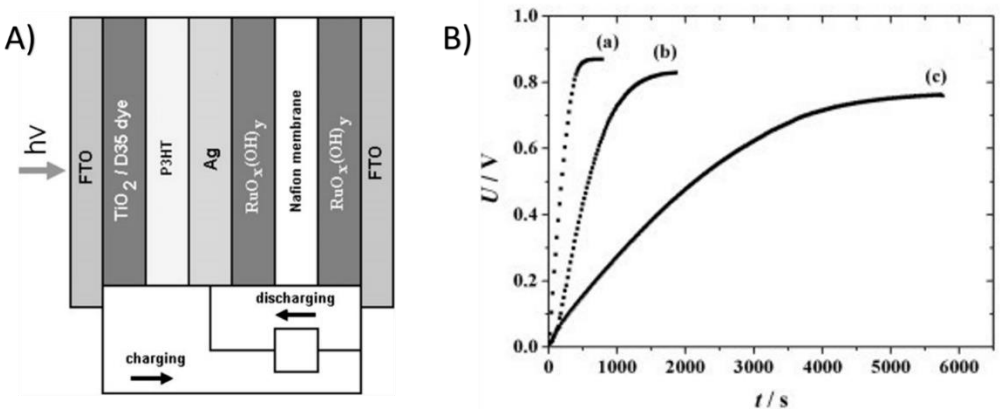

Figure 22: (A) Scheme of the 3-electrodes HS device proposed by Skunik-Nuckowska and co-workers and (B) photo-charge profiles with illumination intensity set at 1 Sun (a), 0.5 Sun (b) and 0.1 Sun (c). Adapted with permission from reference [47]**. Copyright (2013) Elsevier**

The highest OPECSE ever attained to date for DSSC-EDLC HS devices was reported by Yang et al.,[51] who achieved an overall efficiency of 5.12%. This work was published almost simultaneously with respect to the one proposed by Skunik-Nuckowska et al.[47] Thus, they both represent the first reported all solid state HS device. Yang and co-workers used a gel electrolyte for the DSSC section and a PVA-H_3PO_4 for the EDLC. The storage was fabricated employing multi walled carbon nanotubes (MWCNTs) as electrodes active material. In this work also a Pseudocapacitor-based HS device was proposed both in planar and flexible configuration. In these cases, the electrodes were composed by a MWCNT-PANI composite films. The use of a pseudo-capacitive material brought to a higher discharge capacity (201.6 mC cm^{-2}) subsequent to photo-charge if compared to the MWCNT-based EDLC photo-capacitor (49 mC cm^{-2}). The discharge capacity of the flexible configuration (191.8 mC cm^{-2}) was found to be nearly the same of the planar one, demonstrating feasibility of stable and reliable flexible integrated HS devices. Nevertheless, the efficiency of the flexible device (0.79%) was much lower in comparison to the planar MWCNT-PANI-based HS device (4.29%).

Chen et al.,[52] fabricated a HS device similar to Hsu and co-workers[50] but using a plastic substrate for the DSSC harvester. The SC active material employed was PEDOT (poly(3,4-ethylenedioxythiophene)), which brought to a remarkable discharge capacity of 300 mC cm^{-2}.

One of the most appealing reports regarding the integration of DSSCs and SCs is the work published by Cohn and co-workers (in Figure 23A and 23B are reported respectively scheme and band diagram of their proposed architecture).[53] In this work the integration was attained by means of a silicon wafer which was modified in such a way that one side was adapted to replace the catalyst activity of platinum in a DSSC, thus empowering triiodide reduction and the other side provided the charge-storage mechanism typical of an electrochemical SC. The processes which led to the fabrication of the silicon multifunctional electrode were mainly two: the first one was the etching of the two silicon wafer sides performed exposing them to an electrolyte containing a 3/8 volume ratio of fluoridric acid and ethanol in order to obtain porous silicon, while the second was a thermal carbon passivation made through chemical vapour deposition, exposing the surfaces to a precursor flow of acetylene, hydrogen and argon (1/40/100) at a temperature of 750°C. For this HS device the electrolyte was a poly(ethylene-oxide)/1-ethyl-3-methylimidazolium tetrafluoroborate (PEO-EMIBF4).

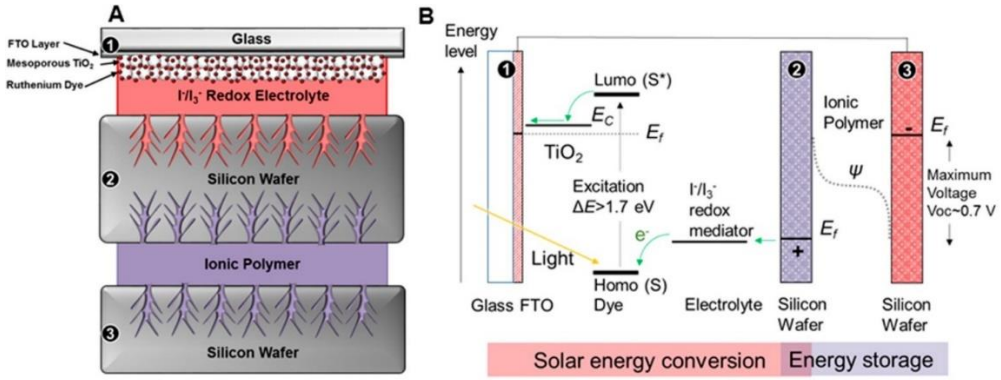

Figure 23: Scheme (A) and band diagram(B) of the Silicon-based HS device. Adapted with permission from Reference [53]**. Copyright (2015) American Chemical Society.**

The PV section efficiency was calculated to be 4.8%. The maximum overall photon-to-electrical conversion and storage efficiency (OPECSE) was 2.1% for a photo-charging time of 1.2 s. During this short time the voltage raised to almost the open circuit voltage of the DSSC, demonstrating to be able to quickly store the

majority of the storable charge. This is not a trivial feature since appears significant obtaining the best overall efficiency for a voltage which is as high as possible.

The principal drawbacks of this configuration were the storage efficiency (43.75%) and above all the discharge capacity after photo-charge which resulted in only 2.1 mC cm^{-2}.

An interesting solution which employed anodic titanium oxide (ATO) nanotubes both as the semiconductor of the DSSC and the active storage material of the SC was proposed by Xu et al.[54]

The storage active material (TiO_2 nanotubes) was treated through plasma-assisted hydrogenation. This treatment increased by a factor of 5 the areal capacitance of the SC, namely from 0.215 mF cm^{-2} to 1.1 mF cm^{-2}. Nevertheless, this value is extremely poor if compared to SC or EDLC literature and lead to the lowest discharge capacity subsequent to photo-charge attained in this research field.

DSSCs have been also successfully integrated with batteries in the last years. Among the others an article that deserves to be mentioned is the work published by Guo et al., [55] in which the authors proposed an innovative powerpack structure (see Figure 24) composed by a Dye sensitized solar module (DSSM) and a Lithium ion battery (LIB). The PV section was composed by 6 DSSCs connected in series and organized in 3 units. Every unit was composed by 2 solar cells, stacked one on top of the other, alternating TiO_2 nanorods (NRs) and TiO_2 nanotubes (NTs) and using different dyes in order to exploit a complementary part of the solar spectrum. The lithium ion battery was obtained with a $LiCoO_2$ cathode and a TiO_2 NTs anode.

The system was photo-charged with a 1.5 AM spectra 1 Sun radiation until almost 3V and subsequent discharge-charge cycles were performed, discharging the device to a minimum voltage of 700 mV. In Figure 25 are reported three consecutive cycles. The overall conversion efficiency was 0.82% and the storage efficiency attained a value of 41%. A negative current of 0.1 mA was applied during discharge phase, obtaining a discharge capacity of 122 mC. Unfortunately, parameters regarding DSSCs or LIB active surface are missing. Thus, a direct comparison with SC-based HS devices is not possible. This work provides evidences concerning the much more complicated approach in designing a suitable PV section in order to drive a LIB instead of a SC. In fact, during the discharge phase a plateau at almost 2V is clearly visible, demonstrating that in order to properly exploit the LIB a higher voltage has to be obtained during charging phase. Otherwise, the stored capacity would have been extremely poor.

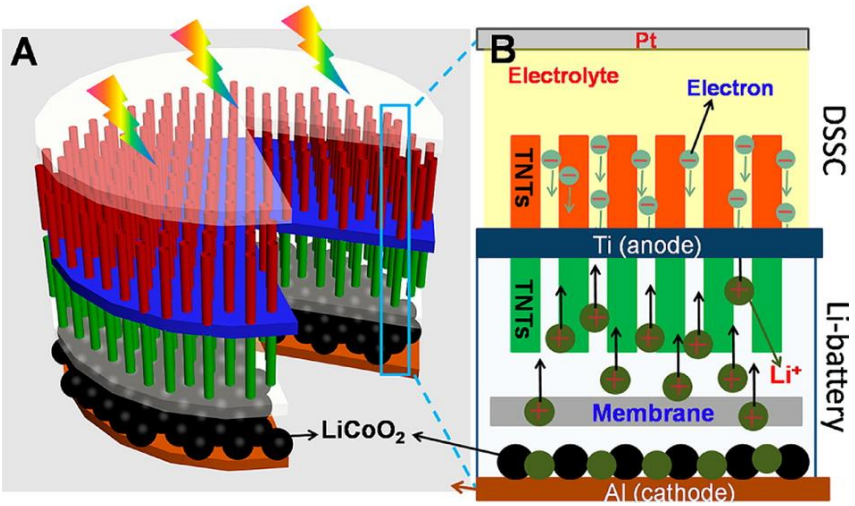

Figure 24: Layout(A) and mechanism(B) of the LIB-based integrated power pack. Reprinted with permission from reference [55]**. Copyright 2012, American Chemical Society**

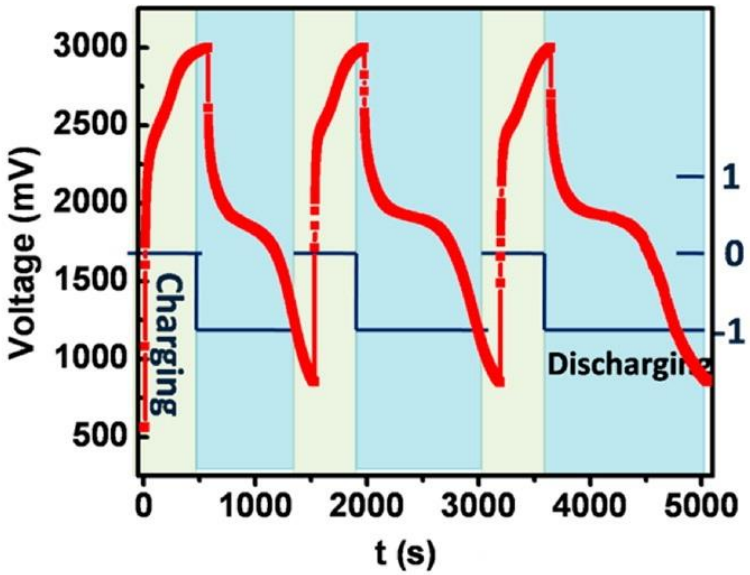

Figure 25: Consecutive photo-charge discharge profiles of the LIB-based power pack. Adapted with permission from Reference [55]**. Copyright (2012) American Chemical Society**

The Perovskite solar cells (PeSCs) fast increase in PV conversion efficiency over an extremely short time period produced in the renewable energy research sector the curiosity to test this new PV technology in charging an energy storage, at first externally.[56], [57]

Some integrated devices were proposed in the last two years, meaning that this research field is constantly evolving and profuse attention was given only recently.

The highest OPECSE among these works was attained by Kim and co-workers.[58] They integrated an organometal halide PeSC with a polyvinyl alcohol (PVA)/phosphoric acid (H_3PO_4)-based solid-state SC. To a PV conversion efficiency of 13.66% corresponded an OPECSE of 10.97%. The maximum photo-voltage obtained during photo-charge was also interesting for a PV harvester endowed of a single solar cell and corresponded to 0.91V. This value was achievable due to the higher open circuit voltage that PeSCs can provide with respect to the other PV technologies, that in this case was 1.06 V. No direct comparison can be made regarding the discharge capacity subsequent to photo-charge with other photo-capacitors present in this state of the art section because the discharge currents were normalized to the mass and not to the SC active surface. In the same work the integration of a polymer-based solar cell with the same SC used for the PeSC-based photo-capacitor was proposed. In this case a remarkable OPECSE of 5.07% and a discrete maximum voltage during photo-charge of 0.7 V were obtained.

Xu et al.,[46] fabricated an integrated PeSC-based photo-capacitor with a PEDOT-carbon electrodes SC. The OPECSE (4.7%) and discharge capacity (8.75 mC cm^{-2}) were modest considering usual PeSCs PV efficiency and mostly because this device utilized pseudo-capacitive material for the SC electrodes.

Li et al.,[59] proposed the first flexible solid-state PeSC-based photo-capacitor employing also a pseudo-capacitor storage section with copper hydroxide nanotubes (CuOHNT) electrodeposited with MnO_2 as SC electrodes.

In Figure 26A is reported the scheme of the obtained photo-capacitor, while in Figure 26B and 26C are reported photo-charge and subsequent discharge curves, respectively, for different discharge currents and after a different number of bending. An OPECSE of 6.97% and a definitely noteworthy, for a flexible photo-capacitor, discharge capacity of 275 mC cm^{-2} were achieved in this work.

Recently, the parallel connection between a PV harvester and an EDLC was successfully demonstrated by Intermite and co-workers.[60]

Noteworthy, authors demonstrated that this configuration allows to obtain a series of benefits, such as the elimination of an electronic circuit which commute light-dark operation or the buffering of discontinuities in renewable energy conversion. Significantly, through this parallel configuration the HS device features an apparent capacitance which is higher if compared to the EDLC alone.

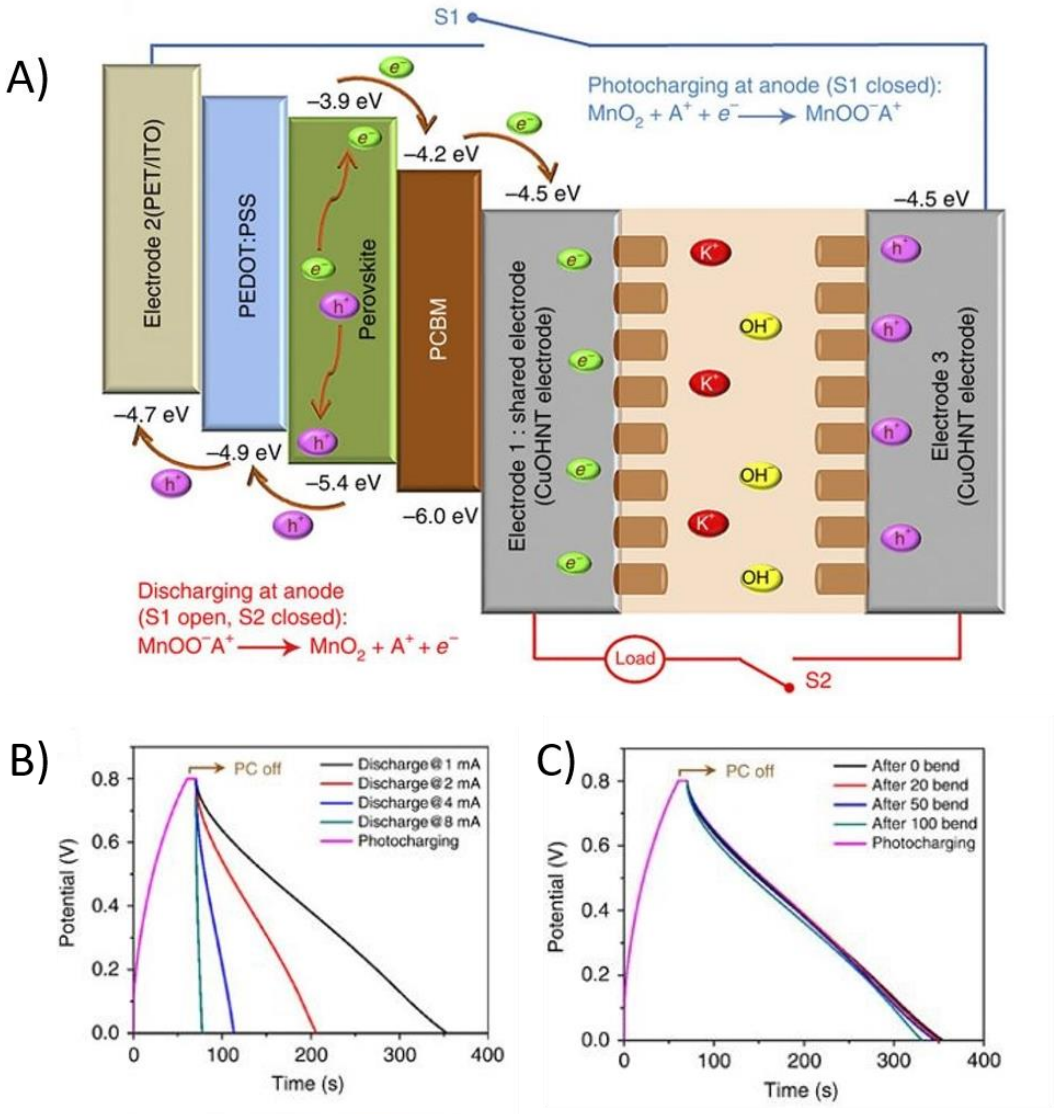

Figure 26: (A) Charging and discharging mechanisms of the flexible solid-state PeSC-based photo-capacitor (B)Photo-charge and discharges profiles recorded with different constant currents ranging from 1 to 8 mA (C) Photo-charge and discharge profiles recorded after bending the flexible device. Adapted with permission from reference [59]**. Copyright 2016, Nature publishing group.**

Table 4: Comparison among the HS devices reported in literature to date in terms of: year, type, PV efficiency, storage efficiency, OPECSE, maximum photo-voltage, discharge capacity, open circuit voltage, short circuit current density and fill factor.

1st Author	Year	HS device	PV eff.	Storage eff.	OPECSE	Max. ph.Voltage.	Disch. capacity (HS) [mC cm-2]	Voc	Jsc (mA cm-2)	FF
T. Miyasaka	2004	DSSC-AC	/	/	/	0,45	75 (at 0.047 mA cm-2)	/	/	/
Murakami	2005	DSSC-AC	/	/	/	0,82	470 (at 0.047 mA cm-2)	0,82	/	/
Hsu	2010	DSSC-PProDOT-Et2	/	/	0.6%	0,75	260 (at 2 mA cm-2)	/	/	/
Hsin-Wei Chen	2010	DSSC-PEDOT	4,37%	/	/	0,69	300 (at 2 mA cm-2)	0,74	8,38	0,71
Zhibin Yang	2012	DSSC-MWCNT	6,10%	83,93%	5,12%	0,72	49 (1.4 mA cm-2)	0,75	13,5	0,61
Zhibin Yang	2012	DSSC-(MWCNT-PANI)	6,10%	70,33%	4,29%	0,72	201,6 (1.4 mA cm-2)	0,75	13,5	0,61
Zhibin Yang	2012	FLEX DSSC-(MWCNT-PANI)	2,31%	34,20%	0,79%	0,73	191,8 (1.4 mA cm-2)	0,75	5,1	0,61
M.Skunik	2013	DSSC-RuOx	2%	40,00%	0,80%	0,88	1440 (at 0.8 mA cm-2)	0,85	5	0,5
Adam Cohn	2015	DSSC-graphene	4,80%	43,75%	2,10%	0,64	2,1 (0.05 mA cm-2)	0,68	11,5	0,61
Jing Xu	2016	DSSC-EDLC TiO2 NTs	3,17%	51,74%	1,64%	0,61	0,75 (0.1 mA cm-2)	0,63	9,03	0,5755
Chien	2015	OPC-graphene	1,57%	/	/	2,3	18 (0.075 mA cm-2)	4,91	0,7225	0,443
A. Scalia	2017	FLEX DSSC-graphene	1,38%	73,91%	1,02%	0,6	6,4 (2 mA cm-2)	0,67	5,56	0,37
A. Scalia	2018	DSSC-AC	2,25%	81,33%	1,83%	2,45	360 (at 0.056 mA cm-2)	2,57	1,8	0,49
A. Scalia	2018	DSSC-AC	2,25%	74,22%	1,67%	2,45	61,2 (at 0.056 mA cm-2)	2,57	1,8	0,49
A. Scalia	2018	DSSC-AC	4,33%	85,91%	3,72%	0,55	20 (at 0.6 mA cm-2)	0,63	11,96	0,34
Wenxi Guo	2012	DSSC-battery	1,95%	42,05%	0,82%	3	122 total device	3,39	1,01	0,57
Junghwan Kim	2016	PeSC-EDLC	13,66%	80,31%	10,97%	0,91	/	1,06	19,44	0,78
Junghwan Kim	2016	PoSC-EDLC	7,85%	64,59%	5,07%	0,727	/	0,79	15,8	0,72
Jing Xu	2016	PeSC-PEDOT	6,21%	73,77%	4,70%	0,7	8.75/7.5 (at 0.25/1.5 mA cm-2)	0,71	18,62	0,48
Chao Li	2016	FLEX PeSC-CuOHNT	10,41%	67%	6,97%	0,8	275 (at 1 mAcm-2)	0,96	16,44	0,66
Intermite	2017	PeSC-EDLC	/	/	/	1	188 (5.5 mAcm-2)	1,1	18,75	0,76
Das	2018	TiO2/hb/CdS-PEDOP@MnO2	6,11%	/	/	0,72	132 Cg-1 (1 Ag-1)	0,746	17,3	0,47

In the HS devices research field, a novel design worth to be mentioned is represented by the work proposed by Das et al.,[61] in which a long PEDOP-MnO_2 electrode served as a storage electrode on one side and as the counter electrode of a TiO2/hb/CdS photo-anode-based solar cell on the other side.

One of the very few reports regarding high-voltage HS devices obtained by PV and EDLC integration is the work published by Chien et al.[62] Their device was constituted by an organic PV module (8 cells in series) and a graphene-based EDLC employing a conventional organic electrolyte. Maximum voltage output during photo-charge was 2.3 V. However, serious constraints regarding the overall system reliability were claimed even by the authors of the study. In fact, an unexpected plateau arose approximately at 2V while photo-charging, demonstrating that the voltage window of the employed storage section was much lower than EDLCs reported in literature using organic solvents. Nevertheless, deep discussion and comparison will be carried out in paragraphs related to the high voltages PV-EDLC integrated devices fabricated during PhD project.

In the following paragraphs are reported HS devices fabricated during the PhD period in chronological order.

4.5 ALL SOLID STATE HIGLY FLEXIBLE POLYMER ELECTROLYTE MEMBRANE-BASED PHOTOCAPACITOR

The innovative HS integrated device proposed in this section was obtained using quasi-solid state electrolytes both for the harvester and storage sections. These were fabricated by means of a photo-polymerization process, which led to a polymer network capable to host liquid electrolytes. In order to give remarkable flexibility feature to the whole structure, flexible metallic grids were employed as electrodes substrates. Namely, titanium grids were employed for the DSSC section and stainless steel grids were utilized for the EDLC. TiO_2 nanotubes (NTs) were grown directly onto the Ti grid via anodic oxidation, while graphene nanoplatelets were deposited onto the stainless steel grids to obtain symmetrical EDLC electrodes. To the best of my knowledge, this photocapacitor still represents the highest OPECSE ever attained for a flexible non-wired DSSC-based HS device.[63]

In Figure 27 are proposed 3-D scheme and pictures of the flexible photo-capacitor.

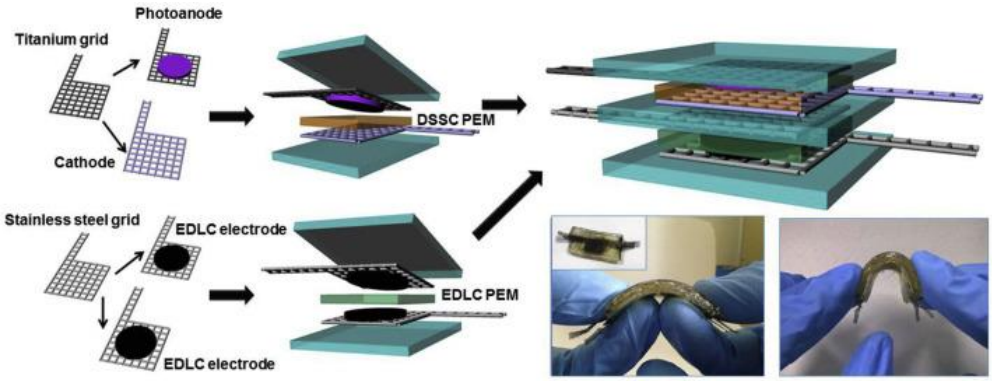

Figure 27: 3-D schemeof the all-solid-state HS device and pictures demonstating its highly flexible layout. Reprinted with permission from reference [63]**. Copyright 2017, Elsevier.**

4.5.1 EXPERIMENTAL SECTION

ELECTRICAL DOUBLE LAYER ELECTRODES PREPARATION

Flexible stainless steel grids were employed as electrodes substrates and current collectors. This choice was made in order to preserve the flexibility of the storage section and of the entire structure. The grid, which presented an open area of 52.25%, was cut into a square shape with 0.5 cm sides and a 4 cm long tail in order to act as electric contact. The electrodes substrates were then cleaned in an ultrasonic bath with two consecutive 10 min steps in acetone and ethanol. Afterwards they were completely dried by means of nitrogen flow and a hot plate set at 100° C. The electrodes of the EDLC were fabricated with a symmetrical loading. Active material was composed of graphene nanoplatelets (GNPs, grade 3, Cheaptubes) and acetylene black (AB, Shawinigan Black) as conductive agent. The ratio between the two components was chosen to be 85/15 in accordance with ref.[64], in which this optimized ratio was demonstrated to lead to stable structured blocks preventing agglomeration of graphene layers. GNPs presented a surface area of 500-700 m^2 g^{-1}.

Low concentration of Poly(vinylidene fluoride) (PVDF) (0.15 wt%) was added as binder using dimetilsulfoxide (DMSO) as solvent. Once a uniform slurry was obtained it was doctor-bladed onto the 0.25 cm^2 EDLC active area. Electrodes were dried first at room temperature and then they were placed onto a hot plate at 100° C to ensure DMSO complete evaporation.

DYE SENSITIZED SOLAR CELL ELECTRODES PREPARATION

TiO_2 NTs were grown onto the Ti grid via room temperature anodic oxidation. For this operation the grids were cut into 4 x 2.5 cm^2 rectangular shape. At first, to clean the surface grid and remove the native oxide layer the grids were chemically etched in a 3% volume fraction hydrofluoric acid in deionized water solution. Then, the grids were anodized in a solution containing 0.5% ammonium fluoride and 2.5% bi-distilled water (weight percentage) in ethylene glycol for 30 min applying a bias of 60 V. As profusely reported in literature the Ti-substrate shape did not influence TiO_2 NTs growth.[65] It *proceeded perpendicularly with respect to the growing plane allowing a complete coverage of the metallic surface with the nanotubular layer*. After this process NTs were amorphous. To obtain the crystallization to an anatase phase an annealing was performed at 450° C for 30 min. The DSSC electrode was obtained as for the EDLC cutting a square shape of 1 cm side with a tail which acted as electrical contact. The photoanode was then soaked in a 0.3 mM N719 solution for 15 hours (the employed solvent was ethanol). Dye excess, which was not adsorbed onto the TiO_2 NTs was removed rinsing the substrate with ethanol.

Counter electrode was fabricated by means of sputtering (Q150T ES, Quorum Technologies Ltd.) technique. A few nm thick layer of Platinum was deposited on both sides of the Ti grid.

The employed Ti grids presented an open area of 40%. For this reason, for the evaluation of the DSSC conversion efficiency a corrective factor referring to the effective area was utilized.

POLYMER ELECTROLYTE MEMBRANE PREPARATION

Two Polymer electrolyte membranes (PEMs) with different thickness were prepared for DSSC and EDLC by means of ultraviolet (UV)-induced polymerization. Bisphenol A ethoxylate dimethacrylate (BEMA) and poly(ethylene glycol) methyl ether metacylate(PEGMA) were used in the ratio of 35:65. Employing this mass ratio between the bi-functional monomer (BEMA) and the monofunctional methacrylate (PEGMA), assured a noteworthy compromise among self-standing capability, flexibility and ionic conductivity of the PEMs. A 3% by weight of photo-initiator (i.e., 2-hydroxy-2-methyl- 1-phenyl-1-propanone, Darocur® 1173) was added to the blend composed by the two oligomers. Then, this mixture was placed between transparent glasses separated by Parafilm tapes (80 μm thickness). For the DSSC section a single film was used while for the EDLC three layers were employed. Afterwards, the blend was UV irradiated for 2 min with a

Hg lamp (intensity of 30 mW cm^{-2}). The photo-polymerized membranes were soaked in two liquid electrolytes. For the DSSC a 0.45 M NaI, 0.056 M I_2 and 0.55 M 4-tert-butylpyridine in methoxypropionitrile (MPN) solution was prepared, while an aqueous electrolyte (2 M NaCl) was used for the EDLC.

HS INTEGRATED DEVICE FABRICATION

The HS device was fabricated in a four electrodes configuration. The two units were linked together in a single structure through a UV photo-polymerization process of a blend composed by silicone polyether acrylate (TEGO® Rad 2010) and Darocur® 1173 (the same photoinitiator used for the PEMs fabrication).

The fabrication started from the EDLC unit. PDMS slides were employed in a 2.5 cm x 4 cm rectangular shape to seal the storage section. This elastomer was chosen as package for its transparency and for the easiness regarding the fabrication process. Two symmetrical electrodes were used for the EDLC. Each electrode was placed in contact with the PDMS slide, positioning the active area of the EDLC in the central region and the tail electrical terminal outside the PDMS slide. The PEM was cut in a square shape with a 1cm side and soaked in a 2M NaCl aqueous solution. It was then interposed between the electrodes. The sealing of the EDLC was obtained by means of light induced polymerization of a liquid mixture composed by TEGO and Darocur 1173 as photoinitiator which was added as 5% in weight with respect to the monomer mass. This blend was deposited on the sides of the PDMS slide so that direct contact with the active material was avoided. The electrodes were disposed in such a way that their contact tails stayed outside the PDMS layer from opposite sides, in order to prevent accidental short circuits. Once the structure was assembled in this way, it was pressed between two lab glasses using clips. UV irradiating for 30 s, the blend polymerized and homogeneously adhered to the PDMS slides.

Afterwards, the counter electrode of the DSSC was placed on top of a PDMS slide employed for the EDLC sealing. Then the 80 μm PEM was deposited onto the counter electrode after swelling in the iodine-based electrolyte. Finally, after inserting the photoanode the final sealing was performed as for the EDLC section with the only difference that this time the whole device was exposed to the UV radiation. Also in this case, contact electrodes were placed on the opposite sides to prevent short circuit.

DEVICES CHARACTERIZATION

PV section was tested with a 91195 Newport solar simulator and a 2440 Keithley. The solar spectrum produced by the simulator was an AM1.5G. While recording the IV curves the terminals of the source measure unit were connected to the DSSC electrodes. Different radiation intensities were obtained with neutral density filters.

The EDLC was tested through cyclic voltammetry (CV) performed with a Metrohm PGSTAT128 and GCD measurements, recorded with the 2440 Keithley.

4.5.2 RESULTS AND DISCUSSION

EDLC CHARACTERIZATION

The storage section was firstly characterized through GCD measurements. The inset in Figure 28 shows GCDs for three different imposed currents, ranging from 0.1 A g^{-1} to 0.4 A g^{-1}. Even if the typical triangular shape was obtained, a somewhat limited coulombic efficiency was experienced mainly for the lowest current applied. However, it must be stated that, in flexible SC literature this feature is occasionally observed. [51], [66]–[68]

This behavior can be ascribed to the excessive SC PEM thickness (240 μm). This thickness was chosen in order to attain a necessary compromise between electrochemical performance and mechanical stability, since this HS device was designed to work particularly under severe bending conditions. The decrease of the PEM thickness in a subsequent work (see paragraph *IN PLANE INTEGRATION OF ENERGY CONVERSION AND STORAGE DEVICES EMPLOYING MULTIPOLYMER ELECTROLYTE MEMBRANE)*, where flexibility was not required, brought to an important increase of the coulombic efficiency.

Long-term stability was tested through 10 000 consecutive cycles. Figure 28 shows the capacitance retention of the flexible EDLC as a function of the cycle number. Evidently, no capacitance fade was experienced over cycling. Stability was tested through cyclic voltammetry (CV) with an imposed scan rate of 1 V s^{-1}.

DSSC CHARACTERIZATION

PV response was tested in a range between 0.15 and 1 Sun. This choice was adopted in order to estimate the DSSC current output as a function of the applied voltage under different illumination conditions. This analysis appears necessary to

appreciate even the behavior of the entire HS device at different illumination conditions.

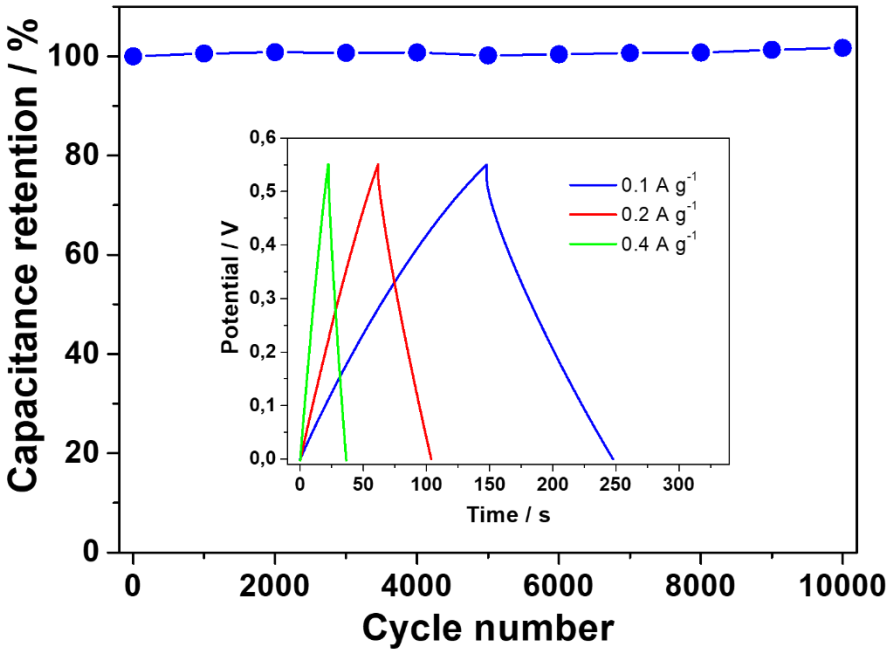

Figure 28: Capacitance retention of the EDLC unit tested through 10 000 consecutive CV cycles. In the inset, GCD measurements of the EDLC flexible section. Adapted with permission from reference [63]**. Copyright 2017, Elsevier.**

Significantly, in this way, the DSSC and the HS device were tested in circumstances close to outdoor real conditions and even in in-field applications conditions, in which the electromagnetic power density is extremely low.

Figure 29A shows the IV measurements performed at 0.15, 0.2, 0.3, 0.5 and 1 Sun, while in table 5 the most important DSSC parameters at different illumination conditions are collected. PV efficiency was calculated as reported in chapter 1.The corrected efficiency was additionally calculated taking into account the effective surface of the grid onto which TiO2 NTs were grown.

FF and V_{OC} remain nearly the same values varying the radiation intensity. Thus, the PV efficiency is strictly related to the ratio between j_{SC} and G. This parameter expresses the current produced by the DSSC for every Watt of radiation which impinges onto the PV device. As reported in table 5 this ratio evidently increases

lowering the illumination intensity. As a consequence, also the PV efficiency increases for low illumination values.

Table 5: PV peculiar parameters of the DSSC flexible device. Adapted with permission from reference [63]**. Copyright 2017, Elsevier.**

Illumination [Sun]	PCE_{corr} [%]	*FF*	V_{OC} [V]	j_{SC} [mA cm^{-2}]	j_{SC}/G [mA W^{-1}]
1	1.38	0.37	0.67	3.34	33.4
0.5	1.46	0.30	0.64	2.30	46.0
0.3	2.03	0.30	0.61	2.00	66.7
0.2	2.59	0.30	0.64	1.60	80.0
0.15	2.96	0.34	0.63	1.26	84.0

Even if the FF at 1 Sun is low with respect to standard DSSCs, an evident improvement was experienced comparing it with a previous work [20] of our group in which the same metallic grids and polymer electrolyte were used but a commercial TiO_2 nanostructure was employed instead of the TiO_2 nanotubes. A so limited FF is mainly ascribable to an excessively high internal series resistance as testified by the slope of the IV curve in the V_{OC} region. This is primarily associated to the non-perfect electrodes/electrolyte interface link, as it is the connection of a solid (current collector) with a quasi-solid section (electrolyte).

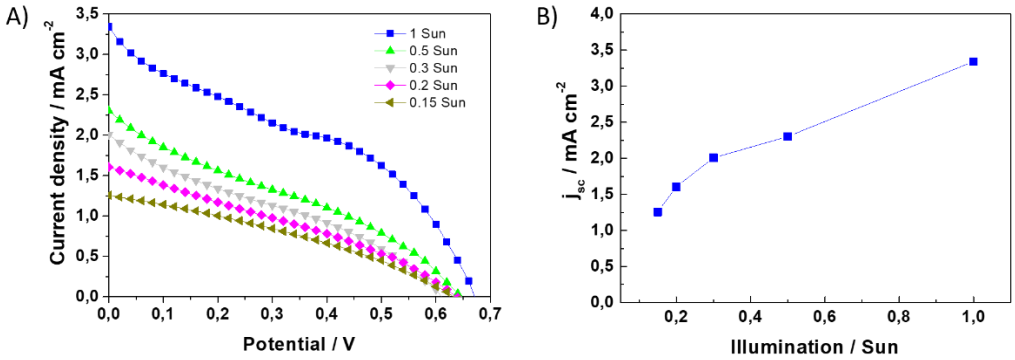

Figure 29: (A) IV profiles of the flexible DSSC recorded at different illumination conditions in the range 0.15 – 1 Sun. (B) Short circuit current density provided by the flexible DSSC as a function of the illumination conditions. Adapted with permission from reference [63]**. Copyright 2017, Elsevier.**

In Figure 29B the j_{SC} is plotted as a function of the illumination intensity. Evidently, a larger variation in the current density values was experienced in the range 0.15 Sun - 0.3 Sun. Moreover, considering the values at 0.2 Sun and 1 Sun it

is evident that the j_{SC} variation was less than proportional. This behavior is related to a higher recombination process occurring between electrons and holes when a higher number of electrons occupies the conduction band of the TiO_2 NTs.

HS DEVICE CHARACTERIZATION

Once the DSSC and the EDLC sections were separately analyzed, integration was investigated. Figure 30A shows the connection among the DSSC harvester, the EDLC storage and the source measure unit, which was employed to detect the EDLC changing bias. The design of the HS device simplified the connection between photo-anode and EDLC symmetrical electrode and consequently between DSSC cathode and the other symmetrical electrode of the storage section. Figure 30B and 30C shows the photo-charging and discharging mechanism respectively. Upon photo-charge, the device and the cables were placed into the solar simulator and light was turned on as in Figure 30D. DSSC and EDLC were electrically connected and the SMU terminals measured the photo-changing EDLC voltage. During this phase EDLC voltage rapidly increased till 0.6 V, approaching the DSSC V_{OC}. Upon discharge, DSSC and EDLC were electrically disconnected, light was turned off and a negative current of 2 mA cm^{-2} was applied to the EDLC in order to completely discharge the storage device. As for the DSSC, the HS device was also tested under different illumination conditions. Figure 30E shows three different charging profiles, obtained respectively at 1, 0.9 and 0.8 Sun.

The evident difference in charging time between tested photo-charging process and GCD measurements is related to a different current density applied per weight of active material. In fact, when the DSSC charged the EDLC, the current density per mass of EDLC active material was about 1 order of magnitude higher with respect to the highest value used during GCDs.[69]

The HS device was tested for all the illumination conditions used to characterize the DSSC, in order to deeply understand its performance in a wide range of environmental conditions.

OPECSE was evaluated as profusely reported in literature (for complete equation and to deeply understand parameters involved see previous paragraph *HS devices significant parameters*):

$$OPECSE = \frac{E_{EDLC}}{E_{SOL}}$$

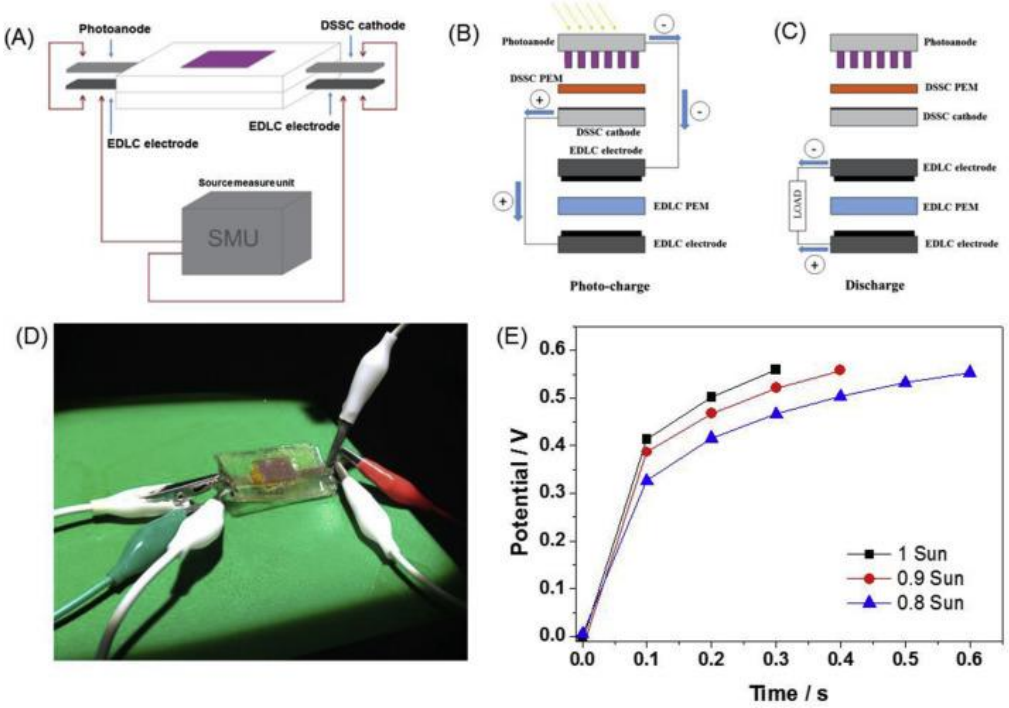

Figure 30: (A) Scheme of the electrical connections among DSSC, EDLC and source measure unit. (B) Photo-charging process scheme. (C) Discharging process scheme. (D) HS device placed in the solar simulator and electrically connected. (E) Photo-charging curves obtained at different illumination conditions. Reprinted with permission from reference [63]**. Copyright 2017, Elsevier.**

Such parameter represents the energy percentage the user can benefit with respect to the whole incident radiation. In this case, the lowest capacitance value obtained through EDLC electrochemical tests (CV performed at 100 mV s^{-1}) was employed to calculate OPECSE. During photo-charge a circular mask of 0.22 cm^2 was used. In addition, as for the DSSC, the corrective factor taking into account the effective area of the grid was used to evaluate the harvester active surface, employed to calculate E_{SOL} (S t G).

As direct comparison, Figure 31 shows the energy performance of the DSSC (conversion) and of the HS device (conversion and storage) for all the investigated illumination conditions. As previously discussed, diminishing the electromagnetic power density, the PV performance improved. In particular, for illumination intensity lower than 0.5 Sun an evident increase is clearly recognizable. However, a different behavior was found for the HS device. In fact, the OPECSE value attained a maximum for a condition of 0.3 Sun. For lower power densities (0.15 and 0.2 Sun) a plateau was achieved for a value slightly lower than the one attained at 0.3 Sun. Interestingly, 0.3 Sun did not correspond to the maximum neither of the

storage efficiency nor of the PV efficiency, but being OPECSE proportional to both these two parameters their product reached the maximum under 30 mW cm^{-2} power radiation density.

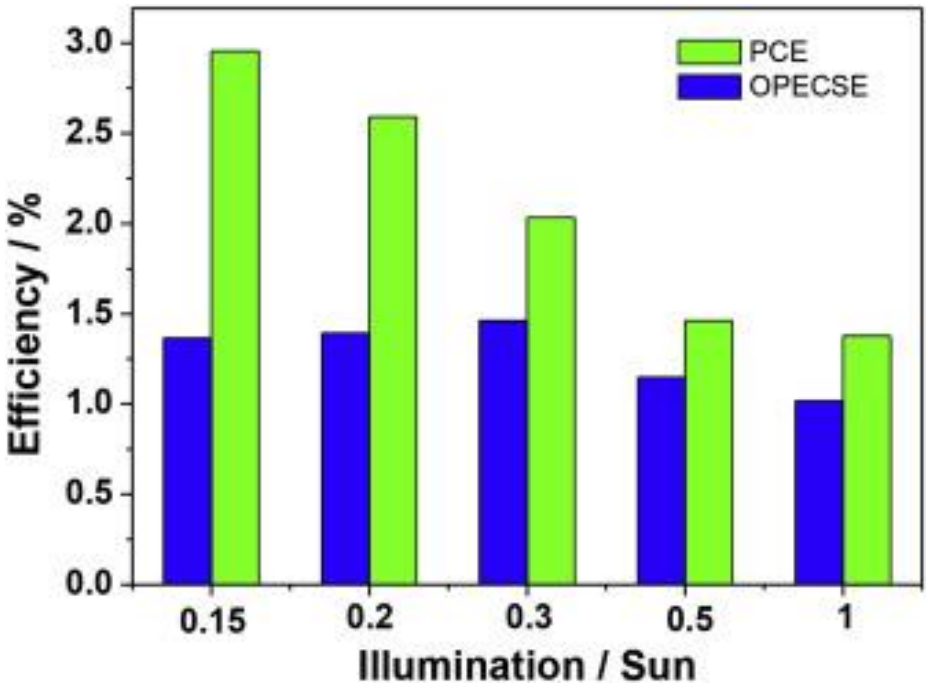

Figure 31: PV and OPECSE efficiecnies as a function of the illumination condition. Reprinted with permission from reference [63]**. Copyright 2017, Elsevier.**

For the sake of completeness, in table 6 all the values regarding PV conversion efficiency, storage efficiency and OPECSE are summarized for every tested illumination condition. Certainly, the decrease of the storage efficiency (0.2 – 0.15 Sun) is related to the EDLC leakage current. Even if this remains constant for every illumination circumstance for lower lighting conditions, the photo-generated current is reduced and the leakage current, which hinders the current charging the EDLC is not anymore negligible as it was for example under 1 Sun illumination.

The plateau of the OPECSE in the range 0.15 – 0.3 Sun is certainly a significant achievement since these radiation conditions are representatives of diffuse radiation or cloudy circumstances, which are typical of a temperate weather for a large period of the year.

Table 6: PV, OPECSE and storage efficiencies. Adapted with permission from reference [63]**. Copyright 2017, Elsevier.**

Illumination condition	PCE_{corr} [%]	η_{ES}[%]	OPECSE [%]
1 Sun	1.38	73.91	1.02
0.5 Sun	1.46	78.76	1.15
0.3 Sun	2.03	71.56	1.46
0.2 Sun	2.59	53.66	1.39
0.15 Sun	2.96	46.28	1.37

In this perspective, reducing the EDLC leakage current might lead to obtain a particularly competitive device, able to store a fixed amount of energy with an extremely small time variation, varying the atmospheric conditions.

The HS device additionally underwent a cycling stability test in order to check its stability over time and upon prolonged operation. To this purpose, a series of consecutive photo-charges and subsequent dark conditions discharges were applied. In Figure 32 the first 5 cycles are shown. These measurements were performed at 1 Sun irradiation intensity.

Upon discharge the SMU was set in order to provide a negative current of 2 Ag^{-1} to the EDLC. This choice was made to guarantee a similar step time with respect to the photo-charge. The average discharge time was found to be 3.2 s.

This work aimed to prove the feasibility of a completely flexible HS device. However, depending on the particular application the storage section size or electrodes loading should be tuned so that the stored charge could be adequate to drive a specific utilizer.

Between two consecutive cycles, when the discharge in dark condition was completed and before the solar simulator was switched on, the EDLC voltage immediately reached 0.05 V. In Figure 32 this behavior is clearly observable and it can be explained by the fact that the discharge phase was extremely fast and some ions in the active porous layers did not have enough time to migrate from the active material.

As this HS device was thought to work predominantly in bending conditions, also its flexibility was tested, recording photo-charge and discharge cycles with different imposed bending angles. Figure 33 shows three photo-charging profiles for no bending angle, 60° and 120° bending angles. In this case, the active material present on the EDLC electrodes was doubled with respect to Figure 30E, thus the different charging time is explained even for the same condition (planar configuration).

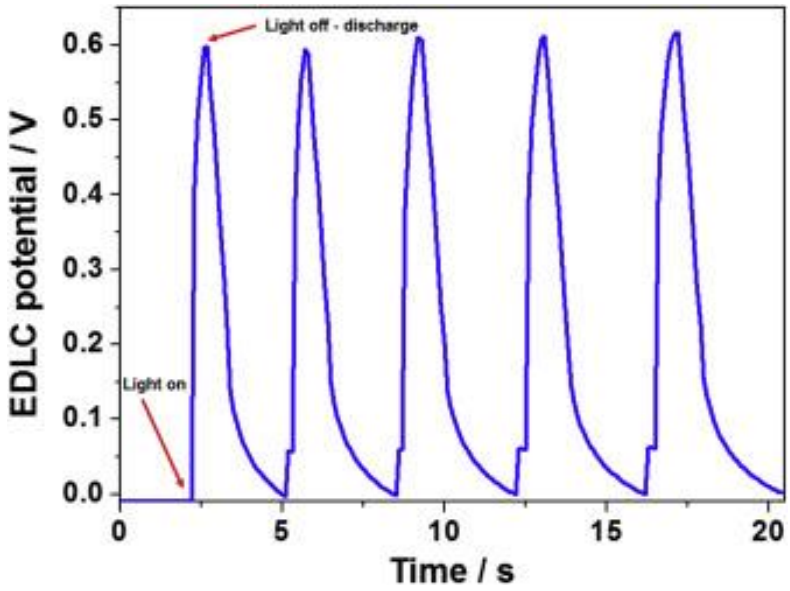

Figure 32: Photo-charge discharge cycles of the flexible quasi-solid-state HS device. Reprinted with permission from reference [63]**. Copyright 2017, Elsevier.**

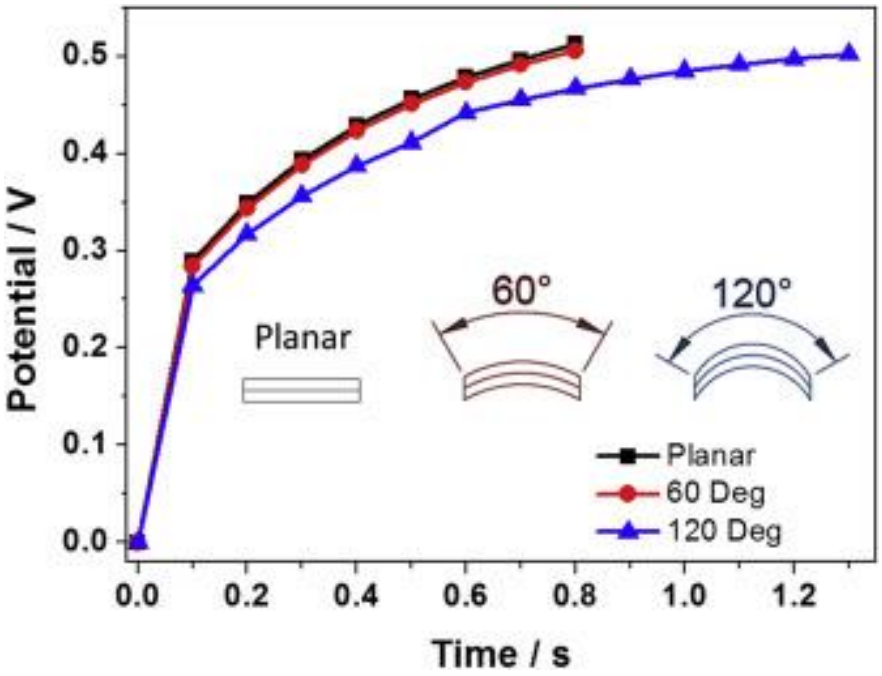

Figure 33: HS device photo-charging curves obtained with different bending angles. Reprinted with permission from reference [63]**. Copyright 2017, Elsevier.**

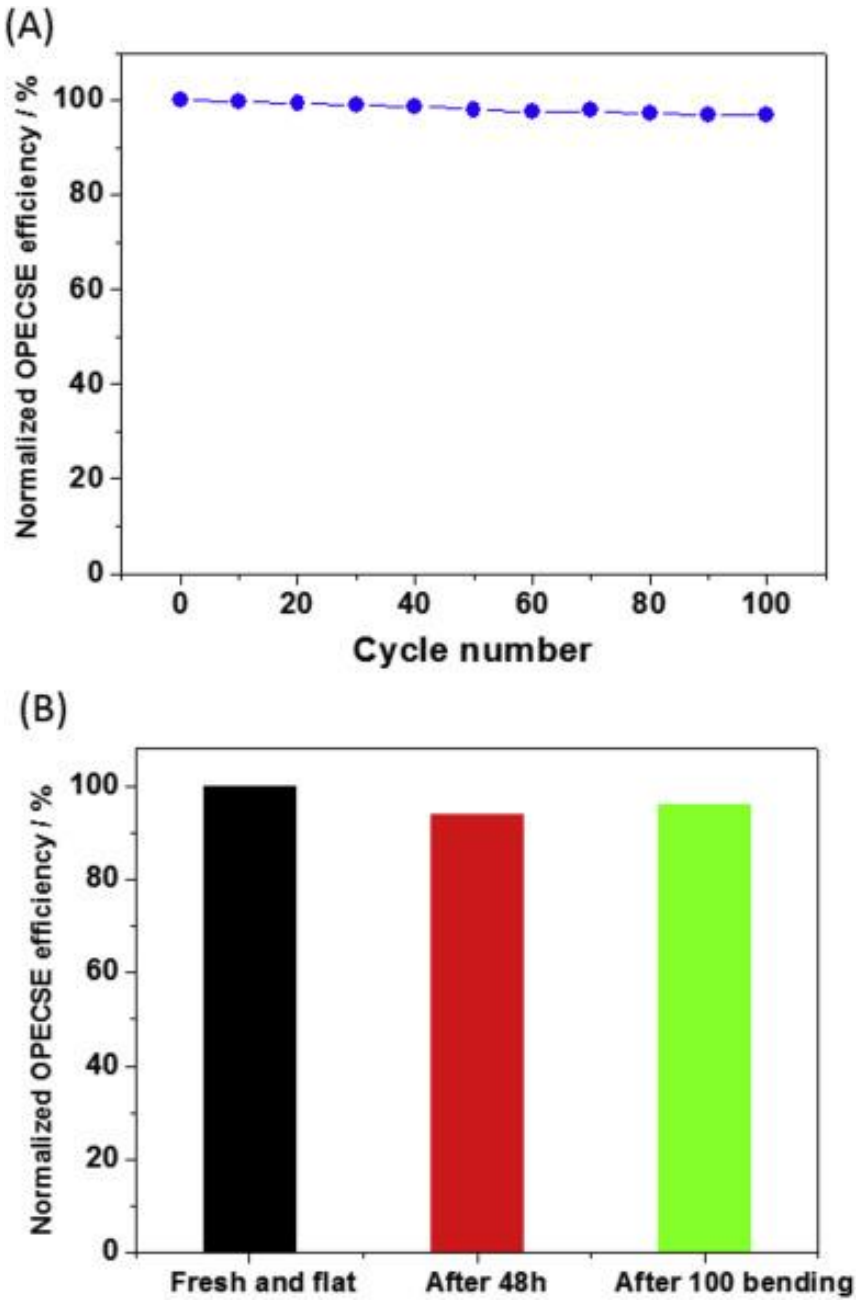

Figure 34: (A) OPECSE value plotted as a function of the cycle number. (B) OPECSE retention of the quasi-solid electrolytes HS device after 48 h rest time and 100 consecutive bendings. Reprinted with permission from reference [63]**. Copyright 2017, Elsevier.**

Remarkably, the less severe tested bending angle did not negatively affect the charging profile. This is certainly a notable point since this bending angle is representative of many practical applications. In the more severe condition which corresponded to a bending angle of 120° the photo-charging step slightly increased with respect to the planar configuration. The increase can be probably related to a non-perfect connection, under a so severe circumstance, between current collectors and PEM, both for the EDLC and DSSC.

The cycling stability of the HS device was tested through 100 consecutive photo-charge discharge cycles. The OPECSE retention is plotted in Figure 34A as a function of the cycle number. The overall efficiency remained constant over cycling. Thus, demonstrating that the proposed architecture possesses interesting reliability characteristics.

Stability of the HS device was tested through other two different tests. At first, OPECSE was calculated after 48 h of rest time. In a second test, OPECSE was calculated after 100 consecutive bending of the flexible architecture. The two tests were performed on two different prototype devices. Results of these two tests are shown in Figure 34B. The decrease in the OPECSE was almost negligible in both cases. 94% and 96% of the initial OPECSE was maintained for the aging and bending tests respectively.

The HS device proposed in this paragraph present flexibility properties that are difficult to be found in literature, to date. In addition, evident increment in overall efficiency was found by lowering illumination conditions, demonstrating that the device lends itself to be exploited in real environment conditions.

4.6 HIGH VOLTAGE PHOTOCAPACITOR: DYE SENSITIZED SOLAR MODULE AND $PYR_{14}TFSI$ IONIC LIQUID ELECTRICAL DOUBLE LAYER CAPACITOR INTEGRATION

In this paragraph, high voltage HS devices feasibility was investigated. The HS device was composed by a dye sensitized solar module (DSSM) and an EDLC employing an ionic liquid electrolyte. DSSM was constituted by 4 serially connected DSSCs in order to increase the open circuit voltage of the PV harvester and ionic liquid was employed to enlarge the EDLC voltage window. As previously mentioned, only another example of photo-capacitor was proposed in literature with a voltage much higher than 1 V. It is related to the fact that the HS devices present in literature deal with a single solar cell integrated with a SC (EDLC or pseudo-

capacitor). The only other work (except works related to my PhD) in which a solar module was utilized as energy harvester was the one proposed by Chien and co-workers.[62] They used an organic solar module in which 8 cells were placed in series and a graphene-based EDLC employing an organic electrolyte. In the results section of this paragraph a precise comparison of our work with Chien et al. report is proposed in order to highlight the remarkable novelty this HS device represents in terms of voltage and discharge capacity.

In this work, both the harvesting and storage sections were fabricated onto conductive glass substrates. Thus, it could be recognized as a step toward HS devices integration in windows facades for self-sustainable buildings. Moreover, this HS device is thought to be integrated in portable electronics or provide energy for off-grid sensor networks.

The PV section was constituted by a 4 serially connected W-type DSSCs-module, while the EDLC consisted of activated carbon as electrodes material and $Pyr_{14}TFSI$ as ionic liquid electrolyte.

The two sections were separately tested before that integration of the whole system was successfully proved through photo-charge and subsequent discharge phases. The system reached a voltage of 2.45 V while the DSSM was charging the EDLC. Upon discharge phase the EDLC was able to deliver a capacity of 1.8 mAh (0.1 mAh cm^{-2}) using a discharge current of 1 mA. This is so far an absolute record in the field of highly stable and reliable integrated HS devices.

4.6.1 EXPERIMENTAL SECTION

DSSM FABRICATION

Referring to the DSSM fabrication, conducting glass were employed as electrode substrates. The DSSM was designed having the plate directly exposed to the sunlight in a 4 x 4 cm^2 square shape and the backward plate in a 4 x 5 cm^2 rectangular shape. This choice was carried out in order to have additional space for contacting the electrodes of the first and last DSSC of the module. Four holes were realized in the backside substrate, approximately at the centre of each DSSC surface to allow the electrolyte to fill the space between photo-anode and counter electrode. The FTO conductive oxide was patterned in both the glass plates in order to create a proper path for the electrons and disconnect the cathode of a DSSC from the photo-anode of the contiguous one.

Then the glass plates were rinsed in two consecutive ultrasonic baths with acetone and ethanol respectively. The counter electrodes were obtained by sputtering different platinum layers. Namely, 3 and 10 nm were deposited in the

DSSCs cathode regions for the back-illuminated and front-illuminated glass plates constituting the DSSM. The sputtering current and deposition rate were set to 30 mA and 0.04 nm s^{-1}. The photo-anodes semiconductors were obtained depositing a DSL 18NR-AO TiO2 paste. In order to deposit the proper amount of TiO_2 paste in the DSSCs regions, two adhesive tapes each with two circular holes, were placed onto the two conductive glass plates. Adhesive tapes thickness was 80 µm and the holes' areas were obtained so that the front-illuminated cells had a circular shape of 10 mm while the back-illuminated cells had an active area of 12 mm. Afterwards, the paste was deposited in the holes by doctor blade. Once the adhesive tapes were removed from the glass substrates, in every conductive plate two circular semiconductor regions and two nanometric thick platinum layers' regions were obtained as proposed in Figure 35.

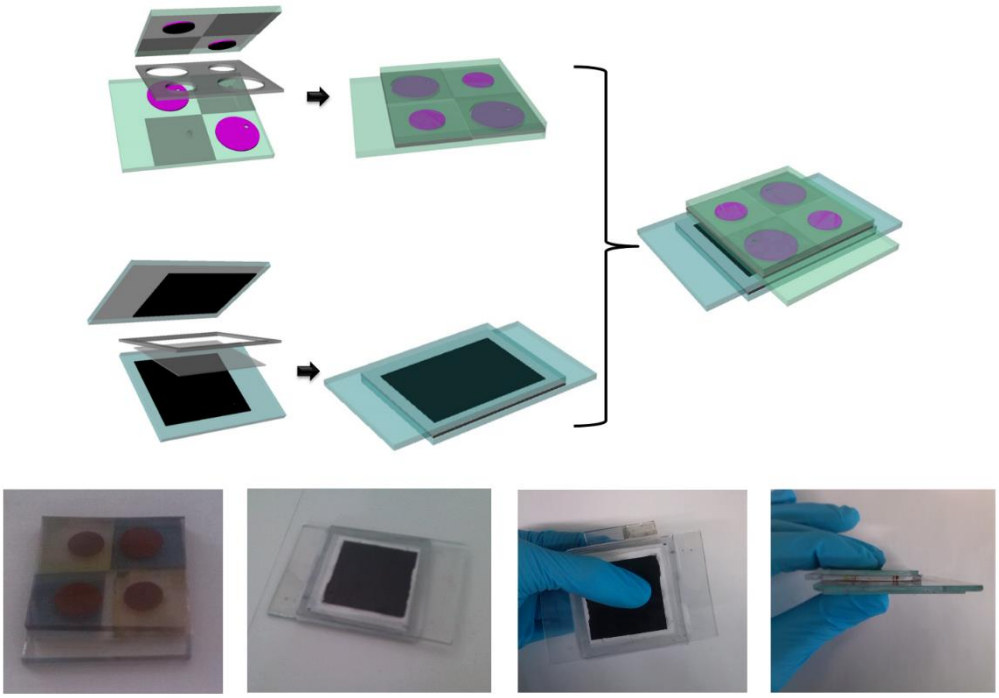

Figure 35: 3-D schemes and pictures of DSSM, EDLC and HS devices. Reprinted with permission from reference [45]**. Copyright 2018, Royal Society of Chemistry.**

Then, the plates were calcined at a temperature of 500° C for 30 min, imposing an increasing and decreasing ramp of 12 h to avoid glasses distortion. In this way, TiO_2 nanoparticles were properly interconnected and the paste solvents and

additives were completely removed. The plates were then soaked for 15 h in the dye solution, which was a 0.3 mM Z907 in ethanol. The device was finally sealed by means of a hot press set at 120° C interposing 2 60-µm Meltonix films between the two glass plates. A methoxypropionitrile (MPN) solvent-based electrolyte was inserted through the 4 holes of the back glass by vacuum backfilling. The electrolyte salts with their apposite concentration were: 0.45 M sodium iodide, 0.056 M iodine and 0.55 M 4-tert-butylpyridine.

4.6.1.2 EDLC FABRICATION

The conductive glasses employed for the EDLC fabrication were cut into 7.5 x 6 cm^2 rectangular shape. As for the DSSCs substrates, the glasses were rinsed in two consecutive ultrasonic baths with acetone and ethanol in order to appropriately clean their conductive surfaces. An aqueous slurry was prepared by proportionally mixing 1g of electrodes material components (active material, binder, conductive component) in 50 mL pure H_2O.

The choice to fabricate an EDLC employing a water-based slurry following Varzi and co-workers previous reports[70]–[72] lead to a more eco-friendly device.

The electrode composition by weight was constituted by 90 % of activated carbon, 5 % of conductive carbon and 5 % of binder. The employed binder was sodium carboxymethylcellulose (CMC). Firstly, CMC was added to water and stirred until the mix appeared homogeneous and highly viscous. Then, in different steps conductive carbon and activated carbon were added, keeping mixing the slurry. The aqueous slurry was then deposited onto the FTO glass in a 4 x 4.5 cm^2 rectangular region delimitated by adhesive tapes, which were subsequently removed after 30 minutes. The electrodes were dried at first overnight at 80° and then under vacuum at 130° C for 12 h. Different coating thicknesses were employed for the EDLC positive and negative electrodes, thus resulting in diverse deposited active material weight. After drying, the deposited material onto the positive electrode was 100 mg (5.55 mg cm^{-2}), while the deposited material onto the negative electrode was 60 mg (3.33 mg cm^{-2}). This choice (validated by 3-electrodes measurements carried out employing an Ag wire as reference electrode) was made in order to account for the asymmetric capacitive response of the employed activated carbon in the $Pyr_{14}TFSI$ ionic liquid electrolyte.

As separators, 260 µm Whatman glass fiber sheets were employed. They were cut in a suitable shape and dried under vacuum in glass oven at 120° C for 12 h. The separator sheet was placed onto an electrode, then some electrolyte droplets were homogeneously deposited onto it, so that the separator was uniformly impregnated. As for the DSSM, meltonix films were employed to seal the EDLC

by means of a hot press. The whole fabrication procedure was performed in a dry room in order to reduce as much as possible moisture contamination.

DSSM AND EDLC INTEGRATION

Integration between DSSM and EDLC was performed by means of a hot press. Two 60 μm meltonix films were placed onto an EDLC substrate electrode and then the DSSM was placed onto the meltonix films (with the glass onto which the four holes were previously drilled in contact with the sealing films), leaving the DSSM contact region outside the EDLC surface so that an easy contacting could be done during measurements. Furthermore, in this way, an optimal sealing of the DSSM holes was guaranteed.

DEVICES CHARACHTERIZATION

PV response of the DSSM was evaluated with a solar simulator (HelioSim-CL60, Voss Electronics) which replicated the electromagnetic solar radiation and a potentiostat (PG510/590 Heka) which measured the photo-generated current for each voltage applied.

The solar simulator produced an electromagnetic power density of 100 mW cm^{-2} with an AM1.5 solar spectra.

Storage section electrical response was estimated through GCD performed with an imposed current of 2 mA and CV with an imposed scan rate of 1 mV s^{-1}. Tests were carried out with a multi-channel potentiostat-galvanostat (VMP3, Biologic Science Instruments).

The EDLC galvanostatic and potentio-dinamyc electrochemical measurements were executed in a climatic chamber set at a temperature of 20° C.

The capacitance was evaluated from the discharge phase of the GCD as reported in chapter 3.

Furthermore, Electrochemical impedance spectroscopy (EIS) was performed on the EDLC in the condition in which it was discharged and left at open circuit voltage in a range of frequencies between 0.1 MHz and 1 mHz employing an amplitude of 10 mV. The instrument utilized to perform this analysis was the Impedance/Gain-Phase Analyzer 1260.

4.6.2 RESULTS AND DISCUSSION

EDLC CHARACTERIZATION

Figure 36A shows the EDLC GCD curve for an imposed current of 2 mA corresponding to a current density of 0.11 mA cm^{-2}. The profile confirms the typical triangular behaviour of double layer capacitor. A deviation from the ideal response due to the moderate $Pyr_{14}TFSI$ conductivity, which is nevertheless reported also in previous works,[72] is observable.

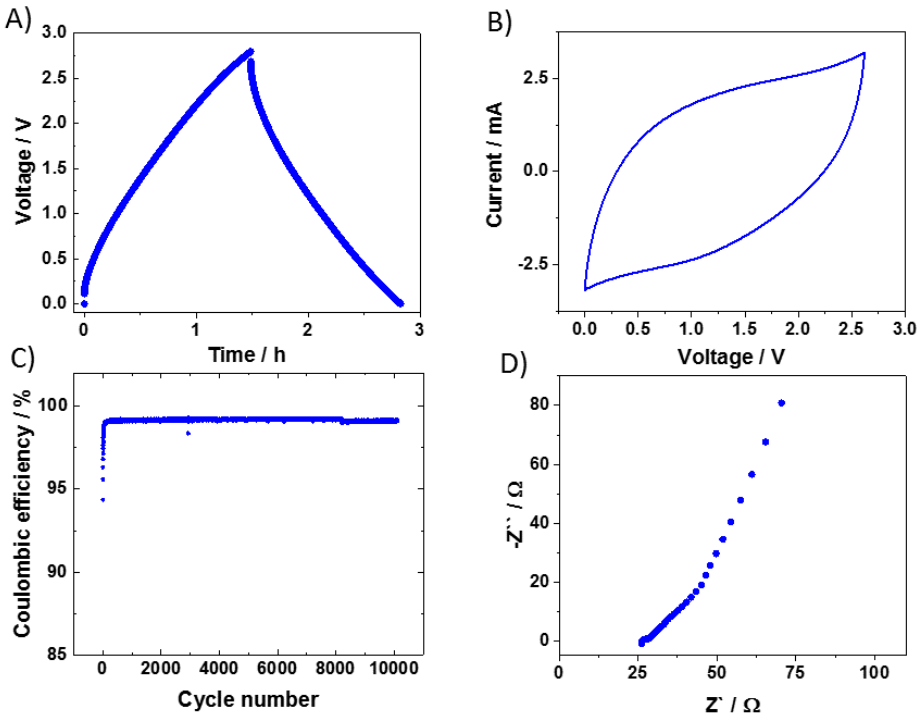

Figure 36: (A) GCD performed at 2 mA. (B) CV performed at 1 mV s-1. (C) Coulombic efficiency retention. (D) EIS analysis. Reprinted with permission from reference [45]**. Copyright 2018, Royal Society of Chemistry.**

As reported in the Experimental section, the capacitance was evaluated from the discharge curve and it was found to be 233 mF cm^{-2}. In comparison with the only other previous work reported in literature related to high voltage photo-capacitor[62] (Chien et. al), the $Pyr_{14}TFSI$ EDLC obtained a capacitance value which is about two order of magnitude higher. Significantly, from the GCD curve in Figure 36A the voltage profile does not show plateaus related to faradaic

reactions until 2.8 V, thus demonstrating the absolute electrochemical stability of the EDLC within a broad voltage window. This window is still higher with respect to the DSSM open circuit voltage, therefore an optimal stability upon photo-charge is guaranteed.

Stressing the comparison with respect to Ref.[62] the proposed $Pyr_{14}TFSI$ EDLC attained a much higher coulombic efficiency and a more defined triangular profile, approximately under the same galvanostatic conditions. More important, the here proposed HS device can be considered the first highly stable photo-capacitor prototype since in Chien et. al GCD measurement an evident irreversible faradaic reaction took place at a voltage lower than 2 V.

Figure 36B shows the CV measurement of the EDLC section (1 mV s^{-1} scan rate). Also in this case the ideal rectangular profile is not obtained. The deviation from the ideal shape is even more pronounced than in the GCD since in this case the completion of a charge-discharge cycle occurs in half the time. A key-role here is played by the FTO conductive glass which limits the EDLC performance in terms of both energy and power.

A long-term stability test was also performed in order to prove EDLC consistency under severe cycling. To this purpose, 10 000 consecutive GCD cycles were carried out at 20 mA. In this case the maximum voltage was maintained at 2.5 V since this was nearly the maximum expected voltage during photo-charge. At the end of the cycling stability test, both capacitance and energy density values were nearly 100% of the preliminary values, demonstrating no fading. Figure 36C shows the coulombic efficiency during the cycling test. Within the very first cycles, coulombic efficiency reached a value above 99% and for all the 10 000 cycles it did not experience any decrement. This is a remarkable achievement for high voltage photo-capacitors since no cycling tests were carried out to date in literature reports.

Figure 36D reports the Electrochemical impedance spectroscopy (EIS) of the EDLC. Equivalent series resistance (ESR) was evaluated as suggested in literature,[21] by the impedance real part estimated at 1 kHz. It provided a value of 26.8 Ω. The other way usually used to assess ESR, namely evaluating the prosecution of the 45° region with the x-axis lead to nearly the same value.

The EIS curve testifies once more for low frequencies that the prevalent contribution to a non-ideal EDLC behaviour as already discuss for GCD and CV measurement is given by the use of FTO glass. In fact, the low frequency region is not vertical as it should be for an ideal capacitive element. Employing the FTO glass evidently causes fading performance for high power applications. In this perspective its use can be dedicated to particular applications in which a somewhat limited current and a high voltage are requested.

DSSM CHARACTERIZATION

PV section was designed as a four serially connected W-type DSSCs module, in which two DSSCs resulted front-illuminated and the other two resulted back-illuminated with respect to the solar radiation. Hence, 100 mW cm^2 was the radiation impinging onto half of the DSSCs present in the W-type module. The remaining half received a solar radiation which was a function of the Pt counter electrode thickness and of the electrolyte transparency.

In accordance with Giordano et al.,[73] a different surface was designed between front- and back-illuminated DSSCs. In this way, each PV cell in the module produced nearly the same photo-generated current leading to a more rectangular current-voltage profile. This is fundamental in order to avoid current discontinuity during photo-charging phase.

Photo-anodes were obtained in circular geometries having 10 and 12 mm diameters for front- and back-illuminated DSSCs respectively, thus resulting in a ratio of 1.44 between the active surface which is back irradiated and the active surface which is directly exposed to the sunlight.

The restricted DSSCs surfaces were chosen in order to feed a limited current to the EDLC, since otherwise a high charging rate would have diminished the charge effectively stored into the EDLC due to the moderate conductivity of the conductive glass substrate.

Regarding DSSCs electrolyte, it was decided to use an iodine-based liquid electrolyte employing Methoxypropionitrile (MPN) as solvent. This choice was carried out due to the higher boiling point of MPN with respect to acetonitrile (ACN), which is the most employed in DSSCs literature for its lower viscosity and higher ionic conductivity. In this perspective, MPN guaranteed to reduce electrolyte evaporation during DSSM sealing. Moreover, also during operations, PV modules temperature increases. For solid state solar cells, it only leads to a decrease in the PV efficiency, while for DSSCs employing a liquid electrolyte it can turn into slow electrolyte evaporation. Hence, a less volatile solvent seemed a good compromise between stability over operations and efficiency.

Figure 37A reports the current-voltage profile recorded at 1 Sun illumination conditions.

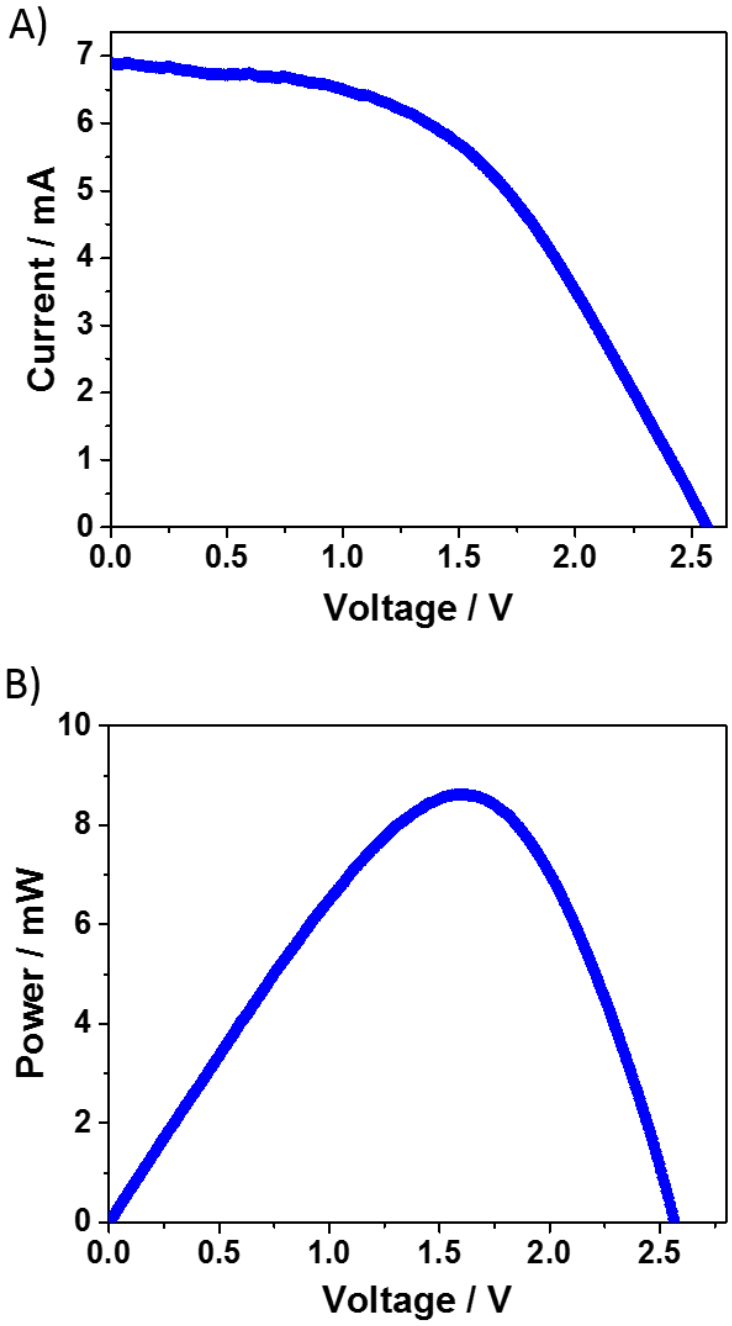

Figure 37: IV and PV curves of the DSSM. Reprinted with permission from reference [45]**. Copyright 2018, Royal Society of Chemistry.**

PV efficiency was evaluated as reported in chapter 1, as the ratio between the electrical power output in the maximum power point and the product of the

incoming electromagnetic power radiation (100 mW cm^2) and the active photo-anode surface (more generally PV cell/module active surface):

$$\eta = \frac{P_{MPP}}{S\ G}$$

The efficiency was evaluated to be 2.25%. Even if this value is lower with respect to DSSM literature reports, this efficiency is higher if compared to the only other report present in literature regarding PV-module-based HS devices (1.57% obtained by Chien and co-workers[62] with an organic 8 serially connected PV module). The current-voltage curve presents a deviation from the ideal rectangular diode profile. However, the current produced remained almost constant even for a voltage which is the 70% of the V_{OC}. In this perspective, the balancing between front- and back-illuminated DSSCs active areas was optimal. This appear a central feature for integration with the EDLC, since discontinuities would have negatively affected the photo-charging behaviour. The evident slope close to the open circuit testifies a significant DSSM series resistance, which is however commonly observed in DSSM literature.[73]–[75] Consequently, the fill factor resulted affected, turning into a value of 0.49. In future works, this FF could be surely improved leading to a substantial increase of the PV efficiency and as a consequence of the integrated device OPECSE.

Figure 37B shows the DSSM power-voltage profile. The curve presented a maximum for 1.61 V. Correspondingly, the maximum OPECSE for the integrated device should be investigated around this voltage.

In table 7 the most relevant DSSM PV parameters are highlighted.

Table 7: DSSM peculiar parameters. Reprinted with permission from reference [45]**. Copyright 2018, Royal Society of Chemistry.**

V_{OC} [V]	I_{SC} [mA]	*FF*	I_{MP} [mA]	V_{MP} [V]	η [%]
2.57	**6.91**	**0.49**	**5.35**	**1.61**	**2.25**

HS DEVICE CHARACTERIZATION

The integrated device was tested through photo-charge and subsequent galvanostatic discharge. Upon photo-charging, 1 Sun (100 mW cm^{-2}) radiation intensity impinged onto the DSSM. This illumination condition is practically the only one used in photo-capacitors literature, thus direct comparison between our device and literature reports is enabled. EDLC electrodes were connected to the DSSM terminals in order to be charged and at the same time potentiostat measured the changing EDLC voltage.

Figure 38 shows photo-charge and subsequent discharge curves for five different imposed constant currents ranging from 1 mA (0.056 mA cm^{-2}) to 10 mA (0.56 mA cm^{-2}).

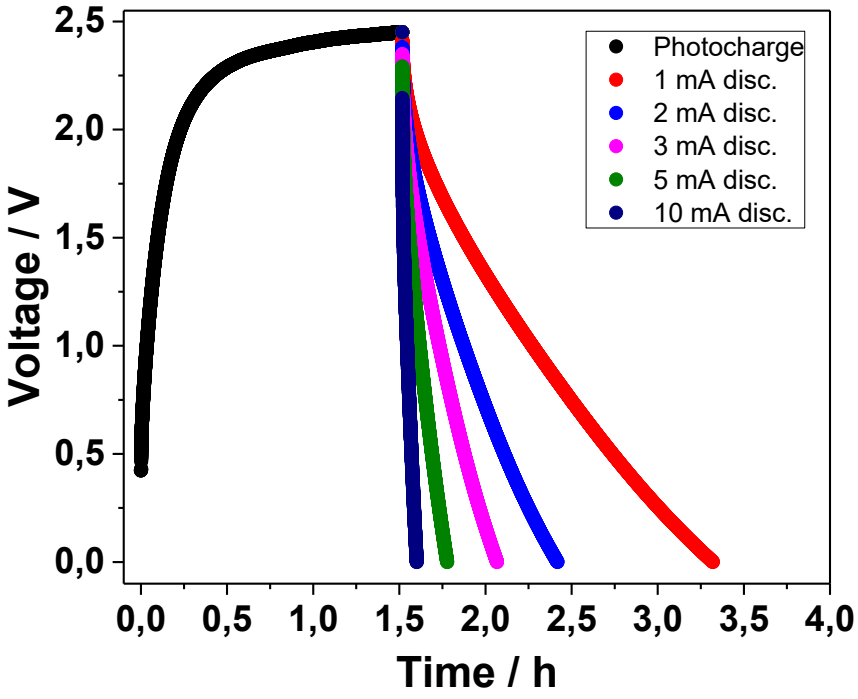

Figure 38: Photo-charging up to 2.45 V and subsequent discharging curves. Discharges were obtained in dark condition employing different current values ranging from 1 to 10 mA. Reprinted with permission from reference [45]**. Copyright 2018, Royal Society of Chemistry.**

In the first part of the photo-charge EDLC voltage linearly increased until it reached a plateau for a value slight lower than DSSM V_{OC}. This behaviour is totally

in accordance with IV DSSM profile since no evident decrease was experienced in photo-generated current with respect to the short circuit current, until the 70% of the DSSM V_{OC} was reached, during the potentiodynamic measurement. When voltage approached 2 V it started to continuously change the slope, accordingly to the decreasing DSSM current, until the profile appeared almost horizontal. The photo-charge was stopped to 2.45 V even if the voltage was still extremely slowly increasing. Keeping charging the system, EDLC voltage would have ideally reached DSSM V_{OC}. However, it seemed inappropriate for a HS device having charging time exceeding 1 h. To this purpose, this test was repeated stopping the photo-charge to 2V (Figure 39). In this case, the charging time was of 13.8 minutes.

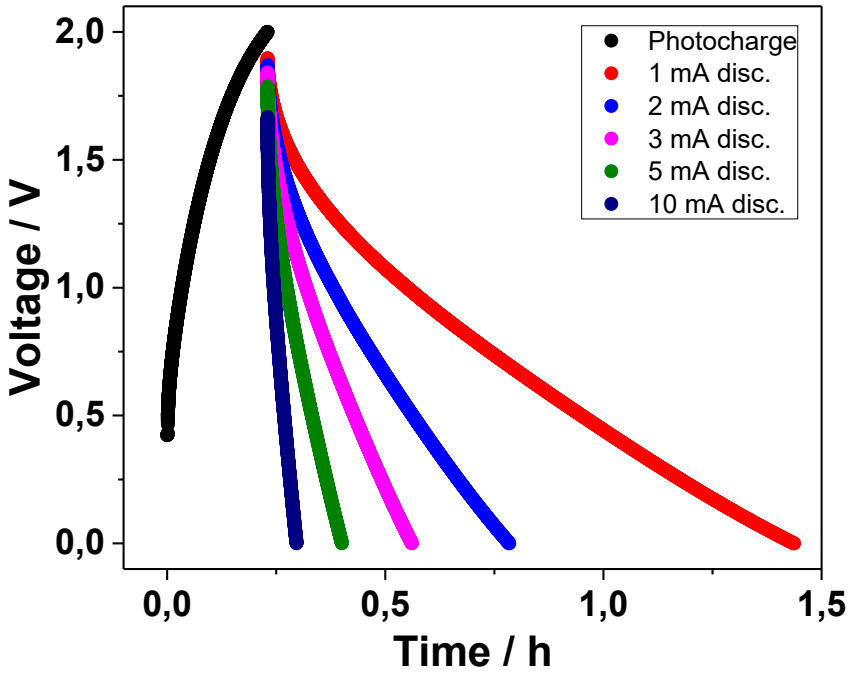

Figure 39: Photo-charging up to 2.45 V and subsequent discharging curves. Discharges were obtained in dark condition employing different current values ranging from 1 to 10 mA. Reprinted with permission from reference [45]**. Copyright 2018, Royal Society of Chemistry.**

It seems certainly a more reasonable value to wait for recharging a storage section that has to serve a sensor grid or an electronic portable device. Also in this case, the discharging curves were applied in a range between 1 and 10 mA referring to the whole EDLC. In both cases, appreciably linear profiles were found. This is not a trivial consideration, since in the only other work presenting a high voltage

PV-EDLC HS device, during discharge phase a fast decrease in voltage was experienced in the initial period of discharge. Thereby, discharge phase persists for few seconds at a voltage higher than 1 V. Chien et al.[62] ascribed this feature to the porosity saturation effect. In the perspective to drive a utilizer this is certainly a shortcoming which reduces potential usage of their powerpack.

In this regard, the work here proposed is the only example present in literature which can drive an electronic utilizer requesting a moderate voltage for more than 1 minute.

Efficiency of the whole device was calculated as previously reported in the dedicated paragraph of this chapter. In this case, the capacitance employed in the OPECSE calculation was evaluated from GCD measurement, turning into a value of 233 mF cm^{-2}.

The OPECSE profile, plotted as a function of the time is totally in accordance with literature (Figure 40A), as evidenced from previous reports.[46], [54], [58] Overall efficiency rapidly increased in the first photo-charge region. This is due to the fact that the energy stored into an EDLC is proportional to the square of the voltage and as already observed from photo-charge profile when an EDLC is connected to a PV device (ideally a current generator), initially, voltage linearly increases with time. However, while increasing the EDLC voltage the PV generator works in a different bias condition and consequently the photo-generated current diminishes. Thus, approaching the voltage plateau, the OPECSE numerator starts stabilizing while the denominator keeps linearly to increase. As time passes, it turns into an OPECSE reduction. Maximum OPECSE was obtained after approximately 8 min of photo-charge reaching 1.83% OPECSE. This is a remarkable value since the other report dealing with EDLC-PV module integration did not report the overall efficiency, but was surely lower being Chien et al. PV efficiency of 1.57%. In fact, OPECSE can be expressed as the product between PV efficiency and storage efficiency (see previous paragraph).

The maximum OPECSE was attained when the EDLC was charged to 1.63 V. Obtaining the best efficiency for a relatively high voltage is certainly a remarkable aspect since real applications such as sensors or electronic portable devices require units of Volts to be driven. In Figure 40B OPECSE was plotted as a function of the EDLC voltage. Interestingly, the condition in Figure 39, which corresponds to arrest the photo-charge at 2 V, gives an OPECSE of 1.65 %. This is the 90% of the maximum value, meaning that in the range between 1.5 V and 2 V the overall efficiency remains almost constant. In addition, 2 V represents also the 80% of the maximum achievable voltage (DSSM V_{OC}). According to literature DSSCs substantially improve their efficiency in real environment, when the

electromagnetic radiation is lower with respect to 100 mW cm^{-2}. Thus, a substantial increase of these OPECSE values can be expected during operations in outdoor environment.

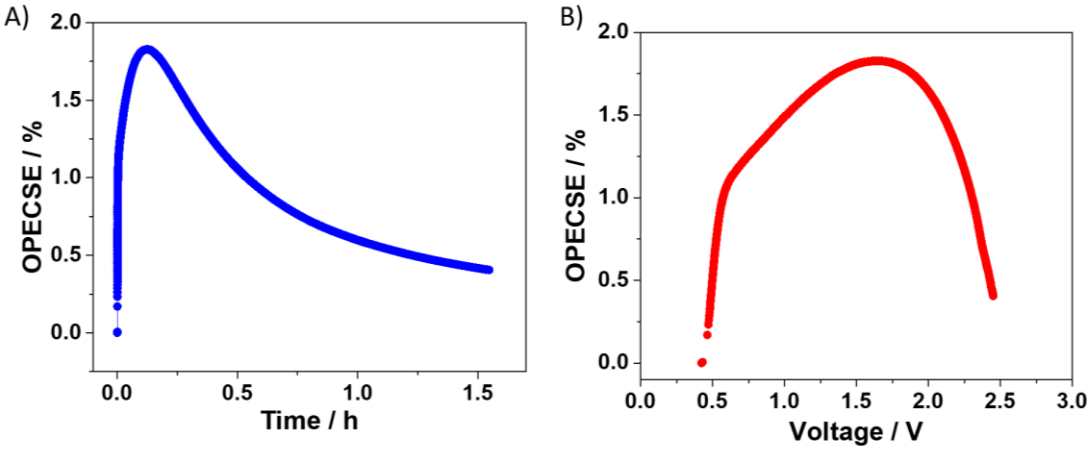

Figure 40: (A) OPECSE plotted as a function of the charging time. (B) OPECSE plotted as a function of the EDLC Voltage. Adapted with permission from reference [45]**. Copyright 2018, Royal Society of Chemistry.**

Table 8 reports for the three more significant conditions (maximum OPECSE, stopping photo-charge at 2 V, stopping photo-charge at 2.45 V) the ratio between EDLC voltage and DSSM V_{OC}, the time required to achieve that condition, the OPECSE calculated in that particular condition and the ratio between OPECSE and maximum OPECSE.

Evidently, for the last examined condition, the required photo-charging time dramatically increased and as a consequence the OPECSE was reduced with respect to the two other conditions.

A central remark from the engineering point of view must be done regarding Figure 40B. For a fixed OPECSE value two different EDLC voltages can be found, which correspond to two different times. In real applications circumstances the points at higher voltages are undoubtedly more appealing, considering also that the additional required time corresponds to few minutes.

Table 8: Voltage, time and OPECSE for the three most representative instant of photo-charge. Adapted with permission from reference [45]**. Copyright 2018, Royal Society of Chemistry.**

Voltage [V]	V/V_{OC} [%]	Time [m]	OPECSE [%]	OPECSE / max(OPECSE) [%]
1.63	63.4	7.9	1.83	100
2	77.8	13.8	1.65	90.1
2.45	93.4	91	0.41	22.2

Since frequently the energy stored into the storage section of a HS device is not immediately required after charging process an innovative test never reported previously in literature was adopted: after photo-charge, discharge profiles were obtained waiting 1 h of rest. The results obtained are reported in Figure 41.

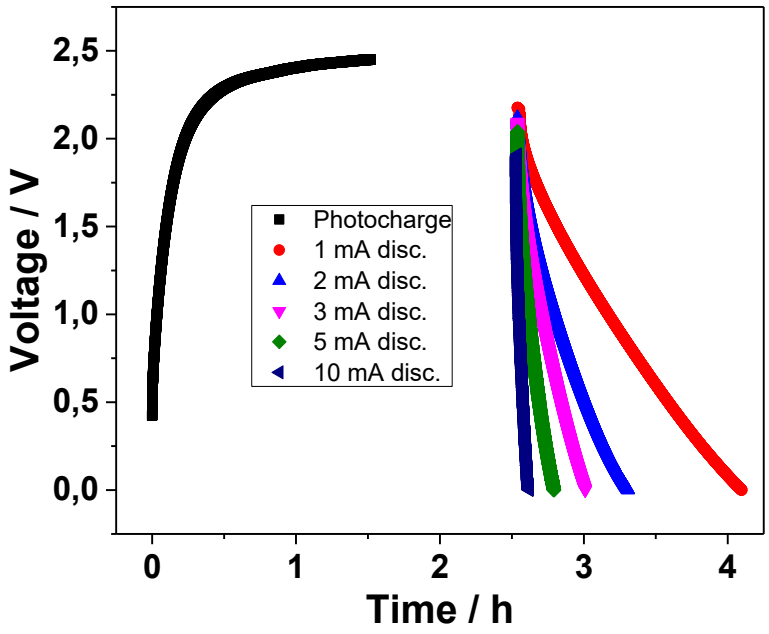

Figure 41: Photo-charging up to 2.45 V and subsequent discharging curves obtained after 1 h rest period. Discharges were obtained in dark condition employing different current values ranging from 1 to 10 mA. Reprinted with permission from reference [45]**. Copyright 2018, Royal Society of Chemistry.**

Figure 42, instead, reports the discharge capacity of the EDLC section after photo-charge, for the three different studied conditions. Respectively, blue squares refer to the condition in which the photo-charge was stopped to 2.45 V, green triangles refer to the condition in which the photo-charge was stopped to 2 V and red circles refer to the condition in which discharge was experienced subsequently to 1 h rest period. As expected, capacity diminished increasing the discharge current. Nevertheless, the capacity discrepancy between the case in which rest period was applied and the case in which discharge started immediately after reaching 2.45 V, was negligible.

For an imposed constant current of 2 mA (0.11 mA cm^{-2}) after reaching 2.45 V, a discharge capacity of 0.1 mAh cm^{-2} was obtained. Impressively, this value is nearly twenty times higher with respect to Chien et al.[62] (0.005 mAh cm^{-2}).

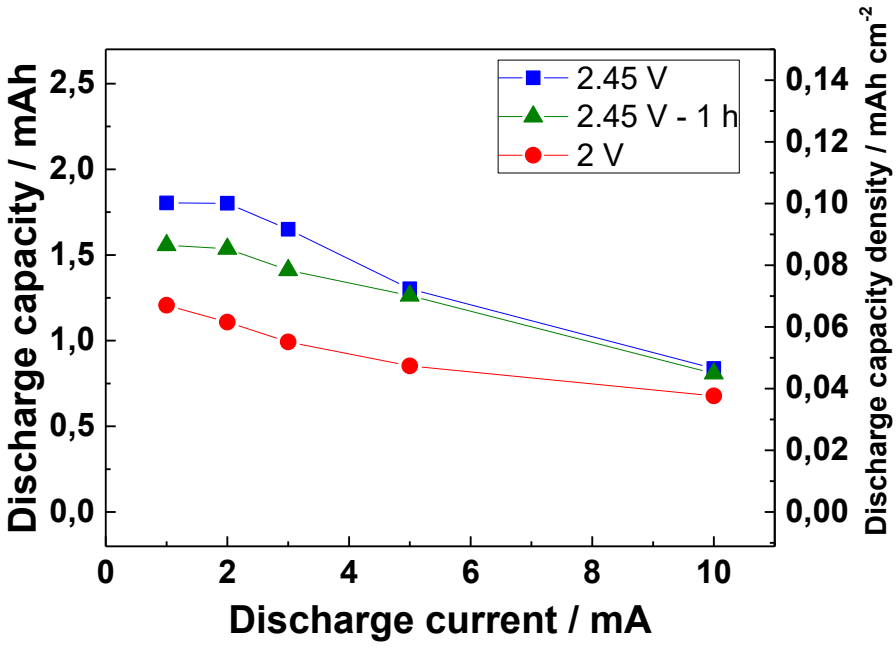

Figure 42: Discharge capacity as function of the discharge current for the three experiments performed. Reprinted with permission from reference [45]**. Copyright 2018, Royal Society of Chemistry.**

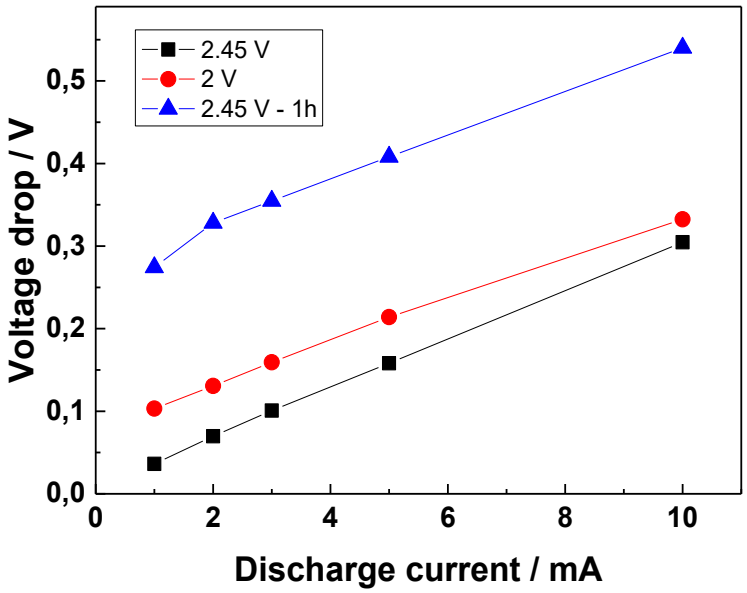

Figure 43: Voltage drop as a function of the discharge current for the three different cases.

This is not related to the current used, since in this work an even higher current density was employed (0.11 mA cm^{-2} with respect to 0.075 mA cm^{-2}).

In order to completely estimate the performance of the DSSM-EDLC integrated device, the voltage drop under the different discharging conditions was evaluated: results are plotted in Figure 43. In the case with 1 h rest period, the voltage drop accounts the total voltage decrement, thus including also EDLC self-discharge. In all cases, the voltage drops linearly increased enhancing the current applied. As expected, with the same current applied, the voltage drop for the case in which photo-charge was stopped to 2V was higher with respect to the "2.45 V photo-charge case". This is related to the fact that in the first case a larger total current variation is experienced, since the positive current during photo-charge is not quasi-null (the slope of the curve testifies how current provided by DSSM is still high when EDLC voltage reached 2V) as in the "2.45 V experiment".

HS device proposed in this paragraph present the highest maximum photo-voltage attained to date in literature. It was allowed by the high large voltage window of the ionic liquid electrolyte employed during EDLC fabrication.

4.7 ALL SOLID STATE ELECTRICAL DOUBLE LAYER HIGH VOLTAGE PHOTOCAPACITOR EMPLOYING PEO-PYR_{14}TFSI ELECTROLYTE

In this section, a novel solid-state-EDLC-based HS device,[76] obtained with similar fabrication procedures with respect to the photo-capacitor proposed in the previous paragraph, is reported. The same harvesting structure was employed; namely a W-type DSSM with 4 serially connected cells. The main difference stands in the EDLC section which was fabricated with a polymeric electrolyte instead of adopting the ionic liquid previously utilized. In particular, the electrolyte is a mixture of polyethylene oxide and N-butyl-N-methylpyrrolidinium bis(trifluoromethanesulfonyl)imide, PEO-Pyr14TFSI. As usual, EDLC was characterized individually in order to evaluate storage section features before efficiently demonstrating the integration with the harvester section. The DSSM was able to photo-charge the EDLC section close to the harvester V_{OC}. In this case, the photo-charging time was lower in comparison to the Pyr_{14}TFSI electrolyte-based HS device, since the capacitance of the all solid-state EDLC was found to be one order of magnitude lower. Also in this case, photo-charge and subsequent discharge profiles were recorded stopping charge to 2.45 V. Thus, direct comparison in terms of discharge capacity can be made between the two devices.

4.7.1 EXPERIMENTAL SECTION

The DSSM harvester was the same employed in the previous paragraph (*HIGH VOLTAGE PHOTOCAPACITOR: DYE SENSITIZED SOLAR MODULE AND PYR_{14}TFSI IONIC LIQUID ELECTRICAL DOUBLE LAYER CAPACITOR INTEGRATION*), thus here fabrication is omitted to avoid redundancy.

ALL SOLID-STATE EDLC FABRICATION

FTO conductive glass was cut in 7.5 x 6 cm^2 plates using a diamond glass-cutter. The plates were then used as substrates and current collectors. The slurry active material was obtained dispersing 90 mg of activated carbon, 5 mg of conductive carbon and 5 mg of binder (CMC) in 5 mL ultrapure water. Subsequently, the aqueous slurry was doctor bladed onto the cut glasses from the conductive sides into a 4 x 4.5 cm^2 area, employing adhesive tapes to delimitate the deposition surface. This limited area was adopted with respect to the whole glass surface in order to properly seal the EDLC and for contacting electrodes during

measurements (leaving additional space from one side). A symmetrical loading was adopted for the two electrodes, which were pre-dried overnight at a moderate temperature (80 °C) and afterwards dried under vacuum at 130 °C for 12 h.

Solid state electrolyte was prepared as reported by Sharova and co-workers [77]. PEO:Pyr_{14}TFSI had a molar ratio of 2:1. A 5% weight (relative to the PEO weight) benzophenone was also part of the electrolyte mixture.

At first, benzophenone was dissolved in Pyr_{14}TFSI. Subsequently, PEO was mixed until the mixture appeared a solid material. Afterwards, the electrolyte was vacuum sealed in a pouch bag and annealed at 100 °C for 12h. Then, small portions were placed between Mylar foils (PPI) and pressed at 100 °C by means of a hot press. In this way, the final thickness was approximately 100 μm. UV irradiating for 6 min[78] electrolyte was therefore cross-linked.

Hence, the obtained polymer electrolyte was placed between two EDLC glasses electrodes and hot-pressed. In Figure 44 the resulting EDLC device is observable.

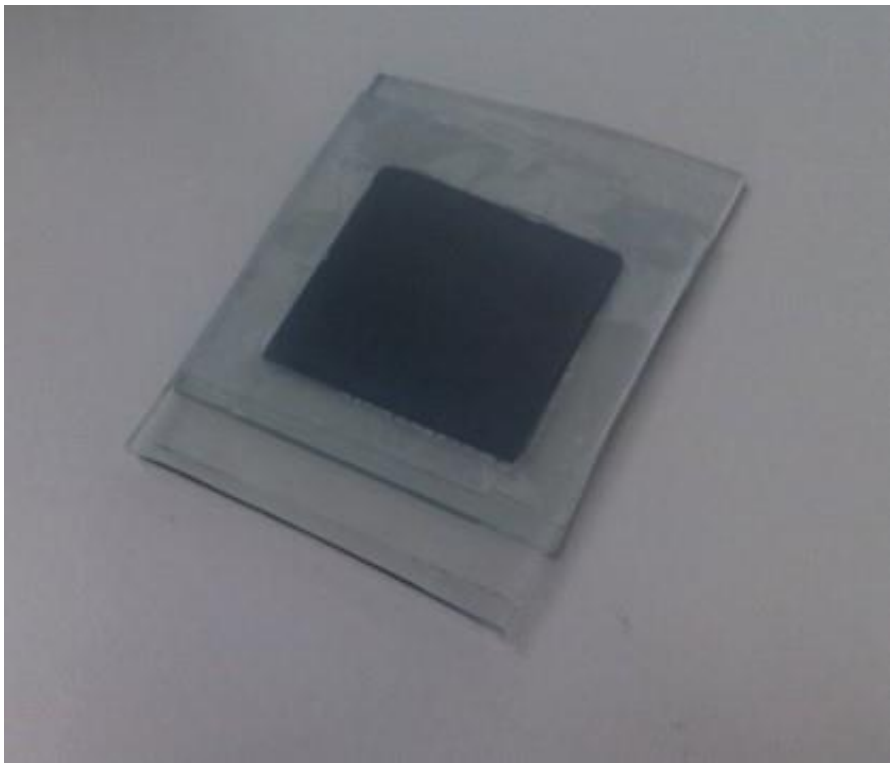

Figure 44: Picture of the all-solid-state EDLC. Reprinted with permission from reference [76]**. Copyright 2018, Frontiers in Chemistry.**

DSSM AND EDLC INTEGRATION

Integration process between harvester and storage sections was obtained as reported in the previous paragraph (HIGH VOLTAGE PHOTOCAPACITOR: DYE SENSITIZED SOLAR MODULE AND $PYR_{14}TFSI$ IONIC LIQUID ELECTRICAL DOUBLE LAYER CAPACITOR INTEGRATION). Figure 45 shows the photo-capacitor front view.

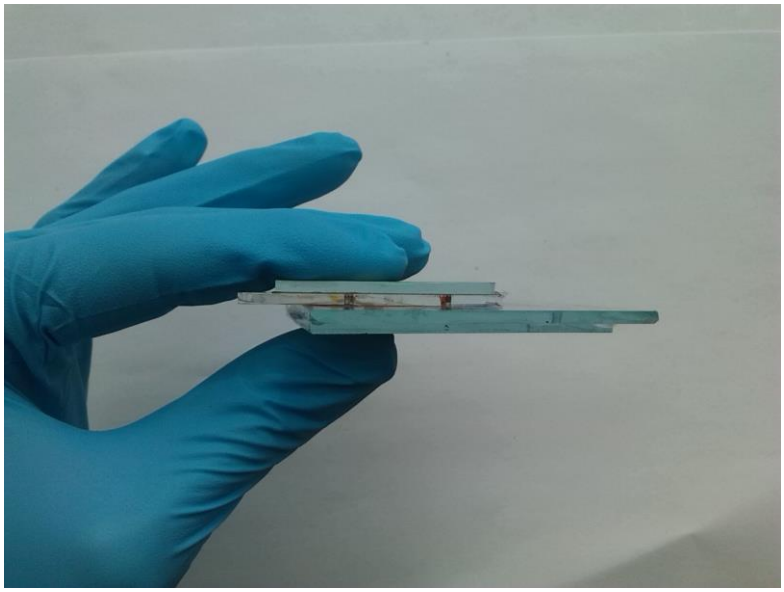

Figure 45: Front view of the HS device. Adapted with permission from reference [76]**. Copyright 2018, Frontiers in Chemistry.**

4.7.2 RESULTS AND DISCUSSIONS

EDLC section was carefully characterized through GCD and EIS. Moreover, a long-term stability was performed in order to ensure that the storage section could have been successfully employed in a HS device which expects dozens or even hundreds of cycles during a single day. Figure 46A shows the GCD measurement profile for an imposed constant current of 2 mA which results in a current density of 0.11 mA cm^{-2}. The shape of the curve clearly demonstrates a deviation from the ideal capacitive response. The moderate FTO glass electrical conductivity and the limited PEO-$Pyr_{14}TFSI$ ionic conductivity are responsible of such a behaviour.

Due to the non-linearity of the discharging curve, the capacitance was precisely evaluated according to the following unconventional equation:

$$\frac{1}{2} C_A V_M^2 = i \int_{t_{i.d}}^{t_{f.d}} V \, dt = E_{EDLC}$$

where C_A stands for the capacitance, V_M is the maximum voltage, $t_{i.d}$ is the initial discharge time and $t_{f.d}$ is the final discharge time and E_{EDLC} is the energy related to discharge.

In this way, the capacitance value was mediated (C_A) through the whole discharge profile and was representative of the energy effectively stored in the EDLC section.

The average capacitance was calculated to be 0.16 F. The normalized value was 9 mF cm^{-2}, which resulted four times higher with respect to the sole example reported in literature (except the works presented in this PhD thesis) dealing with high voltage photo-capacitors.[62]

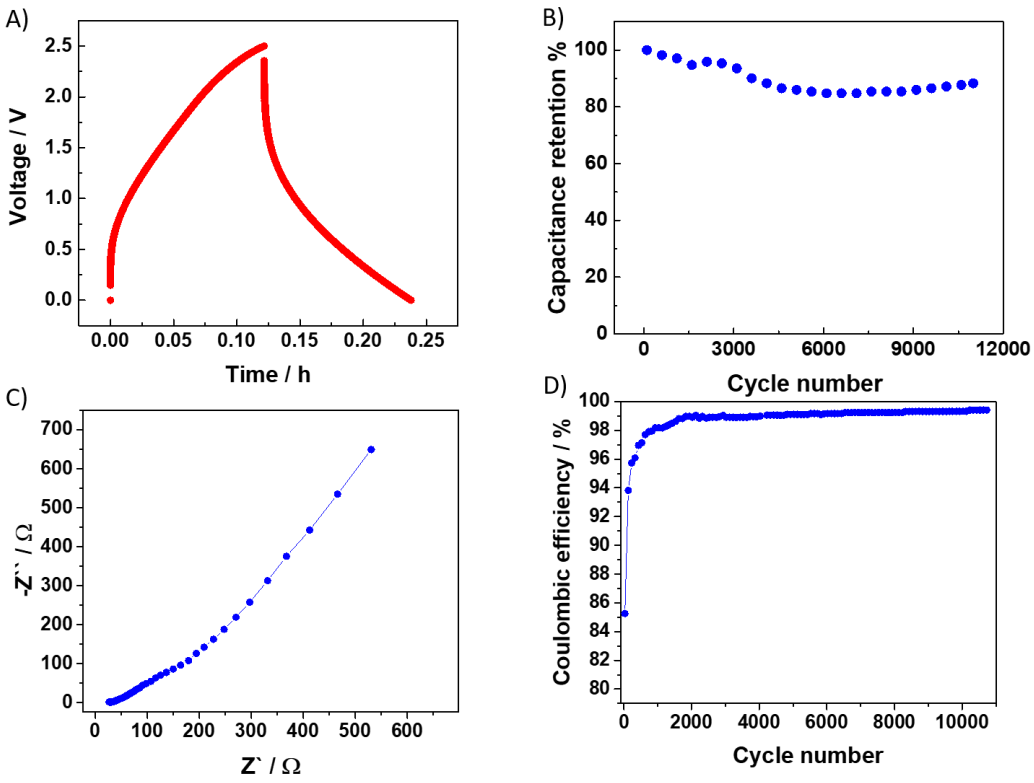

Figure 46: (A) GCD measurement performed at 2 mA. (B) Capacitance retention of the all-solid-state EDLC. (C) EIS. (D) Coulombic efficiecny of the storage section. Reprinted with permission from reference [76]. **Copyright 2018, Frontiers in Chemistry.**

This achievement obtains even more significance, given that the all-solid-state EDLC resulted more performing than an organic liquid electrolyte-based EDLC, thus proving remarkable electrochemical performance.

Furthermore, the polymer electrolyte-based EDLC did not show evident degradation through GCD. Conversely, in Chien et al. a plateau at 2V is clearly observable, demonstrating that the EDLC here presented possesses remarkable stability in the tested voltage window, which is difficult to find in high voltage PV-EDLC integrated devices literature.

Figure 46B reports the EDLC capacitance retention for more than 10 000 GCD cycles performed at 20 mA (1.11 mA cm^{-2}). A slight decrease in capacitance was experienced during the first 3,000 cycles. Afterwards the capacitance stabilized at about 90% of its initial value.

Figure 46C shows the PEO-Pyr_{14}TFSI-based EDLC EIS. In accordance to Zhang et al.[21] the equivalent series resistance (ESR) was estimated at a frequency of 1 kHz by the real part. This procedure led to a value of 33.8 Ω. Nearly the same value was found (36 Ω) from GCD evaluating the ESR by the ratio between voltage drop and applied current. Also in this case, certainly, a predominant part of the ESR was related to the FTO glass substrate resistance. However, if compared to the previous work in which the pure ionic liquid was employed as electrolyte (26.8 Ω), the PEO-Pyr_{14}TFSI provided an evident ESR increase. In the intermediate frequency region, a linear profile with a slope close to 45° is observed, which is ascribed to the limited ion diffusion in the electrodes pore structure. In the low frequency region, the profile is not parallel to the y-axis, meaning that the EDLC does not outperform as an ideal capacitor even for extremely low frequencies.

In Figure 46D the coulombic efficiency related to the long-term stability performed at 20 mA (1.11 mA cm^{-2}) is reported as a function of the cycle number. It stayed always higher than 99% except for an initial activation process region.

IV measurement is reported in the previous paragraph together with the corresponding power-voltage curve.

Figure 47 compares the GCD curves of the PEO-Pyr_{14}TFSI-based EDLC with the pure ionic liquid EDLC. Completely different charging-discharging times were obtained for the same current applied (2 mA), thus providing an order of magnitude difference in capacitance values.

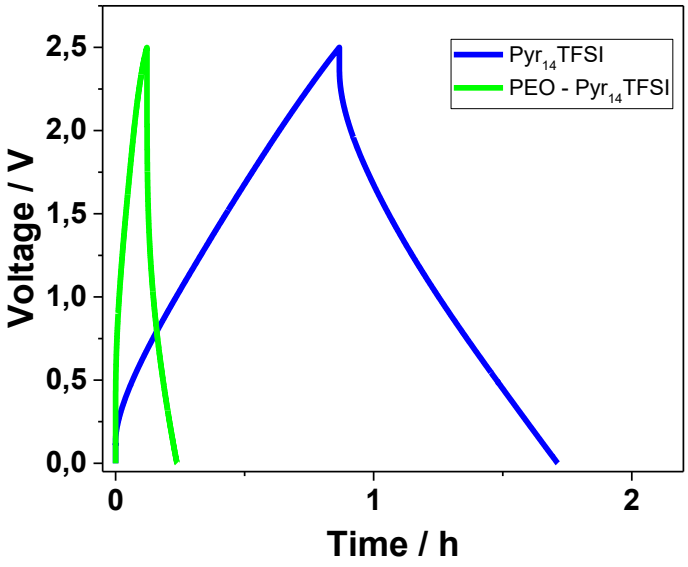

Figure 47: GCD measurements of the EDLC proposed in this paragraph (solid-state electrolyte) and of the $Pyr_{14}TFSI$-based EDLC of the previous paragraph.

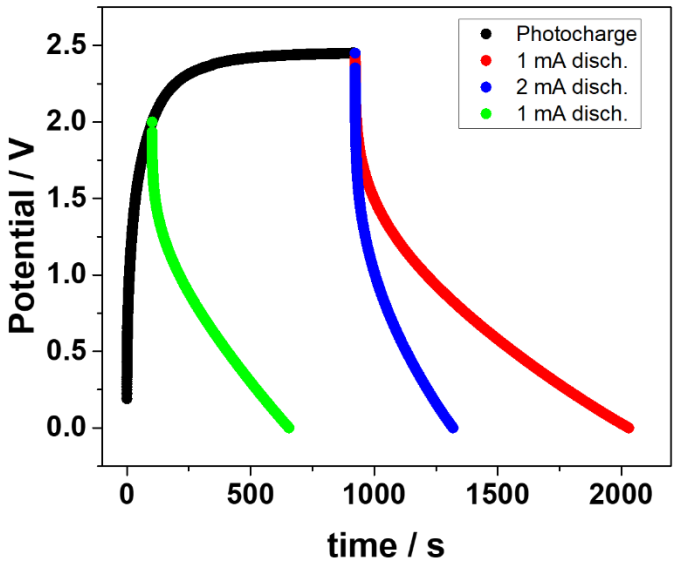

Figure 48: Photo-charge and discharges curves. Reprinted with permission from reference [76]**. Copyright 2018, Frontiers in Chemistry.**

Figure 48 shows the photo-charge-discharge profiles of the al-solid-state-EDLC-based HS device. As experienced in previous works, in the first part of the photo-charge, EDLC voltage rapidly increased. When it reached 2 V the curve started to change the slope and after 300 s it became nearly horizontal. Increasing the EDLC voltage, constrained the DSSM to work in a condition in which the generated current continuously diminished. Thus, if initially, a PV-harvester connected to a storage section works as an ideal current generator, for long periods it acts as an ideal voltage generator and the voltage provided to the storage unit is the V_{OC}. As in the related work[45] the charge was stopped to 2.45 V. Thus, in this case, direct comparison between the two HS devices in enabled.

As evidenced in Figure 48, two negative currents were applied in dark conditions, namely 1 mA (0.056 mA cm^{-2}) and 2 mA (0.11 mA cm^{-2}). The first current provided a discharge capacity of 0.017 mAh cm^{-2}. Compared to the liquid counterpart ($Pyr_{14}TFSI$) discharge capacity was decreased by a factor 6.

In Figure 48 is also reported the case in which the charge was limited to 2V. This test was made in order to investigate the HS device performance upon shorter photo-charging time, since this situation can be related to applications requiring subsequent user requests.

Figure 49A shows OPECSE as a function of the charging time. The plotted profile is totally in accordance with literature and presents a maximum for the first seconds of the test. The highest value was calculated to be 1.67%. Then, from the time related to the highest value, OPECSE decreased exponentially, since EDLC voltage approached the plateau and the stored energy did not increase considerably. Conversely, radiation kept to imping onto the solar module without producing a significant power output.

The first 50 s of photo-charge are shown in the inset in Figure 49A. This condition was highlighted, since 50 s appear an interesting charging step to be exploited in applications requiring power periodically, such as sensor stations performing intermittent measurements. Interestingly, a 50 s charging time corresponds to an EDLC voltage of 1.7 V and to a still remarkable efficiency, corresponding to 60% of the maximum OPECSE.

In Figure 49B the OPECSE is also plotted as a function of the EDLC voltage. In this case, the maximum was found for 0.6 V and afterwards it decreased almost linearly.

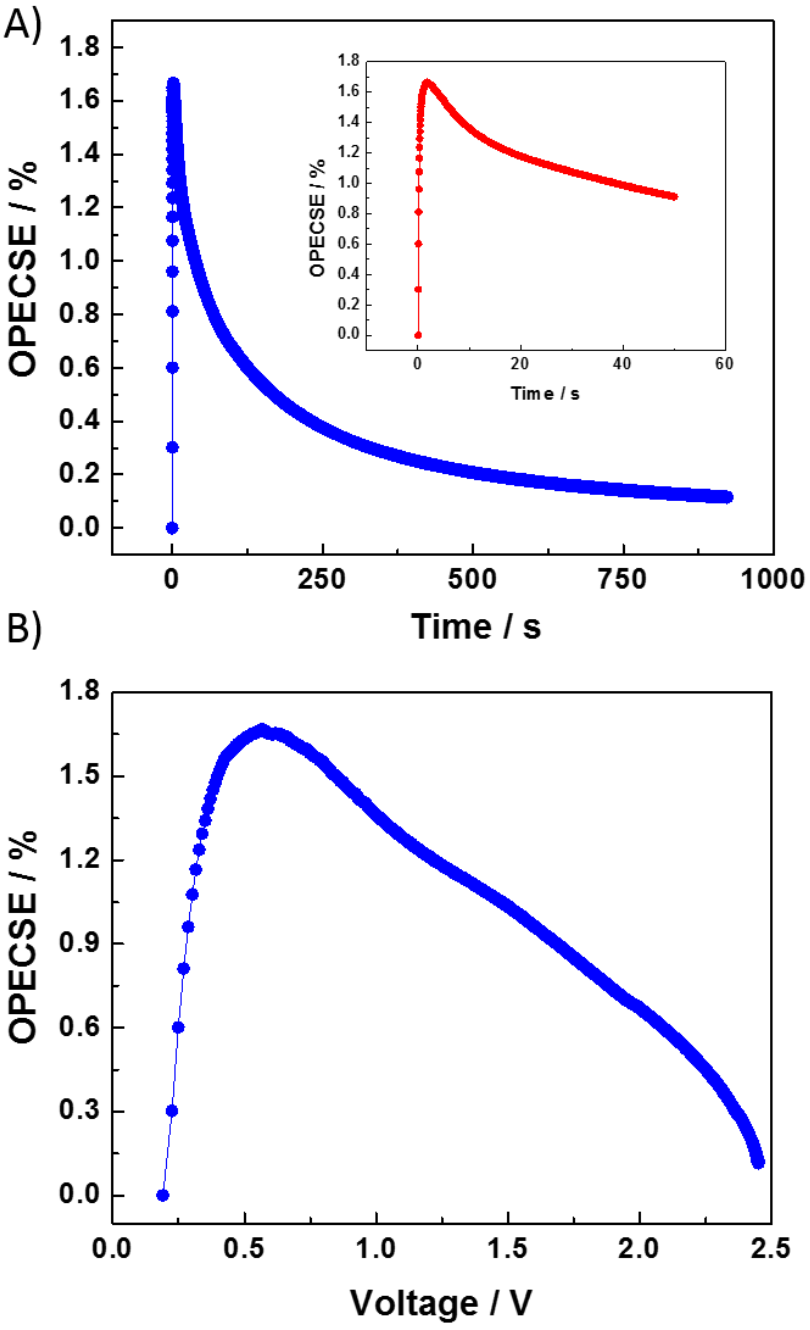

Figure 49: (A) OPECSE plotted as a funtion of the time. (B) OPECSE plotted as a function if the voltage. Reprinted with permission from reference [76]**. Copyright 2018, Frontiers in Chemistry.**

In this work, the principal aim was assessing the feasibility of all-solid-state EDLC employment in HS devices. Voltage window of the utilized polymer electrolyte exceeded the maximum voltage achieved while photo-charging the storage unit. Thus, allowing to obtain a highly stable and reliable integrated device.

Overall, it must be stated that EDLCs of the HS devices proposed in paragraph 4.6 and 4.7, which were obtained onto conductive glass substrates cannot be compared to conventional EDLCs since the poor electronic conductivity of the FTO deposited onto the glass substrate is much less if compared to conductivity of conventional metal substrates. This hindered EDLCs performance especially in terms of current density (lower than 1 mA cm^{-2}).

4.8 IN PLANE INTEGRATION OF ENERGY CONVERSION AND STORAGE DEVICES EMPLOYING MULTIPOLYMER ELECTROLYTE MEMBRANE

In this paragraph a novel polymer-based platform is used for the production of an original two-electrodes HS device. The multifunctional polymeric layer was prepared with two poly(ethylene glycol)-based sections which were separated by a perfluorinated barrier. The whole platform was fabricated by means of oxygen-inhibited UV-light crosslinking procedure.

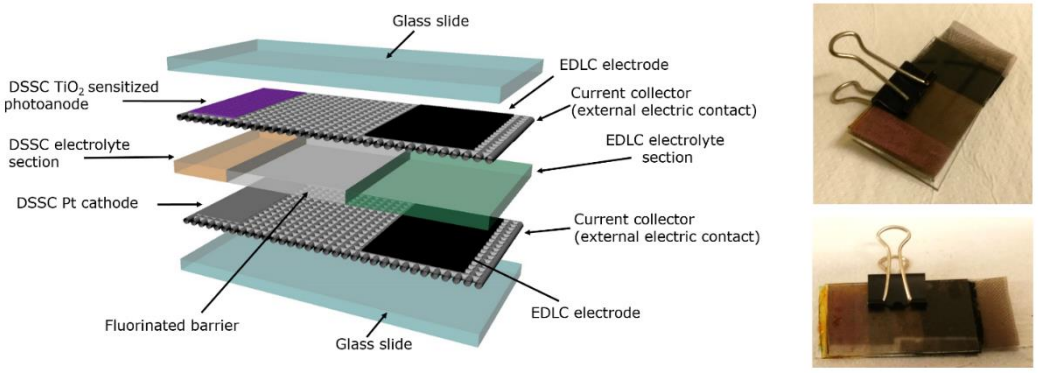

Figure 50: Scheme and pictures of the multifunctional polymer electrolyte photo-capacitor. Reprinted with permission. Copyright 2018, Elsevier.

The harvesting section of the polymeric layer was designed in order to enable iodide/triiodide diffusion in a DSSC, while the opposite side permits ions diffusion in an EDLC storage unit. The obtained HS integrated device possesses a planar

architecture which is considerably simplified if compared to literature reports, thus lending itself to easy and smart exploitation in low power electronics. The maximum OPECSE was 3.72%. This is one of the highest values reported so far in literature for DSSC-EDLC HS devices. Figure 50 shows scheme and pictures of the integrated HS device.

4.8.1 EXPERIMENTAL SECTION

ELECTRODES PREPARATION

Titanium grids were employed as current collector and substrates. Grids were cut in 6 x 2.5 cm^2 pieces before cleaning with two ultrasonic baths, respectively in acetone and ethanol. Then, they were dried by means of a hot plate set at a temperature of 100 °C under nitrogen flow.

DSSC electrode directly exposed to sunlight was manufactured by doctor blading a uniform 80 μm thick layer of TiO_2 commercial paste (18NR-AO) in a 1 × 2.5 cm^2 portion onto one side of the Ti grid. The grid was then sintered at a temperature of 515 °C for 30 minutes.

The grid was incubated for 12 h in a 0.3 mM N719 solution employing ethanol as solvent. The DSSC cathode was fabricated by sputtering a 5 nm thick Pt layer onto the second Ti grid, employing a mask to avoid Pt deposition onto the whole mesh and confining the Pt deposition to the DSSC section.

EDLC electrodes were obtained by depositing 80 μm thick layers of active material slurry: Norit SA SUPER activated carbon mixed with 5% poly(vinylidene fluoride) added in excess of dimethyl sulfoxide (DMSO). The EDLC surface was designed to be 2 × 2.5 cm^2. After a 3 h rest period, electrodes were dried by means of a hot plate set at 100 °C to ensure DMSO evaporation. A 1 × 2.5 cm^2 free space was designed on the far right hand side of the grids for electrical connections during measurements and a 2 × 2.5 cm^2 free space was left between DSSC and EDLC electrodes for hosting the fluorinated polymer separator.

MULTIFUNCTIONAL POLYMER ELECTROLYTE MEMBRANE PREPARATION

The polymer membrane was fabricated by means of oxygen-inhibited UV-curing. At first, photo-initiator (3% by weight with respect to the whole blend) was

added to perfluoropolyether Fluorolink MD700 monomer. The liquid mixture was casted onto the central (2 × 2.5 cm^2) part of the rear Titanium grid. This section was delimited by two 100 µm tapes in order to avoid liquid propagation mixture in EDLC or DSSC regions. The structure was sandwiched between two transparent glasses before irradiating.

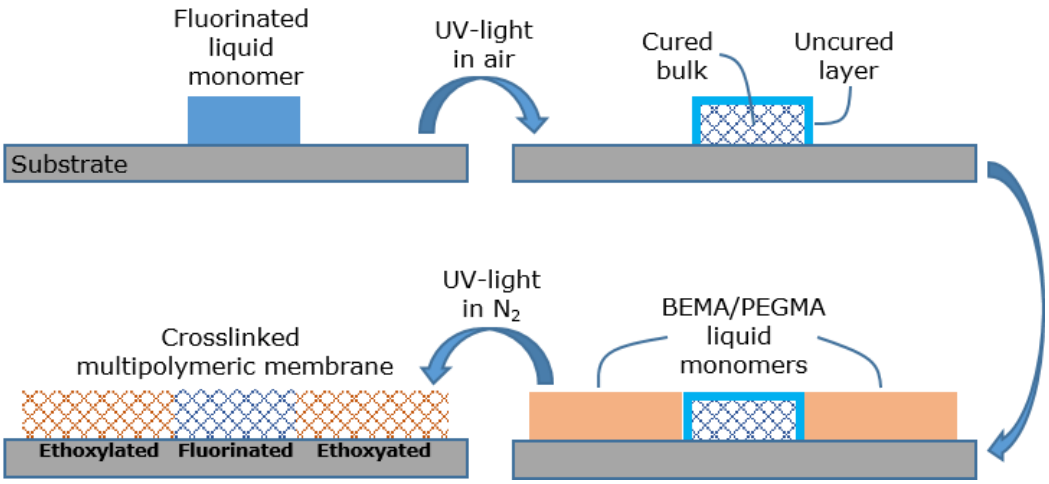

Figure 51: Scheme of the preparation process of the multifunctinal polymer electrolyte. Reprinted with permission. Copyright 2018, Elsevier.

UV radiation intensity was 30 mW cm^{-2}, generated by a medium vapour pressure Hg lamp in air atmosphere. The blend was left underneath UV lamp for 2 min. Even if the inner part was perfectly cross-linked after UV irradiating, the presence of oxygen inhibited the crosslinking of the surface. This left a thin layer of uncured liquid reactive monomer on the external sides and edges of the fluorinated section. Subsequently, 100 µm tapes were removed and a polymer blend composed by 35 wt% BEMA and 65 wt% PEGMA was casted in contact with the barrier layer on both edges of the fluorinated barrier. Tapes were placed on the borders of the rear glass in such a way that also the new electrolyte regions had a thickness of 100 µm. Also in this case a 3 wt% radical photo-initiator was added to the blend in order to promote UV-polymerization. The structure was, also in this case, sandwiched between two transparent glasses and irradiated for 2 min but with the adjustment to flow nitrogen onto the polymer matrix in order to avoid that oxygen inhibited surface crosslinking, thus obtaining a compact and fully cross-linked multifunctional matrix. Afterwards, the electrolyte sections were swelled in two different liquid electrolytes, adding some drops onto the corresponding EDLC or DSSC section. For the EDLC region was employed a 2 M sodium chloride

aqueous electrolyte, while for the DSSC section an iodine-based liquid electrolyte was used: 0.45 M sodium iodide, 0.056 M iodine and 0.55 M 4-tert-butylpyridine dissolved in acetonitrile (ACN). Then, the upper Ti grid containing the DSSC photoanode was placed onto the multifunctional polymer matrix in order to obtain the final device. The assembly was consolidated by applying a clip as can be seen in Figure 50. The complete multifunctional polymeric membrane fabrication procedure is sketched in Figure 51.

4.8.2 RESULTS AND DISCUSSION

POLYMER MEMBRANE CHARACTERIZATION

In Figure 52 are presented: pictures of the multifunctional polymeric membrane before and after swelling in liquid electrolytes and attenuated total reflectance Fourier transform infrared (ATR-FTIR) spectroscopy performed on the three membrane sections before swelling.

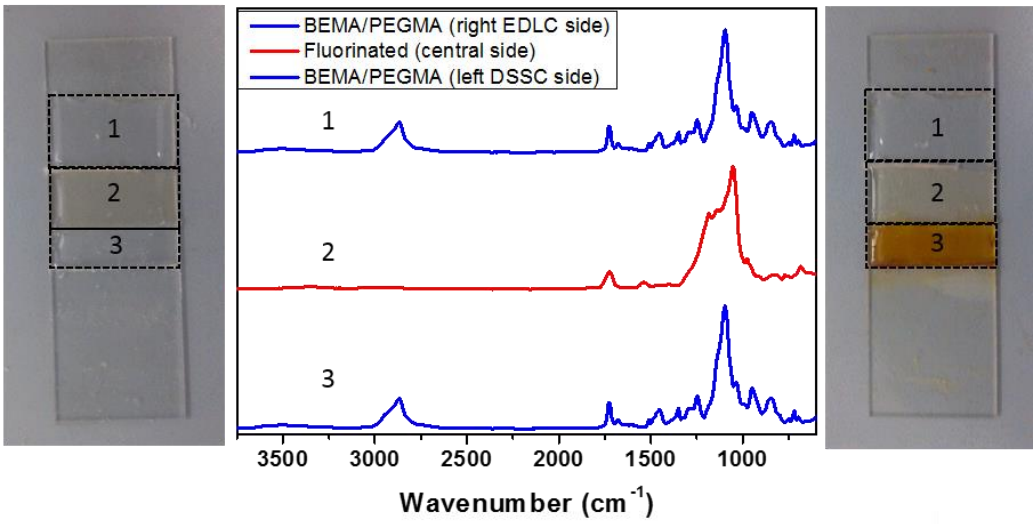

Figure 52: ATR-FTIR spectra of the three different sections of the multifunctional polymer membrane and pictures of the multifunctional polymeric membrane before and after swelling. Reprinted with permission. Copyright 2018, Elsevier.

ATR-FTIR analysis enabled to evidently discriminate the BEMA/PEGMA profile from the fluorinated barrier unit. In the external regions are observed signals

of the methylene groups (~2800 cm^{-1}) and of the carbonyl unit of the acrylic groups (1730 cm^{-1}). In the barrier layer the characteristics C–F stretching is observed at 1074 and 1127 cm^{-1}. In addition, in both the ethoxylated and fluorinated sections, the characteristic signal of (meth)acrylic double bonds at 1640 cm^{-1} is absent, confirming the complete crosslinking upon UV-curing.

Contact angle measurements were performed employing a coloured solution (see Figure 53). A drop of the liquid was carefully laid by means of a pipette at the interface between two different (BEMA/PEGMA) and fluorinated barrier regions. When the liquid got in contact with the heterogeneous surface it instantaneously moved toward the ethoxylated side. As can clearly recognized by photographs taken with 10 s interval time the liquid was completely adsorbed by BEMA/PEGMA membrane section in less than 2 min. Conversely, the fluorinated barrier did not show coloured solution presence being hydrophobic in nature. Thus, demonstrating its capability to act as separator for the two ethoxylted sections containing two different liquid electrolytes.

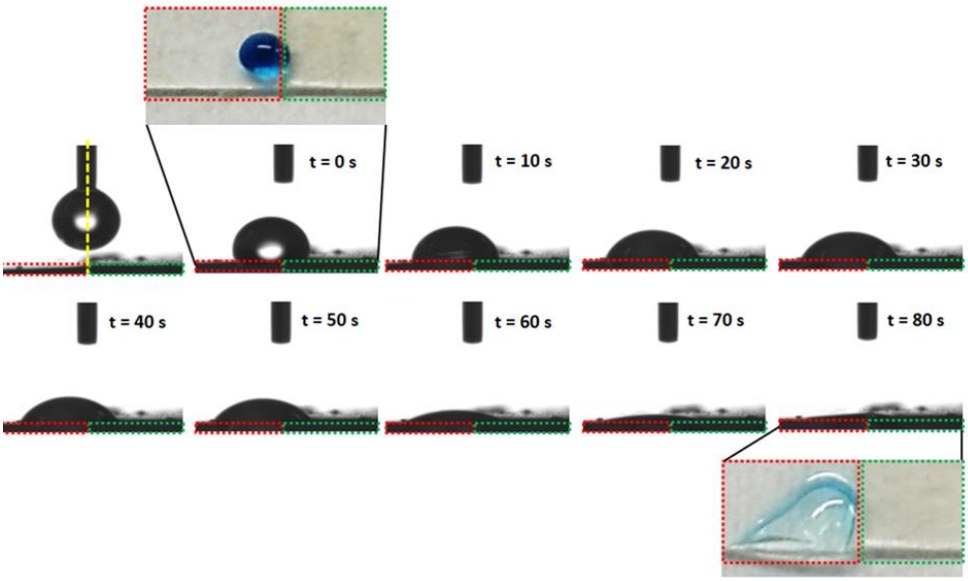

Figure 53: Contact angle measurements for 80 s. Pictures were taken at intervals of 10 s. Reprinted with permission. Copyright 2018, Elsevier.

EDLC AND DSSC SECTIONS CHARACTERIZATION

Storage unit was carefully characterized by GCD, CV, long-term stability and EIS. Evidently, an improved electrochemical response was experienced with respect to the previous HS device based on the same polymer electrolyte. [63] This was ascribed to a thinner PEM thickness (nearly 100 μm in this work with respect to 240 μm in the previous publication). Such a different choice was performed since in the previous flexible configuration an extremely remarkable mechanical stability was sought, expecting a huge amount of bendings during the HS device lifetime. In this new proposed structure, the PEM does not need to be bent, being fabricated in a planar configuration. GCD measurement testify an increased coulombic efficiency (see Figure 54A). In fact, only for the lowest current applied a value approaching 95% was obtained. In all the other cases, presenting a higher current density, a value close to 99% was attained. The improvement is likely ascribed to the much lower path ions need to accomplish in the polymer matrix. This results in a lower electrolyte bulk resistance.

Overall, the triangular shape accounts for noteworthy electrical double layer capacitor characteristics. Capacitance was evaluated through equation reported in chapter 3 in the paragraph *Galvanostatic charge discharge*.

Figure 54B shows EDLC CV profiles obtained for a scan rate range between 1 and 20 mVs^{-1}. For the lowest applied scan rates a somewhat defined rectangular shape is obtained. Increasing the scanning, led to a less rectangular profile with a higher resistive component, even if highly symmetrical behaviour was still obtained in charging and discharging phase.

In this case capacitance was calculated through the equation reported in chapter 3 in the paragraph *Cyclic voltammetry*.[21]

The capacitance values calculated from GCD and CV are plotted in Figure 54C. Values obtained from GCD cycles were found to be generally higher with respect to values obtained through CVs. This occurred even if the time interval needed to complete a CV cycle was higher if compared to the corresponding GCD (1 mVs^{-1}/0.07 Ag^{-1}; 5 mVs^{-1}/0.1 Ag^{-1}; 10 mVs^{-1}/0.17 Ag^{-1}; 20mVs^{-1}/0.35 Ag^{-1}). This can be related to the resistive behaviour observed during CV measurements, which led to a distorted rectangular profile.

Long-term performance was tested through consecutive CVs. Figure 54D shows capacitance retention of the EDLC unit for more than 10 000 cycles. As can be clearly observed, results demonstrated an appreciably capacitance retention. Indeed, at the end of the test, EDLC retained 97% of its initial capacitance.

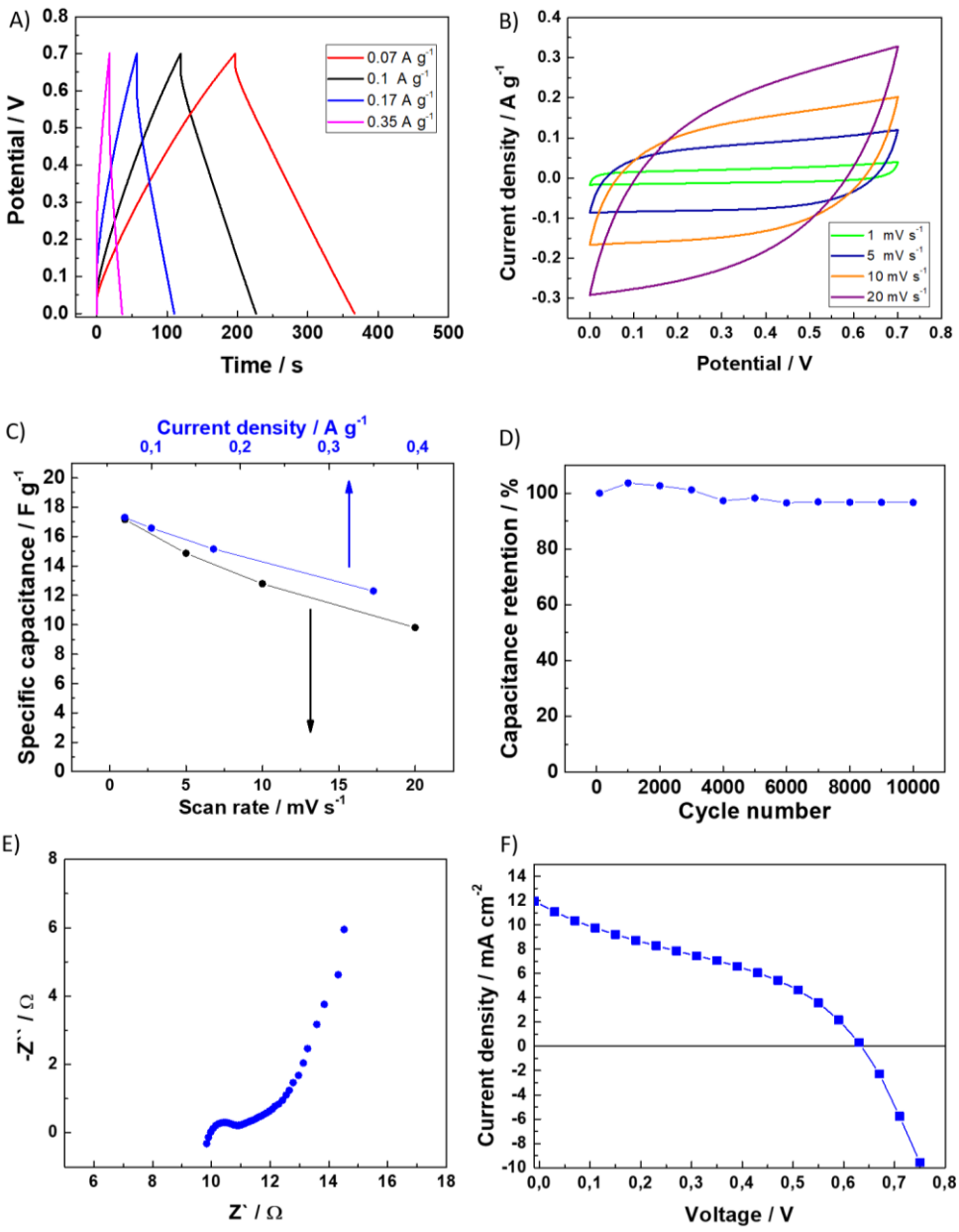

Figure 54: (A) GCD measurements performed in the current range between 0.07 A g^{-1} and 0.35 A g^{-1}. (B) CV measurements performed in the current range between 1 mV s^{-1} and 20 mV s^{-1}. (C) Specific capacitances values reported as function of scan rates and current density. (D) Capacitance retention. (E) EIS of a 1 × 2 cm^2 EDLC. (F) IV measurement of the DSSC part. Reprinted with permission. Copyright 2018, Elsevier.

EIS was also performed onto a 1 × 2 cm^2 EDLC unit (see Figure 54E). The equivalent series resistance resulted 21.8 Ωcm^2, which is in accordance with the best literature reports recently published in the field of all-solid-state EDLC.[38], [39]

Figure 54F shows the DSSC IV characteristic under 1 Sun irradiation (STC conditions). Peculiar parameters are summarized in Table 9: η_C stands for the PV efficiency corrected with respect to the active surface of the Ti grid.

A worthy short circuit current density was obtained if compared to previous works.[20], [63] This was probably due to the use of ACN instead of MPN, having the first a lower viscosity with respect to the latter. However, unfortunately, a low FF (34%) was achieved due to a high series resistance of the cell, which was nevertheless already shown for these quasi-solid-electrolytes-based (BEMA/PEGMA) DSSC.[20], [63]

This behaviour is certainly related to a non-perfect electrode-electrolyte interfacial contact.

Table 9: Peculiar PV parameters of the DSSC section. Reprinted with permission. Copyright 2018, Energy.

η [%]	η_C [%]	V_{OC} [V]	j_{SC} [mA cm^{-2}]	V_{MP} [V]	j_{MP} [mA cm^{-2}]	*FF* [%]
2.60	4.33	0.63	11.96	0.43	6.05	34

HS DEVICE CHARACTERIZATION

Integration was tested through photo-charge and subsequent constant current discharge. The EDLC electrodes were electrically connected to a Source measure unit (2440 Keithley) in order to obtain photo-charging and constant current discharging voltage profiles, which are shown in Figure 55A. During photo-charge, the integrated device was placed in the solar simulator, while generating 100 mW cm^{-2} electromagnetic power density (STC). Charge was stopped to 0.55 V even if the EDLC voltage was still slowly increasing. As aforementioned, this plateau is related to the energy harvester V_{OC}, which hinders the maximum achievable voltage upon charging. Discharge response was investigated in a current densities range

between 0.6 mA cm^{-2} (3 mA discharge current of the whole EDLC) and 2 mA cm^{-2} (10 mA discharge current of the whole EDLC). As clearly evidenced in Figure 55A, an increasing voltage drop was found upon discharging the storage unit by applying a higher current density.

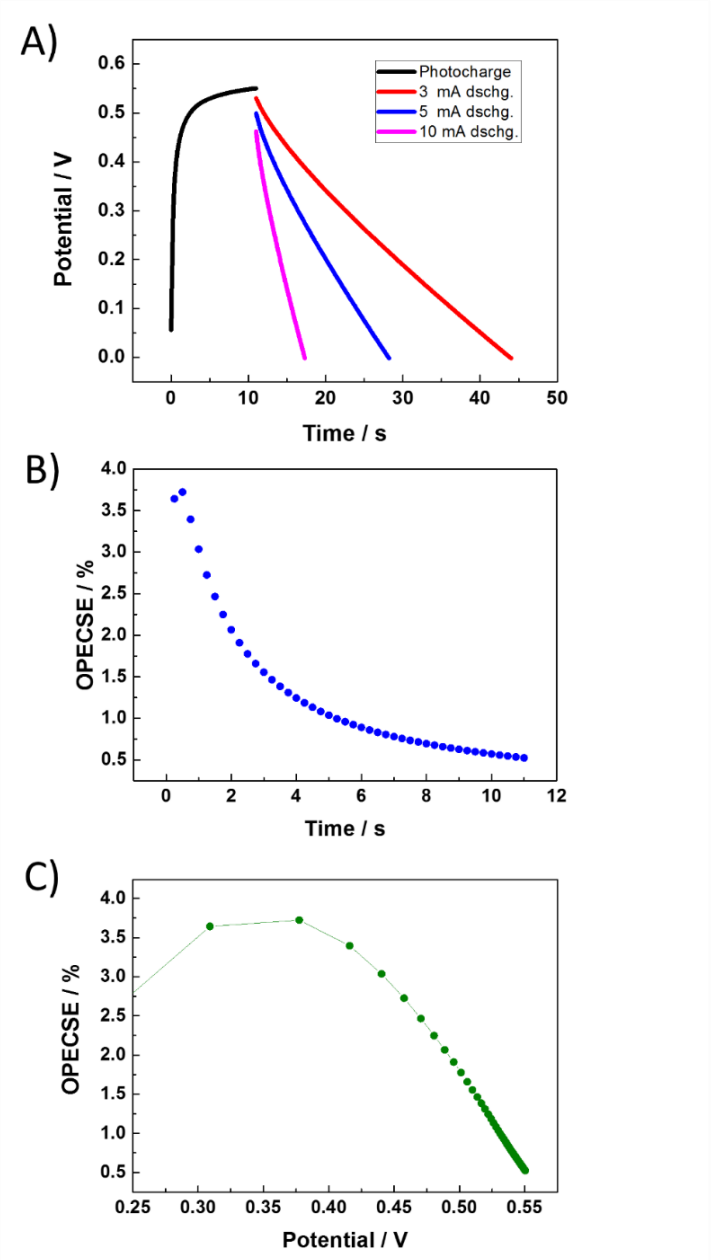

Figure 55: Photo-charge and discharges curves of the multifunctional-polymeric-membrane HS device. (B) OPECSE plotted as function of time. (C) OPECSE plotted as a function of the EDLC voltage. Reprinted with permission. Copyright 2018, Elsevier.

As reported in the paragraph "*HS device significant parameters*" overall efficiency was calculated through OPECSE equation. Results are plotted in Figure 55B and 55C, as a function of time and EDLC voltage, respectively.

The highest OPECSE was attained within a second of photo-charge. For such a short time, the EDLC voltage was already close to 0.4 V. It appears a noteworthy result, since this value represents the 70% of the final voltage.

After reaching 3.72% as maximum OPECSE, the overall efficiency decreased following the usual exponential trend. This behaviour is once again explained with EDLC voltage saturation, which limited the stored energy while electromagnetic power density was constantly impinging onto the PV harvester.

As can be seen in Figure 55C, OPECSE decreased only after EDLC reached 0.45 V. In this perspective, the multifunctional-based HS device possesses remarkable integration properties which renders this novel technological concept promising for industrial applications.

In addition, low cost of materials employed and easy scaling up of manufacturing procedures makes this 2-elctrodes integrated device a promising candidate to intrude the next generation low power electronics market.

5.CONCLUSIONS

Harvesting-storage (HS) integrated systems based on renewable harvesters and reliable storage sections could represent a valuable option to partly replace fossil fuels employment in the next future. Since, dye sensitized solar cells (DSSCs) and electrochemical double layer capacitors (EDLCs) structures are quite similar (both characterized by having two electrodes and an electrolyte in between), integration of the two devices was largely studied and practically obtained in the last ten years.

In this PhD, integration between DSSCs and EDLCs was implemented both in rigid and highly flexible configurations, in order to overcome some of the limitations currently affecting this class of devices.

At first, the approach was to mechanically connect harvester and storage by employing a thermoplastic film or UV polymerizing a silicone blend, obtaining 4 electrodes configurations.

Subsequently, attention was given to different conceptual structures, as the one obtained employing a multifunctional polymeric membrane which brought to a "2 electrodes" configuration.

In the first flexible structure,[63] metallic grids were employed as electrodes substrates and a quasi-solid polymeric membrane was manufactured to act as electrolyte. TiO2 nanotubes (NTs) were grown onto the titanium grid by means of room temperature anodic oxidation, reducing recombination rate and increasing electron diffusion length with respect to commonly used TiO2 nanoparticles. TiO2 NTs employment led to an increased fill factor if compared to a flexible DSSC obtained in a previous work.[20]

The photovoltaic (PV) section and the entire HS system were tested under different illumination conditions, demonstrating that by lowering the incoming electromagnetic radiation, both the harvester and the integrated device performances evidently improved.

A second configuration was obtained by coupling a dye sensitized solar module (DSSM) and an ionic liquid(IL)-based EDLC. DSSM was fabricated in such a way that the open circuit voltage of the PV-harvester was much higher if compared to the single PV-cell integrated devices literature reports. $Pyr_{14}TFSI$ ionic liquid voltage window was large enough to photo-charge the EDLC section up to 2.45 V. This work represents the first report dealing with reliable and efficient high voltage PV-based integrated devices.[45]

This configuration was also proposed in a third report with a solid state electrolyte regarding the EDLC section. The PEO-$Pyr_{14}TFSI$ electrolyte, allowed

long photo-charge/discharge cycling life, providing appealing performance above the state-of-the-art reported in the literature.[40]

The last HS device obtained architecture was appreciably simplified with respect to common literature reports. DSSC and EDLC electrodes were hosted onto the same metallic grid, which effectively enabled a direct electronic path between the PV-harvester and the storage units.

This newly HS device configuration was fabricated using a multifunctional polymer electrolyte membrane, which was cross-linked by oxygen-inhibited UV-curing. This configuration allowed to reach a much higher OPECSE with respect to previous HS structures obtained during this PhD period. In table 10 is proposed a comparison of the HS devices obtained during PhD period.

Table 10: Comparison of the HS devices obtained during PhD period.

HS device Paragraphs of chapter 4	OPECSE [%]	Flexibility	Structure simplification	Max. photo-voltage [V]	Dsch. Capacity [mA cm^{-2}]
4.5, [63]	1.02	Tested		0.6	6.4
4.6, [45]	1.83			2.45	360
4.7, [40]	1.67		EDLC assembly	2.45	61.2
4.8, In press	3.72		Device assembly	0.55	20

Moreover, during this PhD period, innovative electrolytes were electrochemically studied and their use was effectively validated for EDLCs. Electrolytes were obtained as co-solutions of $Pyr_{14}TDI$ ionic liquid and propylene carbonate. The maximum voltage window (3.3 V) was attained for the most concentrated solution (75 wt% IL). However, it did not turn into the highest energy density due to a lower capacitance with respect to the most diluted concentration (25 wt% IL), which instead provided the best performance in terms of specific energy (19.5 Wh kg^{-1}) and power (4.7 kW kg^{-1}).

FUTURE WORKS

Future activity will be devoted to obtain integrated HS devices which more and more embrace currently electrical needs. In this perspective, obtaining an even higher maximum photo-voltage with respect to 2.45 V (4 cells in series in the PV

module), already attained in [45] and [76], represents a crucial step in order to extend HS devices applications scenario. ILs or ILs-PC co-solutions have so far attained voltage windows of 3.5 V. Thus, manufacturing PV modules employing even 6 cells in series appears feasible.

Another HS devices field which has already been studied in [69] and deserve to be further investigated is flexibility. In fact, obtaining highly performing HS flexible integrated devices could lead to the exploitation of bendable surfaces. In addition, HS devices could be used in the field of flexible electronics, which nowadays is obtaining more and more significance.

Finally, EDLC discharge capacity subsequent to photo-charge requires improvement. To this purpose, new electrodes materials, with higher capacitance, deserve to be studied and applied in HS devices.

LIST OF PUBLICATIONS

1 **A. Scalia**, A. Varzi, A. Moretti, P. Ruschhaput, A. Lamberti, E. Tresso, S. Passerini, *Electrolytes based on N-Butyl-N-Methyl-Pyrrolidinium 4,5-Dicyano-2-(Trifluoromethyl) Imidazole for High Voltage Electrochemical Double Layer Capacitors*, ChemElectroChem. 5 (2018) 1. doi.org/10.1002/celc.201801172

2 **A. Scalia**, F. Bella, A. Lamberti, C. Gerbaldi, E. Tresso, *Innovative Multipolymer Electrolyte Membrane Designed by Oxygen Inhibited UV-Crosslinking Enables Solid-State in Plane Integration of Energy Conversion and Storage Devices*, Energy. 166 (2019) 789. doi.org/10.1016/j.energy.2018.10.162

3 **A. Scalia**, A. Varzi, A. Lamberti, T. Jacob, S. Passerini, *Portable high voltage powerpack by solid-state supercapacitor and dye-sensitized solar module integration*, Front. Chem. 6 (2018) 443. doi:10.3389/FCHEM.2018.00443.

4 **A. Scalia**, A. Varzi, A. Lamberti, E. Tresso, S. Jeong, T. Jacob, S. Passerini, *High energy and high voltage integrated photo-electrochemical double layer capacitor*, Sustain. Energy Fuels. 2 (2018) 968–977. doi:10.1039/C8SE00003D.

5 **A. Scalia**, F. Bella, A. Lamberti, S. Bianco, C. Gerbaldi, E. Tresso, C.F. Pirri, *A flexible and portable powerpack by solid-state supercapacitor and dye-sensitized solar cell integration*, J. Power Sources. 359 (2017). doi:10.1016/j.jpowsour.2017.05.072.

6 M. Gerosa, A. Sacco, **A. Scalia**, F. Bella, A. Chiodoni, M. Quaglio, E. Tresso, S. Bianco, *Toward Totally Flexible Dye-Sensitized Solar Cells Based on Titanium Grids and Polymeric Electrolyte*, IEEE J. Photovoltaics. 6 (2016) 498–505.

ACKNOWLEDGEMENTS

Passion, is a good word to start this acknowledgements section. A PhD is an amazing travel full of satisfactions, honours and awards that are difficult to find and reach in other works or even in life experiences. However, as all the PhD candidates know, the way till the achievement is also studded of bad moments, anxiety and a permanent sense of stress. The joining feeling of all the PhD students I have met during these years, that let them overcome difficulties of research activity is the passion they put in every working lab day, the passion they keep after every paper rejection, the passion they have to restart after every fail.

During this incredible journey, I have met a lot of people deserving my gratitude and acknowledgment. I would like to start from my big office: Bianca Dumontel, Luca Spigarelli, Andrea Ancona, Marta Canta, Luisa Racca, Alessandro Pedico, Federica Barbaresco, Carmine Lops, Francesca Susa, Amjid Rafique, Tanveer Ahmed Gadhi. I have spent precious, funny and nice moments with all of them during lab activities, lunches and hilarious office break moments. Among them, a special thank goes to Pietro Zaccagnini. At first, as Master thesis student and subsequently as friend and colleague Pietro transmitted me his admirable approach for research and his unrestrainable enjoyment in exploring new topics.

I thank Andrea Lamberti for being a leader and not a boss. This was fundamental in order to create a relationship based on trust and respect between us. Moreover, his endless proactive behaviour has been a model that I hope I have partly stolen.

I thank Prof. Candido Fabrizio Pirri for giving me the possibility to join his group and work on a so interesting and innovative topic.

To conclude with my tutors, I infinitely thank Prof. Elena Maria Tresso that I have met when I was a Master student and that immediately gave me trust and motivation and provided me precious scientific advices during my whole research route.

Mara Serrapede has been always patient and available to all my doubts and questions, especially during the first year when I had no knowledge regarding the fascinating world of electrochemistry. She also demonstrated important inspiring skills that made intriguing our collaboration.

Stefano Bianco has always been an excellent co-tutor, demonstrating me availability in every moment of the Master thesis project and during my PhD. He has also been a fundamental support to all my scientific requests.

I also truly acknowledge Claudio Gerbaldi and Federico Bella for providing me continuous and rigorous scientific assistance during laboratory work and during the

uneasy activity of papers writing. Since the beginning of my PhD they opened the door of their lab for me. Moreover, a true and sincere friendship grew with time.

I would like to thank Dr. Alberto Varzi for accepting my request to spend a period abroad under his supervision and as a consequence of the reciprocal respect and appreciation of the work done together, for agreeing to prolong the initial fixed 6 months' period. I believe I have learnt an enormous amount of electrochemistry notions by him and the year spent under his supervision makes me confident that at the moment I can say that, with still a lot to improve, I can be considered a specialist in my field.

Before arriving in Germany I did not know Stefano Passerini. Not even his reputation in the electrochemistry world. What was really singular to me was the endless passion he put in his job after years and years of experience and the admirable desire to stress and deeply understand even the less relevant choice his students made during research. With a gigantic group to manage at the best, it is difficult to imagine a similar availability to every doubt of every student. But in his case it was the typical behaviour.

I would like to thank the other components of the best Chinese-Italian-Korean office ever: Dr. Kim Guk-Tae, Chen Zhen, Ma Yuan, Ma Yanjao.

I also acknowledge the Italian group at the HIU: Daniele Di Lecce, Ulderico Ulissi, Mario Marinaro, Arianna Moretti. With them I spent funny lunch breaks and nice evenings in Ulm.

I truly acknowledge Monica Barale. At first, always kind, smiling and present for every bureaucratic doubt. She quickly became a reference point during these three years especially for extra working problems and without doubt she will remain it in the future.

Thanks to Nicolò Cancemi, Valentina Dall'Asta, Giulia Tomasino, Francesco Galuppo, Roberto Cavaliere for being good friends even if the distance did not allow us to see each other often. They have always demonstrated to be next to me when I asked for their help or sustain.

I thank Wanderson Hilary Polanco Rijo and Diego Pettorossi for being the funniest and craziest roommates ever. They were exactly what I needed in that period and now they are precious and present friends.

I thank Marina Scalia and Salvatore Ferrari for being my second family in Turin. Since I arrived here, they were close to me and provided affection in every occasion in which I needed their presence.

I have to acknowledge Giuseppina Buttitta since the person I am today is a consequence of the time spent together. She made me grow up as a man and as an inspired person. She made me believe in myself, always stimulating my curiosity

and bearing my extremely strange character. For all of these reasons I will always be grateful to her.

I acknowledge Francesca Magro for having loved me as her own son.

I dedicate this thesis to my brother, Riccardo. I value him for the man he is. I am proud of him, since he succeeded in carrying out the objectives he prefixed for his life.

I thank my parents for supporting me and giving freedom to my choices. They have grown me with important moral principles that constituted the basis of my life.

I thank Angela Roccasalva for moving mountains, for making me live unforgettable moments and for being unique.

Finally, I thank myself, for never giving up when the success of the experiments seemed hopeless, for being confident, for feeling passion and demonstrating the capability to go through the difficulties of this amazing period.

REFERENCES

[1] L. El Chaar, L. A. Lamont, and N. El Zein, "Review of photovoltaic technologies," *Renew. Sustain. Energy Rev.*, vol. 15, no. 5, pp. 2165–2175, 2011.

[2] B. Parida, S. Iniyan, and R. Goic, "A review of solar photovoltaic technologies," *Renew. Sustain. Energy Rev.*, vol. 15, no. 3, pp. 1625–1636, 2011.

[3] S. D. Stranks and H. J. Snaith, "Metal-halide perovskites for photovoltaic and light-emitting devices," *Nat. Nanotechnol.*, vol. 10, no. 5, pp. 391–402, 2015.

[4] K. Wongcharee, V. Meeyoo, and S. Chavadej, "Dye-sensitized solar cell using natural dyes extracted from rosella and blue pea flowers," *Sol. Energy Mater. Sol. Cells*, vol. 91, no. 7, pp. 566–571, 2007.

[5] H. S. Jung and J. K. Lee, "Dye Sensitized Solar Cells for Economically Viable Photovoltaic Systems," *J. Phys. Chem. Lett.*, vol. 4, pp. 1682–1693, 2013.

[6] L. M. Gonçalves, V. de Zea Bermudez, H. A. Ribeiro, and A. M. Mendes, "Dye-sensitized solar cells: A safe bet for the future.," *Energy Environ. Sci.*, vol. 1, no. 6, p. 655, 2008.

[7] M. Freitag *et al.*, "Dye-sensitized solar cells for efficient power generation under ambient lighting," *Nat. Photonics*, vol. 11, no. 6, pp. 372–378, 2017.

[8] J. Gong, K. Sumathy, Q. Qiao, and Z. Zhou, "Review on dye-sensitized solar cells (DSSCs): Advanced techniques and research trends," *Renew. Sustain. Energy Rev.*, vol. 68, no. July 2016, pp. 234–246, 2017.

[9] S. S. and S. P. S. Shalini1,*,†, R. Balasundaraprabhu1, T. Satish Kumar2, N. Prabavathy1, "Status and outlook of sensitizers/dyes used in dye sensitized solar cells (DSSC): a review," *Int. J. energy Res.*, vol. 31, no. August 2007, pp. 135–147, 2007.

[10] F. Bella, C. Gerbaldi, C. Barolo, and M. Grätzel, "Aqueous dye-sensitized solar cells," *Chem. Soc. Rev.*, vol. 44, no. 11, pp. 3431–3473, 2015.

[11] A. Sacco, "Electrochemical impedance spectroscopy: Fundamentals and application in dye-sensitized solar cells," *Renew. Sustain. Energy Rev.*, vol. 79, no. August 2016, pp. 814–829, 2017.

[12] K. Kakiage, Y. Aoyama, T. Yano, K. Oya, J. Fujisawa, and M. Hanaya, "Highly-efficient dye-sensitized solar cells with collaborative sensitization by silyl-anchor and carboxy-anchor dyes," *Chem. Commun.*, vol. 51, no. 88, pp. 15894–15897, 2015.

[13] T. M. Brown *et al.*, "Progress in flexible dye solar cell materials, processes and devices," *J. Mater. Chem. A*, vol. 2, no. 28, pp. 10788–10817, 2014.

[14] D. Pugliese, A. Lamberti, F. Bella, A. Sacco, S. Bianco, and E. Tresso, "TiO2nanotubes as flexible photoanode for back-illuminated dye-sensitized solar cells with hemi-squaraine organic dye and iodine-free transparent electrolyte," *Org. Electron. physics, Mater. Appl.*, vol. 15, no. 12, pp. 3715–

3722, 2014.
[15] M. Gerosa *et al.*, “Toward Totally Flexible Dye-Sensitized Solar Cells Based on Titanium Grids and Polymeric Electrolyte,” *IEEE J. Photovoltaics*, vol. 6, no. 2, pp. 498–505, 2016.
[16] F. Bella *et al.*, “A UV-crosslinked polymer electrolyte membrane for quasi-solid dye-sensitized solar cells with excellent efficiency and durability.,” *Phys. Chem. Chem. Phys.*, vol. 15, no. 11, pp. 3706–11, 2013.
[17] F. Bella, A. Lamberti, A. Sacco, S. Bianco, A. Chiodoni, and R. Bongiovanni, “Novel electrode and electrolyte membranes: Towards flexible dye-sensitized solar cell combining vertically aligned TiO2 nanotube array and light-cured polymer network,” *J. Memb. Sci.*, vol. 470, pp. 125–131, 2014.
[18] J. K. Lee *et al.*, “Effects of polyaniline additive in solvent-free ionic liquid electrolyte for dye-sensitized solar cell,” *Bull. Korean Chem. Soc.*, vol. 31, no. 11, pp. 3411–3414, 2010.
[19] Z. Lan, J. Wu, D. Wang, S. Hao, J. Lin, and Y. Huang, “Quasi-solid state dye-sensitized solar cells based on gel polymer electrolyte with poly(acrylonitrile-co-styrene)/NaI+I2,” *Sol. Energy*, vol. 80, no. 11, pp. 1483–1488, 2006.
[20] M. Gerosa *et al.*, “Toward Totally Flexible Dye-Sensitized Solar Cells Based on Titanium Grids and Polymeric Electrolyte,” *IEEE J. Photovoltaics*, vol. 6, no. 2, 2016.
[21] S. Zhang and N. Pan, “Supercapacitors performance evaluation,” *Adv. Energy Mater.*, vol. 5, no. 6, pp. 1–19, 2015.
[22] Z. Lin *et al.*, “Materials for supercapacitors: When Li-ion battery power is not enough,” *Mater. Today*, vol. 21, no. 4, pp. 419–436, 2018.
[23] P. Simon and Y. Gogotsi, “Materials for electrochemical capacitors,” *Nat. Mater.*, vol. 7, no. 11, pp. 845–854, Nov. 2008.
[24] S. Zhang and N. Pan, “Supercapacitors performance evaluation,” *Adv. Energy Mater.*, vol. 5, no. 6, pp. 1–19, 2015.
[25] A. Balducci, D. Belanger, T. Brousse, J. W. Long, and W. Sugimoto, “Perspective—A Guideline for Reporting Performance Metrics with Electrochemical Capacitors: From Electrode Materials to Full Devices,” *J. Electrochem. Soc.*, vol. 164, no. 7, pp. A1487–A1488, 2017.
[26] J. Chmiola, G. Yushin, Y. Gogotsi, C. Portet, P. Simon, and P. L. Taberna, “Anomalous increase in carbon capacitance at pore sizes less than 1 nanometer,” *Science (80-.).*, vol. 313, no. 5794, pp. 1760–1763, 2006.
[27] F. Béguin, V. Presser, A. Balducci, and E. Frackowiak, “Carbons and electrolytes for advanced supercapacitors,” *Adv. Mater.*, vol. 26, no. 14, pp. 2219–2251, 2014.
[28] P. Simon and Y. Gogotsi, “Materials for electrochemical capacitors.,” *Nat. Mater.*, vol. 7, no. 11, pp. 845–854, 2008.
[29] A. González, E. Goikolea, J. A. Barrena, and R. Mysyk, “Review on supercapacitors: Technologies and materials,” *Renew. Sustain. Energy Rev.*,

vol. 58, pp. 1189–1206, 2016.
[30] Y. Zhang *et al.*, “Progress of electrochemical capacitor electrode materials: A review,” *Int. J. Hydrogen Energy*, vol. 34, no. 11, pp. 4889–4899, 2009.
[31] C. Zhong, Y. Deng, W. Hu, J. Qiao, L. Zhang, and J. Zhang, “A review of electrolyte materials and compositions for electrochemical supercapacitors.,” *Chem. Soc. Rev.*, vol. 44, no. 21, pp. 7484–7539, 2015.
[32] K. Fic, G. Lota, M. Meller, and E. Frackowiak, “Novel insight into neutral medium as electrolyte for high-voltage supercapacitors,” *Energy Environ. Sci.*, vol. 5, no. 2, pp. 5842–5850, 2012.
[33] S. Pohlmann, B. Lobato, T. A. Centeno, and A. Balducci, “The influence of pore size and surface area of activated carbons on the performance of ionic liquid based supercapacitors,” *Phys. Chem. Chem. Phys.*, vol. 15, no. 40, p. 17287, 2013.
[34] S. Pohlmann, C. Ramirez-Castro, and A. Balducci, “The Influence of Conductive Salt Ion Selection on EDLC Electrolyte Characteristics and Carbon-Electrolyte Interaction,” *J. Electrochem. Soc.*, vol. 162, no. 5, pp. A5020–A5030, 2015.
[35] S. Pohlmann, R. Kühnel, T. A. Centeno, and A. Balducci, “The Influence of Anion – Cation Combinations on the Physicochemical Properties of Advanced Electrolytes for Supercapacitors and the Capacitance of Activated Carbons,” *ChemElectroChem*, vol. 1, pp. 1301–1311, 2014.
[36] A. Brandt, S. Pohlmann, A. Varzi, A. Balducci, and S. Passerini, “Ionic liquids in supercapacitors,” *MRS Bull.*, vol. 38, no. July, pp. 554–559, 2013.
[37] S. Pohlmann, T. Olyschläger, P. Goodrich, J. Alvarez Vicente, J. Jacquemin, and A. Balducci, “Azepanium-based ionic liquids as green electrolytes for high voltage supercapacitors,” *J. Power Sources*, vol. 273, pp. 931–936, 2015.
[38] G. A. Tiruye, D. Muñoz-Torrero, J. Palma, M. Anderson, and R. Marcilla, “Performance of solid state supercapacitors based on polymer electrolytes containing different ionic liquids,” *J. Power Sources*, vol. 326, pp. 560–568, 2016.
[39] G. Ayalneh Tiruye, D. Muñoz-Torrero, J. Palma, M. Anderson, and R. Marcilla, “All-solid state supercapacitors operating at 3.5 v by using ionic liquid based polymer electrolytes,” *J. Power Sources*, vol. 279, pp. 472–480, 2015.
[40] A. Scalia, A. Varzi, A. Lamberti, T. Jacob, and S. Passerini, “Portable high voltage powerpack by solid-state supercapacitor and dye-sensitized solar module integration,” *Front. Chem.*, vol. 6, p. 443, 2018.
[41] R. S. Kühnel, N. Böckenfeld, S. Passerini, M. Winter, and A. Balducci, “Mixtures of ionic liquid and organic carbonate as electrolyte with improved safety and performance for rechargeable lithium batteries,” *Electrochim. Acta*, vol. 56, no. 11, pp. 4092–4099, 2011.
[42] S. Pohlmann, R. S. Kühnel, T. A. Centeno, and A. Balducci, “The Influence of Anion-Cation Combinations on the Physicochemical Properties of

Advanced Electrolytes for Supercapacitors and the Capacitance of Activated Carbons," *ChemElectroChem*, vol. 1, no. 8, pp. 1301–1311, 2014.

[43] S. Pohlmann, T. Olyschläger, P. Goodrich, J. A. Vicente, J. Jacquemin, and A. Balducci, "Mixtures of azepanium based ionic liquids and propylene carbonate as high voltage electrolytes for supercapacitors," *Electrochim. Acta*, vol. 153, pp. 426–432, 2015.

[44] "B._E._Conway_Electrochemical_Supercapacitors_Scientific_Fundamentals_and_Technological_Applications.pdf." .

[45] A. Scalia *et al.*, "High energy and high voltage integrated photo-electrochemical double layer capacitor," *Sustain. Energy Fuels*, vol. 2, no. 5, pp. 968–977, 2018.

[46] J. Xu, Z. Ku, Y. Zhang, D. Chao, and H. J. Fan, "Integrated Photo-Supercapacitor Based on PEDOT Modified Printable Perovskite Solar Cell," *Adv. Mater. Technol.*, pp. 1–5, 2016.

[47] M. Skunik-Nuckowska *et al.*, "Integration of solid-state dye-sensitized solar cell with metal oxide charge storage material into photoelectrochemical capacitor," *J. Power Sources*, vol. 234, pp. 91–99, 2013.

[48] T. Miyasaka and T. N. Murakami, "The photocapacitor: An efficient self-charging capacitor for direct storage of solar energy," *Appl. Phys. Lett.*, vol. 85, no. 17, pp. 3932–3934, 2004.

[49] T. N. Murakami, N. Kawashima, and T. Miyasaka, "A high-voltage dye-sensitized photocapacitor of a three-electrode system.," *Chem. Commun. (Camb).*, no. 26, pp. 3346–3348, 2005.

[50] C. Y. Hsu, H. W. Chen, K. M. Lee, C. W. Hu, and K. C. Ho, "A dye-sensitized photo-supercapacitor based on PProDOT-Et2 thick films," *J. Power Sources*, vol. 195, no. 18, pp. 6232–6238, 2010.

[51] Z. Yang *et al.*, "An integrated device for both photoelectric conversion and energy storage based on free-standing and aligned carbon nanotube film," *J. Mater. Chem. A*, vol. 1, no. 3, pp. 954–958, 2013.

[52] H. W. Chen *et al.*, "Plastic dye-sensitized photo-supercapacitor using electrophoretic deposition and compression methods," *J. Power Sources*, vol. 195, no. 18, pp. 6225–6231, 2010.

[53] A. P. Cohn *et al.*, "All Silicon Electrode Photocapacitor for Integrated Energy Storage and Conversion," *Nano Lett.*, vol. 15, no. 4, pp. 2727–2731, 2015.

[54] J. Xu *et al.*, "Supercapacitors: Integrated Photo-supercapacitor Based on Bi-polar TiO $_2$ Nanotube Arrays with Selective One-Side Plasma-Assisted Hydrogenation (Adv. Funct. Mater. 13/2014)," *Adv. Funct. Mater.*, vol. 24, no. 13, pp. 1814–1814, 2014.

[55] W. Guo, X. Xue, S. Wang, C. Lin, and Z. L. Wang, "An integrated power pack of dye-sensitized solar cell and Li battery based on double-sided TiO2 nanotube arrays," *Nano Lett.*, vol. 12, pp. 2520–2523, 2012.

[56] P. Du *et al.*, "Self-powered electronics by integration of flexible solid-state

graphene-based supercapacitors with high performance perovskite hybrid solar cells," *Adv. Funct. Mater.*, vol. 25, no. 16, pp. 2420–2427, 2015.
[57] A. Gurung *et al.*, "Highly Efficient Perovskite Solar Cell Photocharging of Lithium Ion Battery Using DC-DC Booster," *Adv. Energy Mater.*, p. 1602105, 2017.
[58] J. Kim *et al.*, "A highly efficient self-power pack system integrating supercapacitors and photovoltaics with an area-saving monolithic architecture," *J. Mater. Chem. A*, vol. 0, no. 5, pp. 1906–1912, 2017.
[59] C. Li, M. Islam, J. Moore, J. Sleppy, C. Morrison, and K. Konstantinov, "Wearable energy-smart ribbons for synchrounous energy harvest and storage," *Nat. Publ. Gr.*, vol. 7, no. May, pp. 1–10, 2016.
[60] S. Intermite *et al.*, "Perovskite solar cell – electrochemical double layer capacitor interplay," *Electrochim. Acta*, vol. 258, pp. 825–833, 2017.
[61] A. Das, S. Deshagani, R. Kumar, and M. Deepa, "Bifunctional Photo-Supercapacitor with a New Architecture Converts and Stores Solar Energy as Charge," *ACS Appl. Mater. Interfaces*, vol. 10, no. 42, pp. 35932–35945, 2018.
[62] C. T. Chien *et al.*, "Graphene-Based Integrated Photovoltaic Energy Harvesting/Storage Device," *Small*, vol. 11, no. 24, pp. 2929–2937, 2015.
[63] A. Scalia *et al.*, "A flexible and portable powerpack by solid-state supercapacitor and dye-sensitized solar cell integration," *J. Power Sources*, vol. 359, 2017.
[64] S. Park and S. Kim, "Effect of carbon blacks filler addition on electrochemical behaviors of Co3O4/graphene nanosheets as a supercapacitor electrodes," *Electrochim. Acta*, vol. 89, pp. 516–522, 2013.
[65] A. Lamberti, A. Chiodoni, N. Shahzad, S. Bianco, M. Quaglio, and C. F. Pirri, "Ultrafast Room-Temperature Crystallization of TiO2 Nanotubes Exploiting Water-Vapor Treatment," *Sci. Rep.*, vol. 5, p. 7808, 2015.
[66] Q. Zhou, C. Jia, X. Ye, Z. Tang, and Z. Wan, "A knittable fiber-shaped supercapacitor based on natural cotton thread for wearable electronics," *J. Power Sources*, vol. 327, pp. 365–373, 2016.
[67] T. G. Yun, M. Oh, L. Hu, S. Hyun, and S. M. Han, "Enhancement of electrochemical performance of textile based supercapacitor using mechanical pre-straining," *J. Power Sources*, vol. 244, pp. 783–791, 2013.
[68] Z. Zhang *et al.*, "Integrated polymer solar cell and electrochemical supercapacitor in a flexible and stable fiber format," *Adv. Mater.*, vol. 26, no. 3, pp. 466–470, 2014.
[69] A. Scalia *et al.*, "A flexible and portable powerpack by solid-state supercapacitor and dye-sensitized solar cell integration," *J. Power Sources*, vol. 359, pp. 311–321, 2017.
[70] A. Varzi *et al.*, "A 4 Farad high energy electrochemical double layer capacitor prototype operating at 3.2 V (IES prototype)," *J. Power Sources*, vol. 326, pp. 162–169, 2016.
[71] A. Varzi, R. Raccichini, M. Marinaro, M. Wohlfahrt-Mehrens, and S.

Passerini, “Probing the characteristics of casein as green binder for non-aqueous electrochemical double layer capacitors’ electrodes,” *J. Power Sources*, vol. 326, pp. 672–679, 2016.

[72] A. Varzi, A. Balducci, and S. Passerini, “Natural Cellulose: A Green Alternative Binder for High Voltage Electrochemical Double Layer Capacitors Containing Ionic Liquid-Based Electrolytes,” *J. Electrochem. Soc.*, vol. 161, no. 3, pp. A368–A375, 2014.

[73] F. Giordano, E. Petrolati, T. M. Brown, A. Reale, and A. Di Carlo, “Series-connection designs for dye solar cell modules,” *IEEE Trans. Electron Devices*, vol. 58, no. 8, pp. 2759–2764, 2011.

[74] H. Seo *et al.*, “The fabrication of efficiency-improved W-series interconnect type of module by balancing the performance of single cells,” *Sol. Energy*, vol. 83, no. 12, pp. 2217–2222, 2009.

[75] M. Son, H. Seo, K. Lee, and S. Kim, “Computational modeling and experimental analysis on the improvement of current mismatch in a W-type series-connected dye-sensitized solar module,” *J. Photochem. Photobiol. A Chem.*, vol. 268, pp. 17–23, 2013.

[76] A. Scalia, A. Varzi, A. Lamberti, T. Jacob, and S. Passerini, “Portable High Voltage Integrated Harvesting-Storage Device Employing Dye-Sensitized Solar Module and All-Solid-State Electrochemical Double Layer Capacitor,” *Front. Chem.*, vol. 6, no. September, pp. 1–8, 2018.

[77] V. Sharova, G.-T. Kim, G. A. Giffin, A. Lex-Balducci, and S. Passerini, “Quaternary Polymer Electrolytes Containing an Ionic Liquid and a Ceramic Filler,” *Macromol. Rapid Commun.*, vol. 37, no. 14, pp. 1188–1193, 2016.

[78] G. T. Kim *et al.*, “UV cross-linked, lithium-conducting ternary polymer electrolytes containing ionic liquids,” *J. Power Sources*, vol. 195, no. 18, pp. 6130–6137, 2010.